INFLUENCE OF DEFECTS ON CRITICAL PARAMETERS IN HIGH TEMPERATURE SUPERCONDUCTORS

by

Predrag Kisa

Dipl. Ing. Metallurgy, University of Belgrade, 1997

Submitted to the Graduate Faculty of

School of Engineering in partial fulfillment

of the requirements for the degree of

Doctor of Philosophy

University of Pittsburgh

2006

UNIVERSITY OF PITTSBURGH

SCHOOL OF ENGINEERING

This dissertation was presented

by

Predrag Kisa

It was defended on

April 4, 2006

and approved by

Jean R. Blachere, Associate Professor Emeritus, Materials Science and Engineering Department

Ian Nettleship, Professor Materials Science and Engineering Department

Michael E. McHenry, Professor Materials Science and Engineering Department

Nicholas G. Eror, Professor Materials Science and Engineering Department
Dissertation Director

INFLUENCE OF DEFECTS ON CRITICAL PARAMETERS IN HIGH TEMPERATURE SUPERCONDUCTORS

Predrag Kisa, Ph.D.

University of Pittsburgh, 2006

Bismuth cuprate high temperature superconductors are currently the only ceramic material that can be successfully processed in kilometer length wires. Bismuth cuprates form three compositions that can be represented with the generic formula $Bi_2Sr_2Ca_nCu_{n+1}O_{8+d}$ n = 0, 1, 2 (with critical temperatures T_c = 20K, 85-94K and 110K respectively). With critical temperatures above 77K (liquid nitrogen boiling point) the only property inhibiting a widespread use is the infield performance, that is, insufficient critical current densities in high magnetic fields. The infield critical current is intimately related to the pinning of the flux vortices that form under the influence of a magnetic field. The intrinsic pinning of flux vortices, is still not well understood in these quaternary systems. The influence of $SrCuO_2$ second phase additions as well as internal cation nonstoichiometry was investigated as a viable way to control the flux pinning properties in the $Bi_2Sr_2CaCu_2O_{8+d}$ (Bi-2212) system. The compositions of $Bi_2Sr_{2+x}CaCu_{2+x}O_{8+y}$ (x = 0.0001-0.6) as well as Nd substituted Ca samples were prepared via freeze-drying. Phase pure stoichiometric Bi-2212 was synthesized via freeze-drying in a reduced oxygen atmosphere. It was further determined that up to 20mol% additions of $SrCuO_2$ can be accommodated in the Bi-2212 structure and that the additions increase critical current. The incorporation of $SrCuO_2$ into Bi-2212 results in change of both lattice parameters and modulation vector.

TABLE OF CONTENTS

LIST OF TABLES

LIST OF FIGURES

NOMENCLATURE

Nomenclature (List of symbols and acronyms used through the text)

YBCO	$YBa_2Cu_3O_{7-x}$, $YBa_2Cu_4O_{7-x}$
(Y-123, 123)	$YBa_2Cu_3O_{7-x}$
RBCO (REBCO, RE-123)	$(RE)Ba_2Cu_3O_{7-x}$, RE= lanthanide series of elements
BSCCO also Bi-2212	$Bi_2Sr_2CaCu_2O_{8+\delta}$
Bismuth cuprate superconductors	Any of the $Bi_2Sr_2Ca_nCu_{n+1}O_{8+\delta}$ n=0, 1, 2 family
XRD	X-ray diffraction
SEM	Scanning electron microscopy
HRTEM	High resolution TEM
DTA	Differential thermal analysis
TGA	Thermo gravimetric analysis
Doping, substitution, addition	Used as synonyms to explain replacement of cations within the crystal structure
T_c	Temperature of the superconductor – normal transition
J_c	Critical current density
λ	Penetration depth (magnetic field penetration distance within the superconductor)
ξ	Coherence length (length at which the superconducting electrons are coupled)

1.0 INTRODUCTION

1.1 OVERVIEW OF SUPERCONDUCTING PROPERTIES

The advent of superconductivity[1] could be considered to have started on 10th of July 1908 when Heike Kamerlingh Onnes at the University of Leiden achieved liquefaction of helium (He). In 1911, his interest in behavior of the resistivity of metals at low temperatures led to detection of abrupt drop in resistivity to 10^{-6} of the previously measured value, when mercury was cooled to 4.2K. During his 1913 Nobel laureate lecture [1] he used the term superconductivity to describe a new state that some of the investigated metals i.e. mercury, tin and led (Hg, Sn, Pb) entered upon cooling below 4.2K. Though the potential for engineering applications was immediately realized, practical application was hindered, since even the small magnetic fields destroyed the state of zero resistivity.

Exclusion of field from the bulk material was first observed by Meissner and Ochenfeld in 1933 [7]. By cooling a single crystal of tin, and polycrystalline Pb tubes in the presence of a magnetic field, they discovered that when the sample became superconducting, it expelled the magnetic field lines that penetrated it when it was in the normal state. Though relation between flux expulsion and superconductivity was

[1] Superconductivity overview, constitutive equations and history is given in classical reference texts [1-5], this short introduction will give only the basic overview without derivations based on the classic papers.

not immediately obvious, C.J. Gorter [8] ascribed internal field equal to zero to be a general characteristics for superconductivity, and concluded that the superconductor was a perfect diamagnet.

Although it was initially believed that superconductors are just ideal, or perfect conductors, the two behave differently. After the Meissner-Ochenfeld experiment, it was realized that superconductors are not simply perfect conductors being characterized with vanishing resistivity (ρ), $\rho = 0$ at $T = T_c$ and no other salient feature. Superconductivity is distinguished in the path independence of transitions to the superconducting state. [Figure 1].

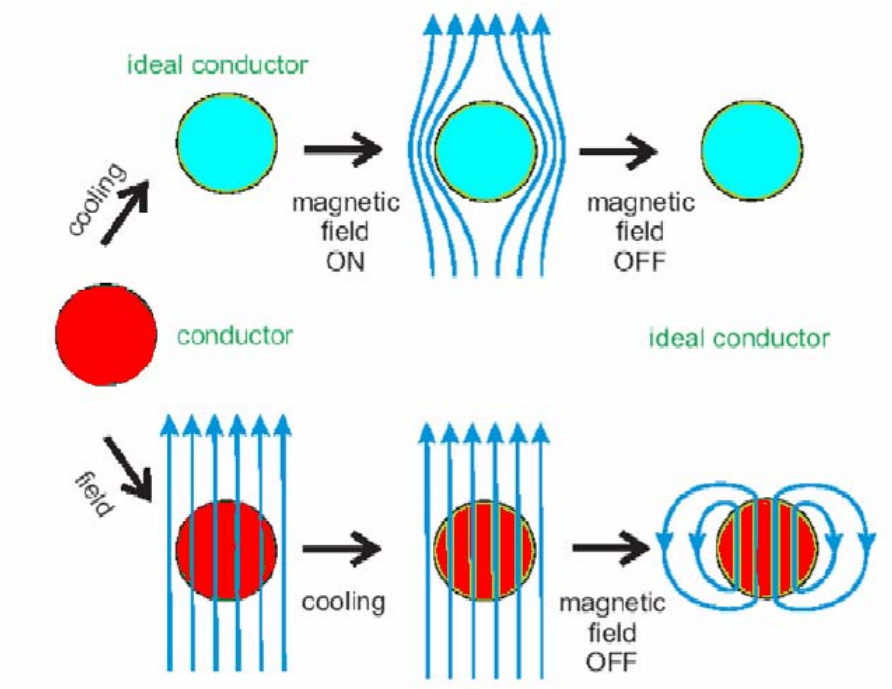

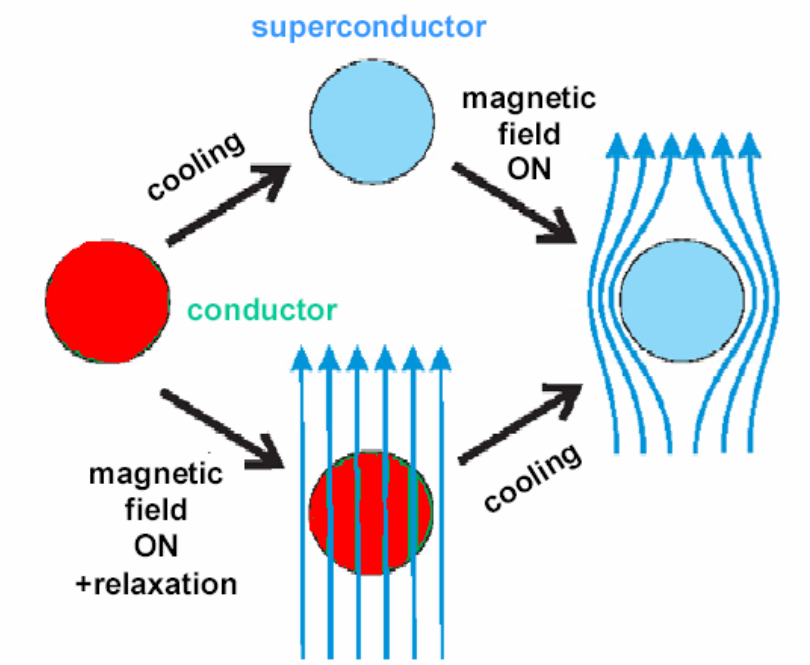

Figure 1 Expulsion of field from ideal and superconducting conductor. Expulsion of magnetic field in superconductors is path independent.

Today all superconductors are considered to be described with the two previously mentioned characterizing properties, the *loss of resistivity* upon reaching the transition temperature and *expulsion of external magnetic field*.

In order to explain the expulsion of magnetic field from the superconductor, the London brothers proposed a phenomenological theory in 1935 [9] with the premise of the previously proposed two fluid model, all free electrons in the superconductor are divided into two groups: superconducting electrons of density n_s and normal electrons of density n_n, with the total density of free electrons $n = n_s + n_n$. As the temperature increases from 0 to T_c, the density n_s decreases from n to 0. Further assumptions are that the magnetic flux penetrates to a certain penetration

depth λ that is independent on the strength of the magnetic field as well as the dimensions of the sample. The *London equations* are given by:

$$E = \frac{\partial}{\partial t}(\Lambda J_s)$$

Equation 1

From the first London equation, in the stationary state (i.e. $\frac{dJ_s}{dt} = 0$) ***E = 0*** that is, there is no electric field inside superconductor.

and

$$B = -\nabla \times (\Lambda J_s)$$

Equation 2

where

$$\Lambda = \frac{m}{n_s e^2}$$

E represents the macroscopic electric field inside the specimen, ***B*** macroscopic magnetic field, $\boldsymbol{J_s}$ current density, ***m*** mass of the charge carrier and ***e*** the charge of carrier. Derivation of the London equations is given in the appendix.

If the second equation is combined with the Maxwell equation

$$\nabla \times B = \mu_0 J$$

Equation 3

$$\nabla \times (\nabla \times B) = \mu_0 (\nabla \times J) = -\frac{1}{\mu_0} \Lambda B$$

$$\frac{1}{\lambda^2} = \frac{\mu_0 n_s e^2}{m}$$

$$\nabla^2 B = \frac{1}{\lambda^2} B$$

Equation 4

where λ represents the London penetration depth of the magnetic field.

If a magnetic field is applied parallel to the surface of a superconductor $\boldsymbol{B=B_0x}$ and the distance into the superconductor is measured in the z direction. The London equations simplified to one dimension (z):

$$\nabla^2 B = \frac{1}{\lambda^2} B$$

$$\frac{\partial B_x(z)}{\partial z^2} = \frac{1}{\lambda^2} B$$

are solved as:

$$B_x(z) = B_{0x} e^{-\frac{z}{\lambda}}$$

Equation 5

showing the exponential decay of magnetic field penetrating the superconductor to a characteristic depth λ.

In 1953 AB Pippard [10] introduced a notion of a coherence length, ξ, over which the electrons in a superconducting medium are coupled. While investigating the influence of substitution on penetration depth [11], he noticed discrepancies between experimental estimations of λ(0) (the penetration depth at zero

temperature) for certain conventional superconductors, and those predicted by the London brothers, Pippard introduced non-local effects into the London equations. Spatial changes of quantities such as n_s in a superconductor may only occur on a finite length scale (the *coherence length,* ξ) and not over arbitrarily small distances. Whenever n_s is varying in space its value may change significantly over distances of order ξ. The coherence length defines the intrinsic nonlocality of the superconducting state. Using the uncertainty principle, Pippard estimated the coherence length for a pure metal to be:

$$\xi_0 = \frac{\hbar^2 k_f}{2mE_g} = \frac{\hbar v_f}{2E_g}$$

Equation 6

where $\hbar = \frac{h}{2\pi}$, *h* Planck's constant, $\boldsymbol{E_g}$ energy gap, $\boldsymbol{v_f}$ electron velocity at the Fermi surface.

First phenomenological theory taking into account the quantum effects was proposed by Ginzburg and Landau in 1950 [1-4]. The proposed theory took into account that the superconducting state is more ordered than the normal state and that the transition from one to the other state is a second order phase transition.

$$\alpha\psi + \beta|\psi|^2 + \frac{1}{2m}\left(-i\hbar\nabla - \frac{2eA}{c}\right)^2\psi = 0$$

Equation 7

$$j = -\frac{e\hbar}{im}\left(\psi^* \nabla \psi - \psi \nabla \psi^*\right) - \frac{4e^2}{mc}\psi^* \psi A$$

Equation 8

The equations (7-8) represent the fundamental Ginzburg-Landau (GL) equations.

Superconducting materials can be differentiated using the GL parameter

$$\kappa = \frac{\lambda}{\xi}$$

such that when $\kappa < \frac{1}{\sqrt{2}}$ they are of type I superconductors and when $\kappa > \frac{1}{\sqrt{2}}$ they are of type II superconductors. All elemental superconductors are type I, with the exception of Nb, V and Tc

The basic difference between type I and type II superconductors is usually illustrated by using Figure 2, which shows the idealized magnetic response of both types of superconductors under an applied field. If an ideal sample geometry is used (i.e. long cylinder) type I superconductors exhibit the full Meissner effect prior to turning “normal” at a critical magnetic field (H_c). Under the same conditions type II superconductors expel the magnetic field up to a lower critical field H_{c1} whereupon magnetic flux begins to penetrate in the form of the quantized flux lines (flux vortices) and superconductivity is lost upon reaching upper critical field H_{c2}.

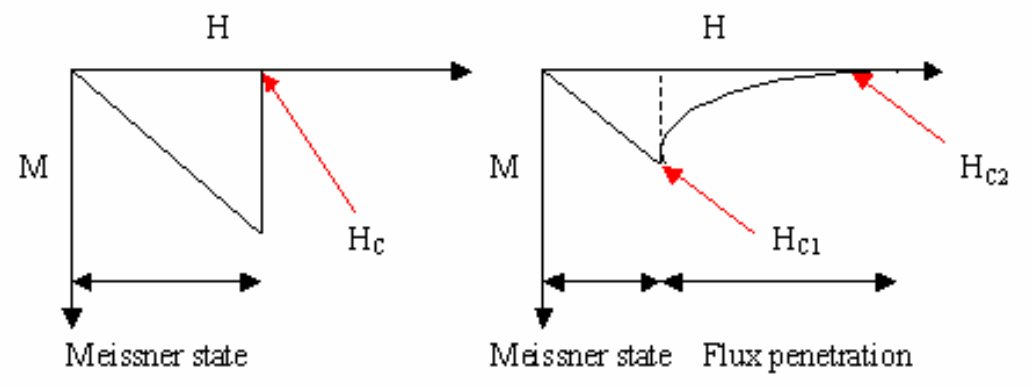

Figure 2 Magnetization (M vs. H) curves for type I and type II superconductors. For a type I superconductor (left) the superconducting–normal transition occurs at H_C and the superconductor exhibits the full Meissner effect prior to turning normal. For a type II superconductor (right) the full Meissner effect is exhibited until H_{C1} when the first fluxoid penetrates. Superconductivity is lost upon reaching H_{C2}.

1.2 FLUX VORTICES

Three types of vortices can be developed in a superconductor. First an Abrikosov vortex (3D vortex), penetrates type II superconductors above a lower critical magnetic field (H_{c1}). These vortices can be regarded as tubes consisting of a normal core of the radius ξ and the shielding current that extends a distance λ from the center. Under an applied current, or through thermal activation, vortices move/hop between pinning sites causing dissipation in current. These vortices appear in alloys of type II superconductors. (Figure 3)

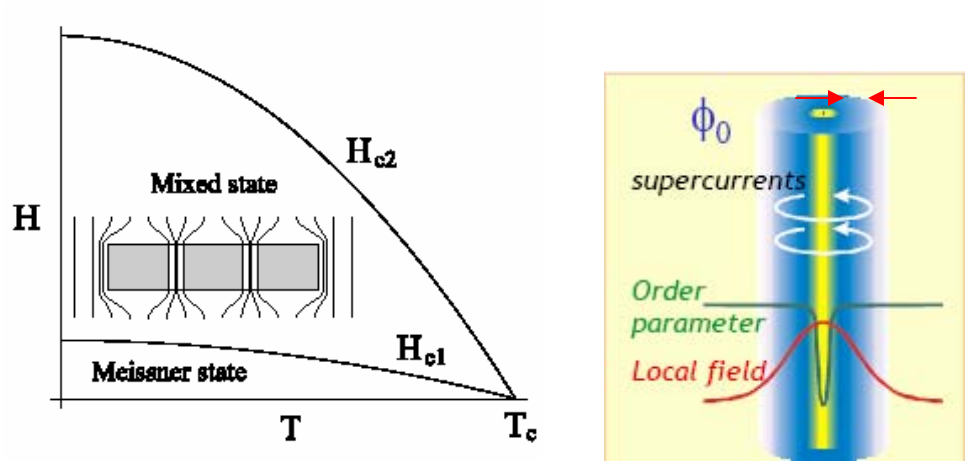

Figure 3 The simple phase diagram of a type-II superconductor. The magnetic field is expelled from the superconductor by supercurrents circulating at the sample edges when the applied field is below the lower critical field H_{c1}. Flux lines will enter the sample above H_{c1} and the cores of the flux lines are overlapping completely at the upper critical field H_{c2} leaving no space for superconductivity in the sample.

A second type of vortices is caused by high anisotropy in high temperature oxide superconductor (HTSC) materials. HTSC materials are characterized with high λ values and low ξ. Small coherence length causes reduction in the pinning energy while the high values of penetration depth soften the flux line lattice (FLL). To complicate the matters further, the layered highly anisotropic structure of HTSC causes formation of two additional vortex configurations. HTSC structures are best described as having sequential distribution of conducting (Cu-O) and insulating layers. As a flux line penetrates HTSC, the vortex can be best illustrated as a string being built of two-dimensional “pancake vortices” (2D) in the superconducting Cu-O layers. The 2D vortices couple over a distance ***s*** between neighboring layers through Josephson coupling. The interaction of 2D vortices in adjacent Cu-O layers is attractive, while they repel within the same conductive layer. In low anisotropy

materials, strong coupling within the 2D assembly, depicts behavior of an Abrikosov flux line (rigid vortex). Weak coupling makes the flux line flexible and allows dissolution (melting) into independent 2D pancake vortices.

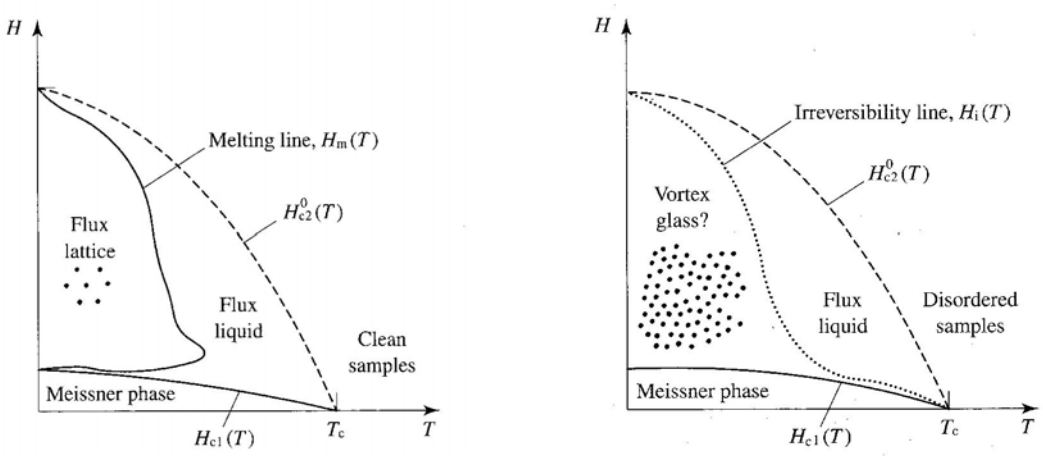

Figure 4 Realistic phase diagram of a type-II superconductor for Clean and Highly disordered high T_c superconductor. [12]

Yet another type of flux line, forming parallel to the CuO layers, are Josephson vortices. Josephson vortex cores lie between two layers, where the superconducting order parameter is reduced or zero. Josephson vortices, exists in a Josephson junctions, formed by a sandwich of two superconducting layers and a thin insulating layer, through which electrons in the form of Cooper pairs can tunnel coherently.

The current applicability of superconductors is mainly dictated by high critical current densities at elevated temperatures and magnetic fields (i.e. T>30K H>1T). The realization of this application for high temperature superconductors could be best achieved through effective pinning of flux vortices.

1.3 CRYSTAL STRUCTURE OF BI-2212.

Upon the initial 1987 discovery of superconductivity in Bi-Sr-Cu-O system by the Raveau group [15, 16] with critical temperature reaching 22K, Maeda's group's further research led to the discovery of a new series of superconductors [17] having the generic formula $Bi_2Sr_2Ca_nCu_{n+1}O_{8+\delta}$ n = 0, 1, 2. The resistivity results interpretation allowed possibility that the new superconductor consists of at least two superconducting phases (Maeda's initial stoichiometry corresponded to Bi:Sr:Ca:Cu –1:1:1:2). Single-phase materials were subsequently refined and identified as $Bi_2Sr_2CuO_{6+\delta}$ (Bi-2201), $Bi_2Sr_2CaCu_2O_{8+\delta}$ (Bi-2212) and $Bi_2Sr_2Ca_2Cu_3O_{10+\delta}$ with critical temperatures of 20, 80 and 110K, respectively.

The crystal structure of Bi-2212 shown in Figure 5 demonstrates one of several possible crystal models. Unlike the $YBa_2Cu_3O_{7-x}$ (YBCO) crystal structure where the reported structure, cation stoichiometry and lattice parameters are in agreement, the BSCCO crystal systems definition poses several challenges. Bismuth cuprate superconductors form solid solutions (further discussed for the case of Bi-2212 in the following chapters), which along with intrinsic nonstoichiometry on both cation and oxygen sub-lattice make the structure determination nontrivial. Several structure models were proposed, differing in space group, lattice constants and position of the oxygen atoms. X-ray diffraction (XRD) coupled with Rietwald refinement is a common method for the structure determination, though the use of neutron diffraction and high-resolution electron diffraction (HRTEM) had also been reported. Different symmetries discussed in the literature for the orthorhombic,

pseudo-tetragonal and even monoclinic (Cc) structure of Bi2212 are I4/mmm (a=3.814, c=30.52 Å) [24, 25, 26], Fmmm [18], Amma [21, 22, 27], A2aa [18]. The two latter designations assume arrangement of oxygen ions along the a-b axis. In general the basic structure is considered to be orthorhombic with lattice vectors a and b ~ 5.4 Å and c ~ 30.9 Å with the space group Cccm.

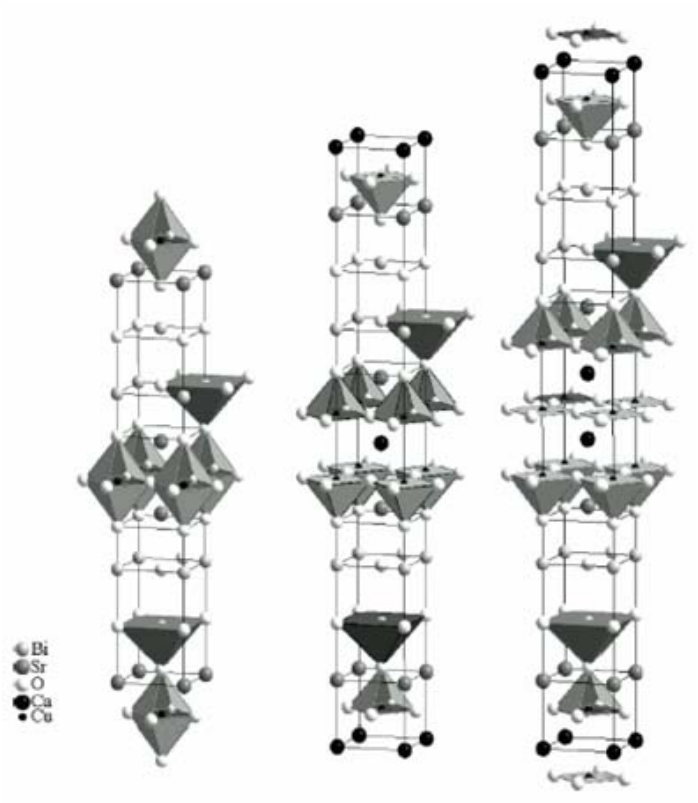

Figure 5 Crystal structures of $Bi_2Sr_2Ca_nCu_{n+1}O_{8+\delta}$ *with* n = 0, 1, 2

All bismuth-cuprate superconducting structures can generally be described as being built from oxygen deficient perovskite layers [$Sr_2CaCu_2O_6$] with intergrowths of NaCl-type $(BiO_y)_2$ double layers. Calcium and strontium ions are located between Cu-O square pyramids. The position of the Ca ions at the cell center has the same polyhedral environment as Y (RE) within the YBCO crystal structure, sharing edges

with eight CuO_5 pyramids and faces with two Sr polyhedra. Strontium ions are positioned similar to Ba in (YBCO); however, Sr is nine-coordinated, leaving large pyramidal sites that are occupied by bismuth. The Bi-O double layers are displaced with respect to each other creating an incomensature modulated structure. The characteristic feature of all cuprate superconductors can also be seen in Bi-2212, the presence of Cu-O planes as well as atypical copper valance (2.33 in YBCO, 2.15-2.6 BSCCO).

To complicate the structure determination further, bismuth based superconductors have a common characteristic, analysis of the diffraction patterns shows additional diffraction spots – usually referred as satellites. Despite the fact that additional diffraction spots (usually weaker than the main reflections) are constantly spaced, indexing in the standard 3-dimensional reciprocal space cannot be performed by using only three reciprocal vectors. One or more additional vectors are needed to index all diffraction spots. The direct consequence is that the diffraction pattern can no longer represent a three-dimensional lattice and the basic property of the crystal translation symmetry is violated. Although the existence of modulated structures in PbO or Na_2CO_3 were known before the discovery of bismuth based superconductors modulation-property relationships were given little attention. Recent discoveries of organic conductors and high temperature Bi based superconductors spurred investigation of modulations in crystals.

Structural analysis of modulated crystals is based on theoretical work of P.M. de Wolff, A.Janner and T.Janssen [31] that had developed a superspace description of multidimensional modulations in crystals. Observed modulation displacements

can involve atomic positions (displacive modulation, [32]), temperature factors, site occupancies (occupational modulation), spin density or combinations of these. It is interesting to note that the recent articles [33, 34] relate superconductivity of the high temperature cuprates to the incommensurability of charge modulation in the Cu–O layers. In a crystal with *n* independent modulation waves, (3+n) - dimensional superspace should be used. Undoped bismuth-based superconductors show only a one-dimensional displacive modulation, however Bi substitution by Pb leads to the observation of two modulation vectors.

The cause of the observed modulation in BSCCO structures is not currently resolved. A majority of the literature relates the modulation to the extra oxygen atoms being inserted into the Bi - O plane, however modulations were also observed in Sr cuprates. [35] It has been proposed that additional oxygen atom(s) expand the Bi – Bi bond length and create Bi rich and Bi poor regions that alternate along one of the shorter axis. Lattice mismatch between the perovskite and the NaCl sublattices has also been proposed as the source of the both modulation and additional oxygen within the structure. In a sense that the perovskite structure yields an average orthorhombic structure with typical Cu^{2+}-O distance of 1.9 Å . Since the typical Bi^{3+}-O bond length is on the order of 2.0–2.5 Å these are not compatible, and consequently Bi-O layers forms an incommensurate structure.

1.4 APPLICATION OF THE SUPERSPACE APPROACH

The Description of the regular (unmodulated) space is represented by:

$$\mathbf{Q} = h\mathbf{a}^* + kb^* + lc^*$$

where $\mathbf{a}^*, b^* and\ c^*$ define the basic lattice vectors in reciprocal space

A modulation wave is defined in reciprocal space by a "wave vector" **q**:

$$\mathbf{q} = q_1\mathbf{a}^* + q_2 b^* + q_3 c^*$$

q is a modulation vector in the a, b or c directions. If the coefficients q_1, q_2 and q_3 are rational the structure is commensurate, that is, the modulation vector(s) is(are) commensurate with the underlying crystal lattice. In the case that at least one of the coefficients q_1, q_2 and q_3, is irrational the structure is incommensurate. The modulation wavelength, $\lambda = \frac{1}{|q|}$, is incommensurate with the basis lattice in that direction.

The scattering vector **Q** in a modulated crystal is the sum of the scattering vector **H**, defined by (*h; k; l*) in the basic lattice and a multiple of the wave vector **q**:

$$\mathbf{Q} = ha^* + kb^* + lc^* + m\mathbf{q} = \mathbf{H} + m\mathbf{q}$$

Reflections with $m = 0$ refers to the main reflection(s); reflections with $m \neq 0$ is referred to as an m^{th} order satellite reflection. In Bi-2212 superconductors, a one-dimensionally incommensurate modulated crystal structure can be identified by four indices: *h; k; l and m*.

1.5 CLASSIFICATION OF DEFECTS

Basic crystal structures are usually defined as periodic arrangement of atoms in space under the provision that local deviation from regularity is possible in the areas defined as lattice defects. An ideal description of the crystal structure is contingent on the movement of atoms around their equilibrium positions with the frequency and amplitude as a function of interatomic forces and temperature. Lattice defects are broadly classified based on their dimensionality as point defects, line defects (1D) and planar defects (2D). In real crystals defects occur frequently and strongly influence diffusion, electrical, magnetic and other properties of materials.

1.5.1 Point defects

Point defects are generally considered as lattice defects of the zero dimensionality. In the crystal lattice, defects are formed as a result of removing an atom from it's crystallographic position, thus forming a vacancy or placing an atom into crystallographicaly inappropriate position. Depending on whether the defects involve one or more types of species they can be vacancies, self-interstitial atoms, interstitial impurity atoms or substitutional atoms. Formation of point defects increases thermodynamic stability of materials due to the increase in configurational entropy. The influence of point defects on superconducting properties was observed and documented in early stages of superconductor development [1, 2, 3]. Specifically, studies in Nb – Ta system (Tc = 10 - 18K) [36] showed difference between well-annealed (no defects) and drawn wires (Figure 6).

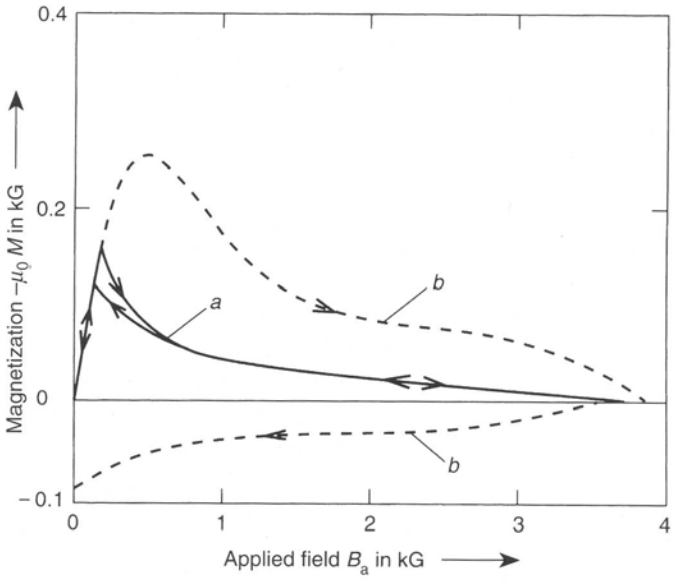

Figure 6 Magnetization of un-deformed (a) and deformed (b) type II Ta-Nb superconductor measured at 4.2 K [1]

The magnetization data of the samples with higher defect concentration exhibited much higher magnetization (B_{c1}), which indicates that higher applied magnetic fields are necessary for the nucleation of vortices. In addition, the width of magnetic hysteresis loops indicates that the critical current density is much higher in the imperfect material. In cuprate superconductors, lowering the oxygen content from the fully oxygenated $YBa_2Cu_3O_x$ (x= 7 to 6.5) results in orthorhombic - tetragonal transition with ordering along Cu-O chains. The lattice symmetry change had been confirmed by neutron diffraction, XRD and HRTEM measurements. Counterintuitively, the influence of ordering on the oxygen sublattice with respect to pinning properties in YBCO materials is detrimental [37] and in the BSCCO systems remains controversial (experimental [47, 48, 49] vs. theoretical [50])

The presumption that additional oxygen incorporates in Bi-2212 as an interstitial O^{2-} leads to the formation of electron holes h^{*}. Using the Kröger - Vink notation this can be written as:

$$\frac{1}{2}O_2 \rightarrow O_i^{//} + 2h^{\bullet}$$

where O''_I is an oxygen interstitial occupying () position. Invoking the mass action law:

$$K_1 = \frac{[O_i^{//}][h^{\bullet}]^2}{p_{O_2}^{1/2}}$$

As in the case of YBCO the defect structure can be thought of as anti-Frenkel type:

$$\frac{1}{2}O_2 + V_i \leftrightarrow O_i^{//} + 2h^{\bullet}$$

$$O_i^{//} + 2h^{\bullet} \leftrightarrow O_i^{/} + h^{\bullet} \leftrightarrow O_i^{x}$$

where

$$[O_i^{x}] >> [O_i^{/}] >> [O_i^{//}]$$

and

$$[h^{\bullet}] + [Y_{Ba}^{\bullet}] = [O_i^{/}]$$

1.6 DEFECTS AND PINNING

Pinning of flux lines represents the fundamental problem in the development and technical application of high T_c superconductors. While pinning in YBCO (Y-123, Y-124, Y-247) type materials is generally good and can be further improved with substitution of Y with RE, the intrinsic pinning in BSCCO systems is generally regarded as poor and limits the application to temperatures below 30K.

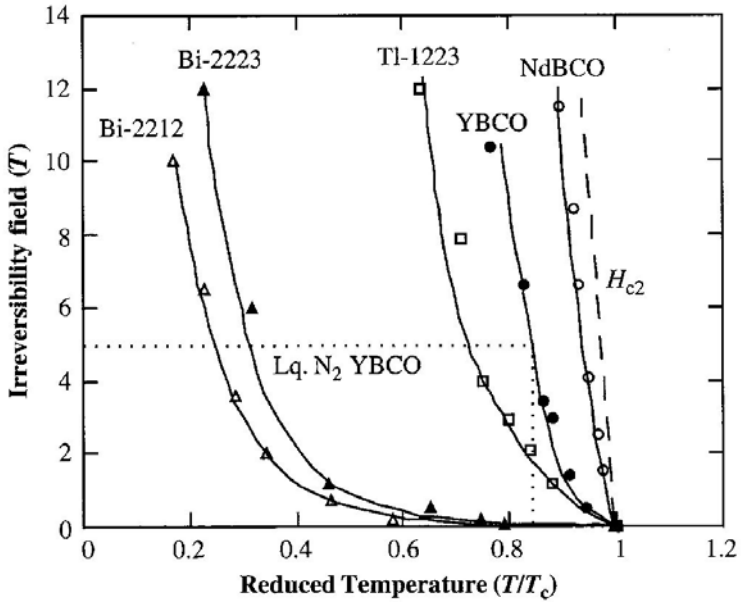

Figure 7 Experimental diagram of irreversibility field versus reduced temperature for several HTSC. The most applicable material is Nd-Ba-Cu-O that shows high values of irrevisibility field. [12]

According to the literature [38-43] vortex–pinning site interactions can be broadly divided into three groups

- Pinning due to scattering of the electron mean free path
- Pinning due to spatial scattering of T_c

- Pinning due to magnetic interaction between flux vortices and defects

The anisotropy of high temperature superconductors strongly influences pinning properties. This is best seen if comparison between YBCO and BSCCO is made (see Table 1). In the case of YBCO, flux vortices could be regarded as flexible tubes threading through the material (similar to dislocations) while in the case of BSCCO systems they are considered to be confined to Cu-O planes weakly paired over insulating blocks via Josephson coupling [44].

Table 1 Comparison of critical parameters of Bi-2212 and Y-123 superconductors

Symbol	Bi-2212 *	Y-123 *	
Tc [K]	75-96	90-92	Critical temperature
λ_{a-b} [nm]	300-500	36-800	Magnetic penetration depth along a-b
λ_c [nm]	16000	125-2600	Magnetic penetration depth along c
ξ_{a-b} [nm]	1.42-1.8	1.2-12.9	Coherence length a-b direction
ξ_c [nm]		0.09-4	Coherence length a-b direction
H_{C1} [mT]	6.3-85	23-95	Lower critical magnetic field
H_{C2} [T]	36-542	3-340	Upper critical magnetic field

- Literature data disagree on the absolute values of critical parameters, the values differ based on the method used as well as the stoichiometry [45, 48, 49]

Higher coherence length in YBCO type materials, allows introduction of 3D defects in the form of precipitates as a means of increasing pinning properties. Y_2BaCuO_5 or $REBaCuO_5$ type particles (211) along with plane and line defects (ion tracks, twin boundaries, screw dislocations) are proven to increase critical current densities in thin-film, melt-textured and bulk YBCO type materials. While fine dispersions of MgO and $SrZrO_2$ had shown similar type of effects in BSCCO type materials, creation of point defects (partial substitution of Bi^{3+} by Pb^{2+}, oxygen vacancies) as pinning centers have shown to be more suitable [47-49]. Substitution

of Pb had shown to lower the extra oxygen content, stabilizing the crystal structure. However the best pinning centers had been proven to be amorphous columnar defects formed through ionic irradiation of BSCCO type materials. The lateral size of defects is on the length scale of coherence length, that is the radius of the vortex, which shows excellent pinning characteristics. Figure 8

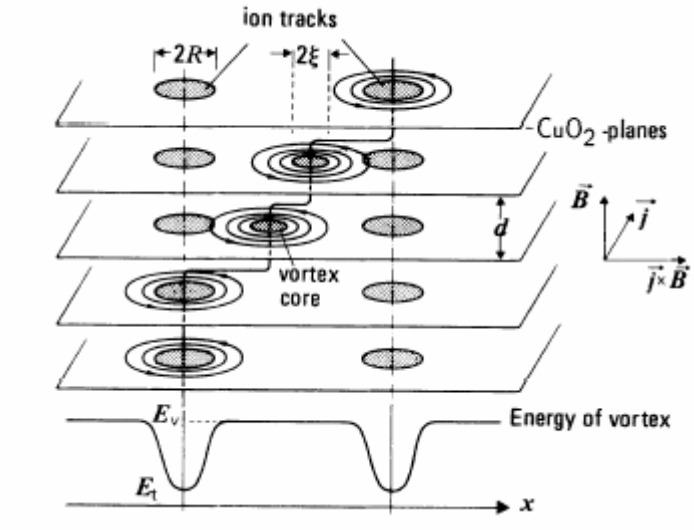

Figure 8 Schematic of the vortex pinning on the ion track threading through Cu-O planes [46]

Study of point defects and their influence on critical parameters (J_c, H_{irr}) has not been fully investigated. Point defects, as a result of intrinsic nonstoichiometry or substitution, as previously noted are of the appropriate scale to pin the flux vortices. Looking at the Figure 7 it can be observed that for the case of the full Nd^{+3} substitution on Y^{+3} sites, irreversibility field is shifted towards higher temperatures, indicating higher stability of flux lattice and consequently higher application temperatures. Study of point defects is also important for the possibility of developing Kroger-Vink diagrams that allow quantification of the influence of

different annealing schedules as well as behavior and interaction of charge carriers. Baetzold and Islam [51-62], as a notable exception, investigated the Y-123 structure using molecular-mechanics calculations, they determined the Y-123 defect energies as a function of intrinsic nonstoichiometry and doping; unfortunately no relation to pinning properties was given. For the case of the Bi-2212 system, which is significantly more complex, only one article describes the energetics of point defects [63].

1.7 PHASE RELATIONSHIPS IN BI-2212 SYSTEM

The discovery of superconductivity in bismuth cuprates prompted feverous research in defining the phase fields containing the single phase Bi-2212 composition [15, 141]. As early as 1988 papers published by AT&T Bell labs [77] investigated the presence of single-phase solid solution in $Bi_2Sr_{3-x}Ca_xCu_2O_{8+\delta}$ (range $0.8 \leq x \leq 2.2$) and found the single-phase region for $1.25 \leq x \leq 1.75$. The material was synthesized from spray-dried nitrates in air at temperatures of 840 - 885^0C. Other research followed and considered possible phase relationships in the $BiO_{1.5}$-SrO-CaO-CuO systems. The investigated phase diagrams generally considered samples synthesized in air, at temperatures of 800 - 900^0C. The influence of CO_2 in the furnace atmosphere was also investigated [99] along with other phase relationships.

Several groups [80-82, 84, 86-88, 94, 99, 108, 116, 123, 126, 131-138,] published detailed, elaborate, descriptions of both the experiments as well as the

starting and final compositions considering all four cations. However, the reported zone of existence of the single-phase material varied. The single phase superconducting region is in intimate relationship with the substitution level and/or intrinsic cation nonstoichiometry (i.e. Pb_{Bi}, Ca_{Sr}, Ag addition, etc) as well as the annealing conditions (temperature, oxygen partial pressure, heat treatment schedule) and possibly the synthesis routes. There is still no general agreement, however, on whether the stoichiometric Bi-2212 lies outside the three-dimensional quaternary phase field for the samples synthesized in air. Research performed by our group indicate that creating single phase Bi-2212 is possible, even in air, if the proper synthesis technique is employed, that is, through utilizing the freeze-drying synthesis method. The initial precursor is formed through the aqueous solution, which upon freeze-drying results in random, uniform distribution of cations. Intimate mixing of cations and short annealing times compared to solid-state technique could be responsible for this observation.

Phase purity of Bi-2212 system is still not understood fully. National Institute of Standards (NIST) researchers investigated the stability of Bi-2212 as a function of oxygen partial pressure as well as silver addition. Their recent paper [138] gives an overview of the current knowledge of the $BiO_{1.5}$-SrO-CaO-CuO system and contributed several additional data points.

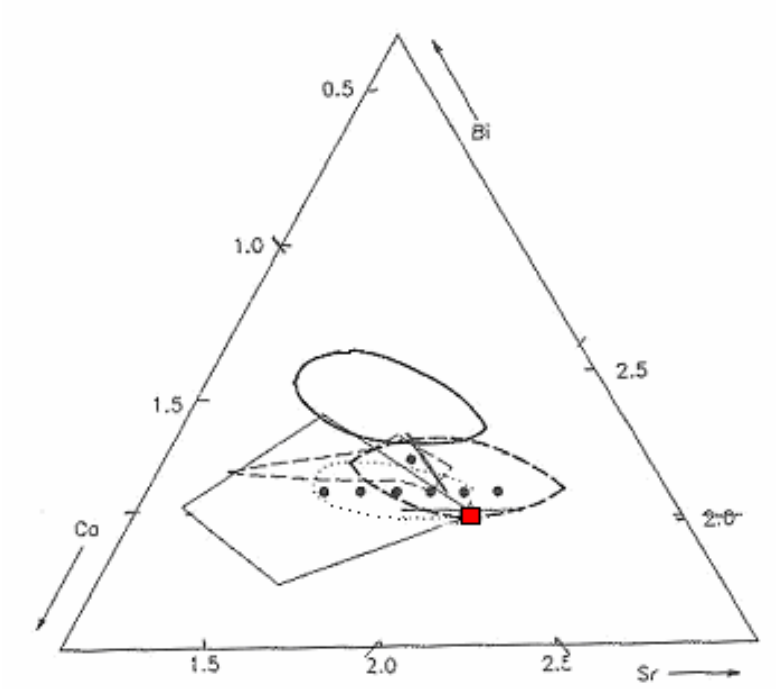

Figure 9. 2212 Solid solution boundaries reported by various investigators. The red square indicates stoichiometric $Bi_2Sr_2Ca_1Cu_2O_{8+\delta}$. [81, 138]

Though plotted data in Figure 9 should not be analyzed casually, since it represents data measured at different temperatures (T=830-865^{0}C) and oxygen partial pressures (p_{O2} = 0.21 and 1 atm), it nevertheless illustrates how challenging is to determine the region of stability in this quaternary system. Looking at the ternary diagram, with the data overlay, it can be concluded that the stoichiometric Bi-2212 composition lays on the boundary of the single-phase field. It is interesting to note that the reported phase pure materials obtained from the starting stoichiometric mixtures were synthesized through wet chemical methods. The addition of silver (Ag), which is commonly used as the sheath material, was found to decrease melting point of Bi-2212 by 4 - 30^{0}C, through the formation of an eutectic with ~4% Ag [138]. A range of temperatures is given due to different Bi-2212 cation

compositions, that have melting temperatures ranging from 825^0C for bismuth rich-copper poor ($Bi_{2.92}Sr_{1.13}Ca_{1.56}Cu_{1.39}O_{8+\delta}$) to 890^0C for copper rich samples ($Bi_{1.88}Sr_{1.73}Ca_{1.23}Cu_{2.16}O_{8+\delta}$) without Ag addition. The 2212 phase field was given by the analytical formula describing a complex hull:

$$0.3101x+0.4853x^2–0.8236x^3+1.1898y–2.1062xy+0.1414x^2y–0.8026y^2 +2.8833xy^2–1.5012y^3+1.2362z–0.0849xz–1.4659x^2z–1.9282yz+1.2505xyz– 3.085y^2z–3.1529z^2+1.2203xz^2+1.6967yz^2-2.3490z^3 = 0.2634$$

Equation 9

where *x* represents the mole fraction of CuO, *y* mole fraction of CaO and *z* mole fraction of SrO. *Equation 9* is applicable within the limits: $0.19 < x < 0.43$; $0.02 < y < 0.27$; $0.06 < z < 0.34$.

It has been also suggested [90, 112, 127, 128] that different cation compositions, forming a single-phase pure volume, have unique charge carrier concentrations and, accordingly, distinct critical superconducting temperatures (Figure 10).

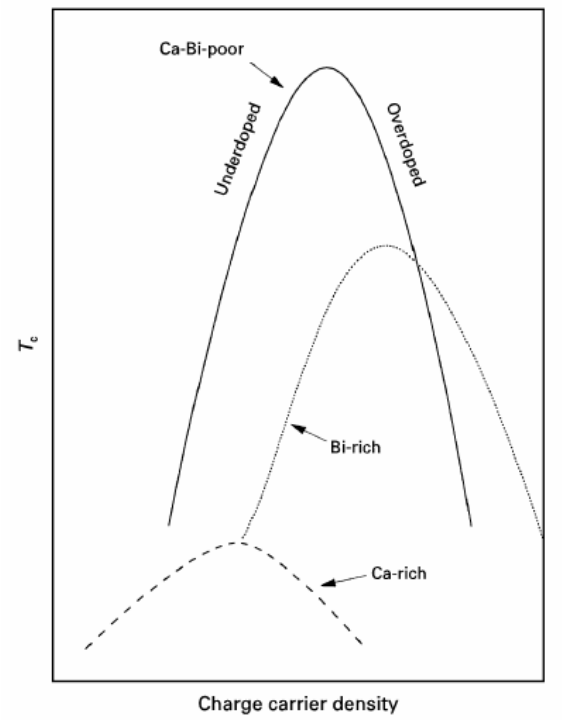

Figure 10. Schematic representation of the correlation between Tc and the charge carrier concentration [136]

Majewski described a nonlinear relationship between charge carrier concentration and the critical temperature for Ca - Bi poor and Bi, Ca rich single-phase regions [136]. As a result, investigation of substitution (doping) effect resulting in the change of pinning properties represents a complex analysis task unless the proper starting and finishing stoichiometries are known.

Majewski suggests that only three superconducting phases exist within the quaternary field [82, 84], those belonging to the $Bi_2Sr_{3-x}Ca_{n-1}Cu_nO_{8+\delta}$ n = 1, 2, 3 series. However, a recent paper [137] discusses the existence of superconductivity in $Bi_2Sr_3Cu_2O_{8+\delta}$ up to 85K.

The reported zone of existence varies from author to author. Knizek [102] suggested that the single-phase composition defined as $Bi_2Sr_{2.9-x}Ca_xCu_2O_{8+\delta}$ cannot be obtained, though within the Ca-rich range ($1.1 \leq x \leq 1.3$) and Sr-rich range ($0.8 \leq x \leq 1.0$) Bi-2212 predominates. The superconducting critical temperature varies from 90 - 85K for resistivity ρ = 2.63-1.85 mΩ cm (x = 0.8-1.3) measured for the polycrystalline sample by a four-probe method. (Figure 11). Under the same substitution conditions the crystal structure also changed such that both the a and c axes are reduced from 5.405 to 5.399 Å and 30.82 to 30.67 Å, respectively.

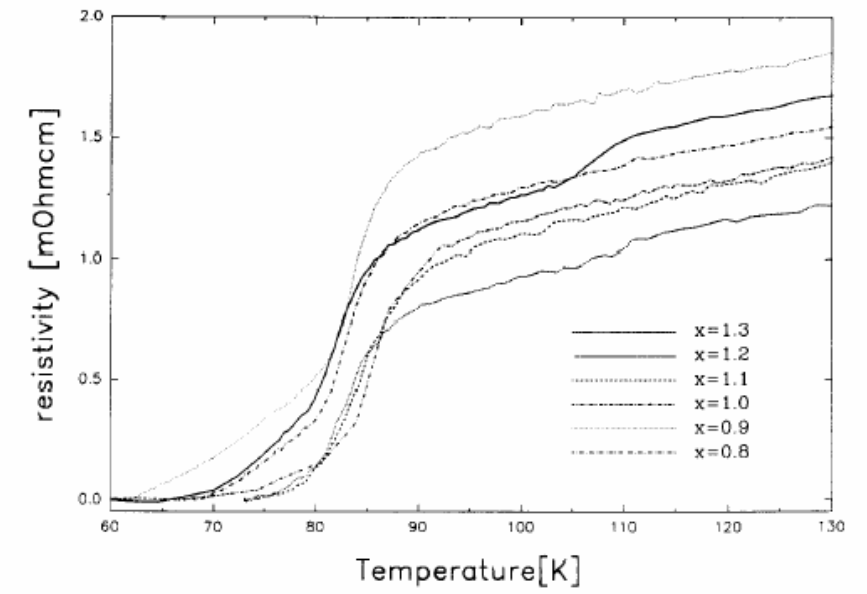

Figure 11. Resistivity vs temperature dependences in $Bi_2Sr_{2.9-x}Ca_xCu_2O_{8+\delta}$ (x = 0.8-1.3) [102]

It is interesting to note that in Knizek's paper the reported lowering in both resistivity and critical temperature follows a decrease in layer spacing.

Although cross substitution of cations had been widely investigated, the main focus has been on the effect of Sr_{Ca} as well as Ca_{Sr} substitution. Idemoto et al. [112]

considered the possibility of cross substitution of all four cations at varying temperatures for Bi-2212 and Bi-2201 systems in air. Phase purity at different temperatures (820-850^{0}C), cation defects, crystal lattice modification as well as densities were determined through combined use of XRD, iodometric titration and pycnometric analysis. Phase purity fields are represented in Figure 12 in the form of the overlaid ternary diagrams at different temperatures.

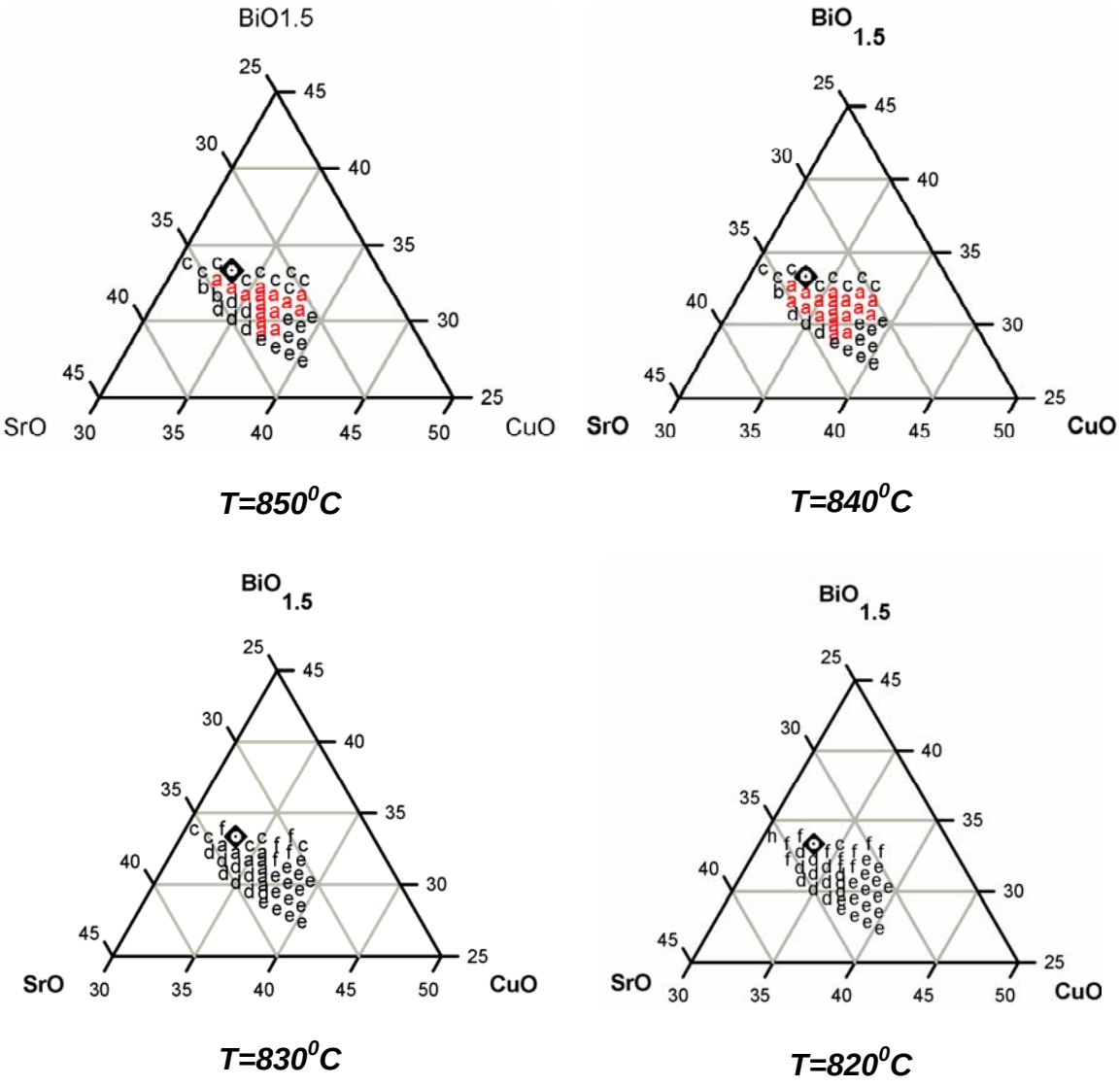

Figure 12 Phase diagrams of the $BiO_{1.5}$-SrO-CuO system (850, 840, 830 and 820°C; 14.0 mol.% CaO) the zone labeled a represents the Bi-2212 without impurity phases present, zones labeled b, c, d, e and f represent Bi-2212 with different impurities present. Stoichiometric composition Bi:Sr:Ca:Cu=2:2:1:2 is labeled with ◘ [112]

1.8 INFLUENCE OF DOPING

1.8.1 Ca Substitution

Within the BSCCO crystal structure, calcium ions occupy similar position as the Y within the YBCO structure, that is, they represent a “spacer” between two Cu-O adjacent layers. Octahedraly coordinated Ca^{2+} with ionic radius r_i~1.12 Å according to Shannon [74] shows good correspondence of ionic radii with Y, Sr and the lanthanide series of elements (La, Ce..Yb) and hence a good choice for the substitution studies. The largest number of research papers explores the consequences of Y and Sr substitution on Ca sites. Full substitution of Y, as well as the lanthanide series elements [146, 147, 149, 151, 153, 157, 158, 160, 165, 171, 173, 176, 180] is possible with the formation of an antiferomagnetic insulator for substitution levels higher than 60% [144, 149, 152, 180]. Substitution of a +3 RE ion for the +2 Ca ion contributes to incorporation of additional oxygen within the structure, which, leads to a lowering of mobile holes (p) as charge carriers and an increase of Tc for the overdoped material. Additional consequences are represented by the decrease in c-axis length, and increase in the a, b axes leading to a lower overall anisotropy of the structure. This suggests that the addition of RE might increase the Josephson coupling between the parallel Cu-O planes and consequently between 2D vortices.

The substitution effects of rare earths on lattice parameters are best summarized in Figure 13. [153] Similar to $REBa_2C_3O_7$ (RBCO) the c axis is shortened, which in RBCO is followed by an increase in upper critical field, lowering

of the penetration depth, and an increase in coherence length [142]. These effects of RE substitutions have not been investigated in the BSCCO system except for Y substitution by Villard [198, 200]. Insertion of a smaller cation on the Ca sites shows similar effects to quenching from higher temperatures [160]. The renewed interest in RE substitution for Y was mainly spurred by recent articles [182-194] showing significantly increased flux pinning; the enhanced pinning properties are mainly attributed to 211 precipitates.

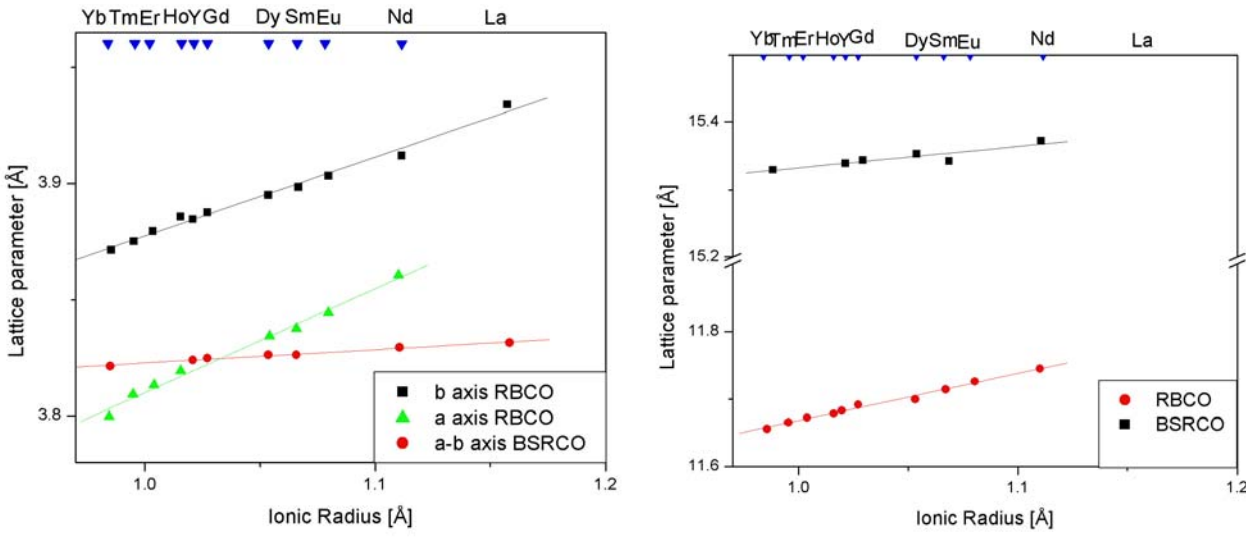

Figure 13 The a-axis length is plotted as a function of rare earth ionic radius by solid circles for $Bi_2Sr_2REC_2O_8$ (BSRCO). Variation of the a and b-axes lengths in RBCO are represented by open and solid triangles, respectively. (b) The c-axis lengths are plotted as a function of rare earth ionic radius - ● BSCCO (c/2 is plotted) and ■, ▲for RBCO [153]

The cause of the increase in flux pining in RBCO is still an open question with the various explanations including the formation of 211 precipitates, Ruderman-

Kittel-Kasuya-Yosida (RKKY) interaction[2], also observed in Nd substituted Bi-2212 [173] etc.

Yoshizaki in one of his early papers [145, 157] investigated the influence on superconducting and magnetic properties in $Bi_2Sr_2(Ca_{1-x}Y_x)Cu_2O_{8+\delta}$ as a function of substitution level. Figure 14 shows the diamagnetic susceptibility for $x \leq 0.3$.

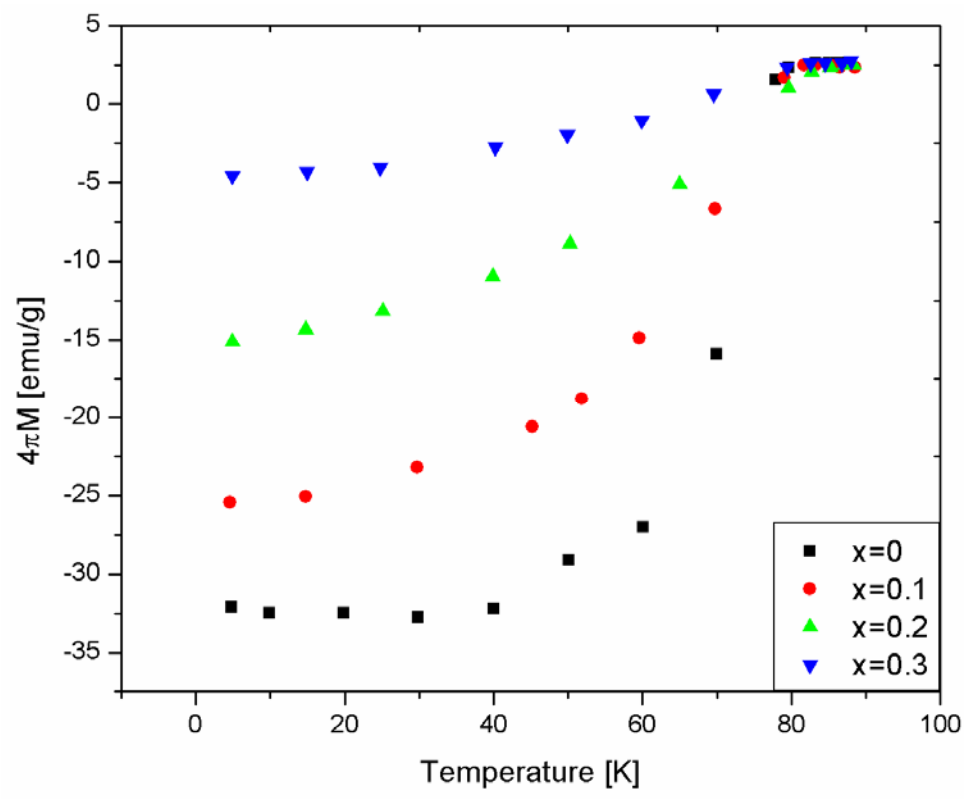

Figure 14. Superconducting diamagnetic susceptibility measured at 10.0mT in the field cooling for polycrystalline samples of $Bi_2Sr_2(Ca_{1-x}Y_x)Cu_2O_{8+\delta}$ x=0-0.3 [145]

As can be seen from Figure 14, there is a small increase in T_C and the author also reports a decrease in superconducting volume deduced from susceptibility data.

[2] RKKY interaction is the indirect exchange interaction between two local spins via the spin polarization of conduction electrons.

Though generally accepted as a measure of superconducting volume, the change in susceptibility, has been also shown to occur with decrease in grain size of the polycrystalline specimen or with increase in pinning.

Oliver [148] contends that substitution of Y^{+3} or Ce^{+4} ions for Ca^{2+} leads to incorporation of extra oxygen into the Bi-O layers, changing the oxygen coordination of Bi^{3+} ions from six to nine. Charge compensation requires that the extra oxygen be compensated by partial reduction of either[3] $Cu^{2.15+}$ or Bi^{3+} or by vacancies on oxygen sites. It is generally observed that the partial substitution of higher valence cations (Ce^{4+}) for Ca induces a faster decrease of charge carriers and that the superconductor-insulator transition occurs at lower substitution levels.

[3] $Cu^{2.15}$ represents the average Cu valence

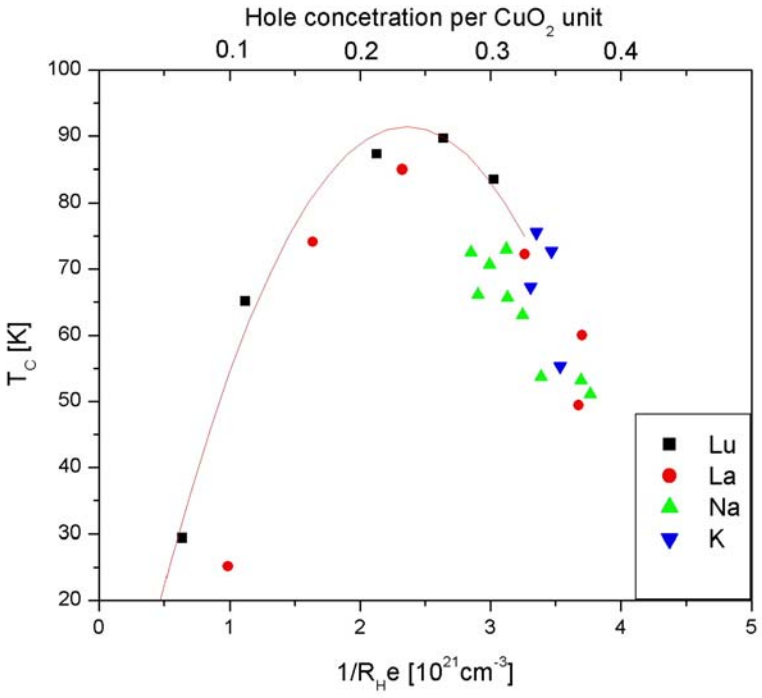

Figure 15. Correlation between Tc and hole concentration $1/R_He$ in the $Bi_2Sr_2Ca_{1-x}Lu_xCu2O_{8+\delta}$; $Bi_2Sr_2Ca_{1-x}Na_xCu_2O_{8+\delta}$; $Bi_2Sr_{2-x}La_xCaCu_2O_{8+\delta}$; and $Bi_2Sr_{2-x}K_xCaCu_2O_{8+\delta}$ systems. Open, half-closed and fully closed symbols correspond to samples made with no additional annealing, with annealing at 600 °C in 1 bar of oxygen, and with annealing at 430°C in 250 bar of oxygen, respectively. [146]

Controlling the hole concentration by different dopants was investigated by Koike [146], Groen [151] and others [159, 160, 164, 165, 171]. It was found that doping destroys antiferomagnetic ordering inducing metal–insulator transition. The maximum Tc in cuprates (La-Sr-Cu-O, YBCO, BSCCO) is generally realized for 0.2-0.3 holes per CuO_2 layer (effective Cu valence of 2.2-2.3), and superconductivity is lost when the concentration of holes drops to 0.07 holes per CuO_2 layer.

Hole concentration through charge compensated samples of $Bi_{2-u}Pb_uSr_{2-x}Ca_{1-y}RE_{x+y}Cu_2O_{8+\delta}$ (u = x; u = y) has also been investigated [156, 158, 160, 162, 167, 203, 208, 210]. The substitution of RE^{3+} that lowers the concentration of mobile

holes is compensated by the introduction of Pb^{+2}. It was determined that RE substitution produced a more favorable ordering of the oxygen within the crystal lattice. Partial substitution of Ca by Y was found to induce more of the 2D type behavior. With increasing Y-substitution level, x, continuous increase in the oxygen content and decrease in the thickness of the SrO-Bi_2O_2-SrO spacer block was observed. The extra oxygen uptake in the structure only partially counteracts the trivalent-Y for divalent-Ca substitution, and consequently the hole concentration in both blocks was found to decrease. The influence of increasing x and oxygen content on H_{irr} was found to be rather ambiguous, it was reported that H_{irr} as well as the pinnining either increases [198, 200, 208] or decreases [210].

1.8.2 Cu Substitution

The five-fold coordination of copper in Bi-2212 superconductor is represented by a square pyramid with similar geometry found in YBCO systems. The three distinct types of Cu-O coordination observed in cuprate superconductors are represented in Figure 16. having planar four fold [(a)-occurring in Bi-2201], square-pyramidal five fold [(b)-Bi-2212; Bi-2223; YBCO)] and octahedral sixfold [(c)-Bi-2223)]. Although similar in coordination, Bi-2212 and YBCO differ in bond length of copper to the apical oxygen. In-plane Cu-O distances in Bi-2212 were reported to be 1.875Å and the apical oxygen was at 2.05Å, while YBCO apical oxygen was at 2.3Å. [75]

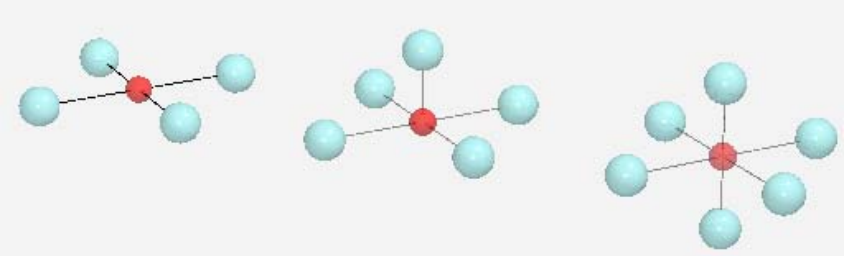

Figure 16. Cu-O coordination polyhedra in BSCCO systems - from the left: a) Bi-2201; b) Bi-2212; c) Bi-2223

Substitution effects of Li and 3-d type elements (Zn, Co, Ni, Ti) for copper (Cu) with an ionic radius r_i = 0.65Å [74] had a direct effect on CuO_2 planes and on the superconducting properties. These dopants had been investigated in terms of superconducting-insulator transitions as well as flux pinning. It is generally observed that the substitution of Li increases the T_c and flux pinning whereas the introduction of more than 10 at% of 3d elements strongly suppresses T_c. Recent results of the

influence of 3d elements on single crystal samples had shown that at small substitutions, (up to 2 at %), fluxon pinning could be strongly enhanced.

A dramatic increase in critical temperature up to 100.9K (magnetization measurement) and superconducting volume percent was reported [211, 235] upon alkaline metal substitution (Li, Na, K, Rb, Cs) without the observation of Bi-2223 (XRD). The XRD patterns showed Bi-2201 and CuO impurity phases present, however.

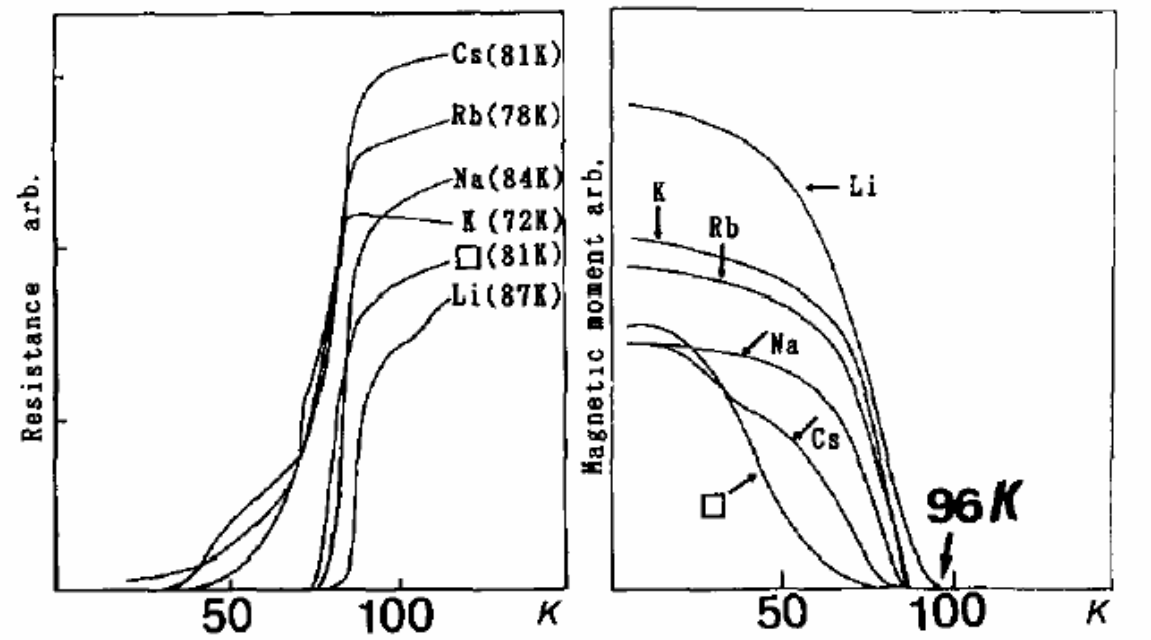

Figure 17. (a) *R-T* curves (T_c mid) and (b) T_c onset-in Meissner effect [211]

Addition of alkaline metals lowers the Bi-2212 melting temperature, for instance Li which has the smallest ionic radii lowers the temperature from approximately 840^0C to 710^0C. Although initially reported synthesis of polyphase mixtures synthesis of single-phase material was reported in later work by the same group. It was observed that the c-axis increase as well as the constant formal

charge of Cu independent of doping level [214]. Interestingly, comparison of the influence of Li partial substitution for Sr and Cu showed similar behavior of doped samples. (Figure 18)

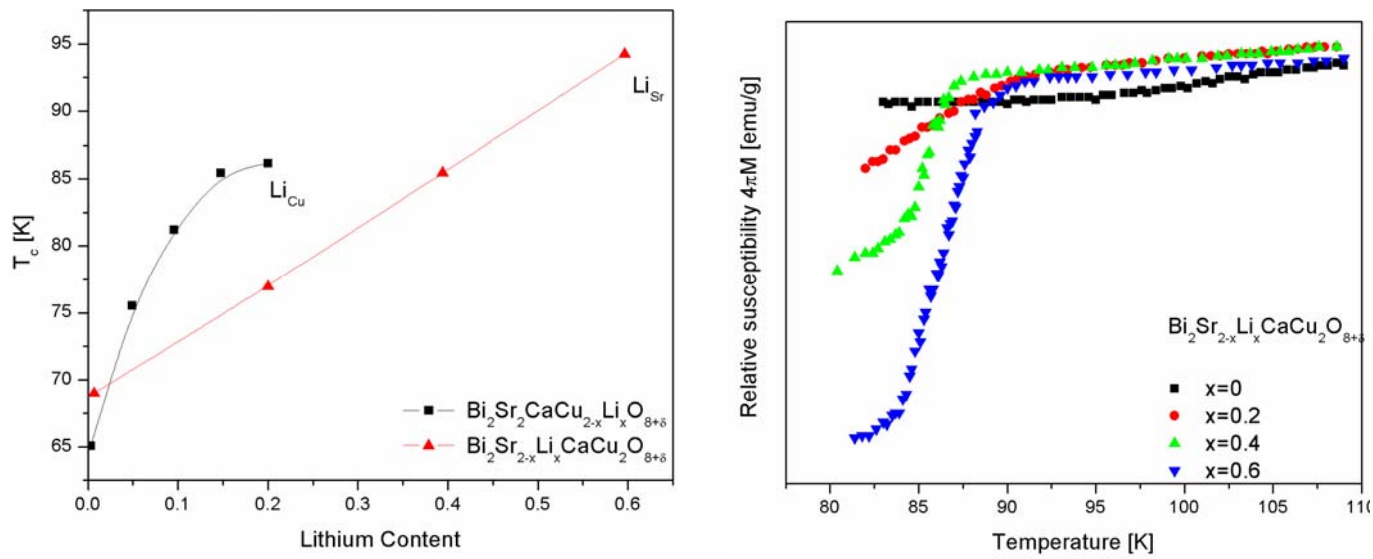

Figure 18 a) Tc's of the superconducting lithium-doped bismuth superconductors vs. the lithium content. ■ T_c's in the Bi-2212 where some Cu ions were replaced by the Li^+ ions; ▲ are the T_c's obtained when some Sr^{2+} ions were replaced by the Li^+ ions.

b) Relative AC susceptibilities of the superconducting $Bi_2Sr_{2-x}Li_xCaCu_2O_{8+\delta}$ series. For x = 0 - 0.6 [219]

Single crystal synthesis confirmed substitution of Li though reported lower critical temperatures were reported (~90-93K) [221, 234] than previously doped polycrystalline samples or electrochemically intercalated samples. [211, 214, 235, 238, 254]

It should be noted, however, that differences exist in the stoichiometry of the polycrystalline materials and single crystals. ($Bi_{2.2}Sr_{1.8}CaCu_{1.2}Li_{0.8}O_{8+\delta}$, T_c = 98K; $Bi_{2.1}Sr_{1.9}CaCu_{1.8}Li_{0.1}O_{8+\delta}$, T_c = 92K)

Soon after the first publication, authors of the initial report of Bi-2212 superconductivity studied the effects of 3d metal partial substitution effects on Cu sites as well as Cu deficiency effects. [212]

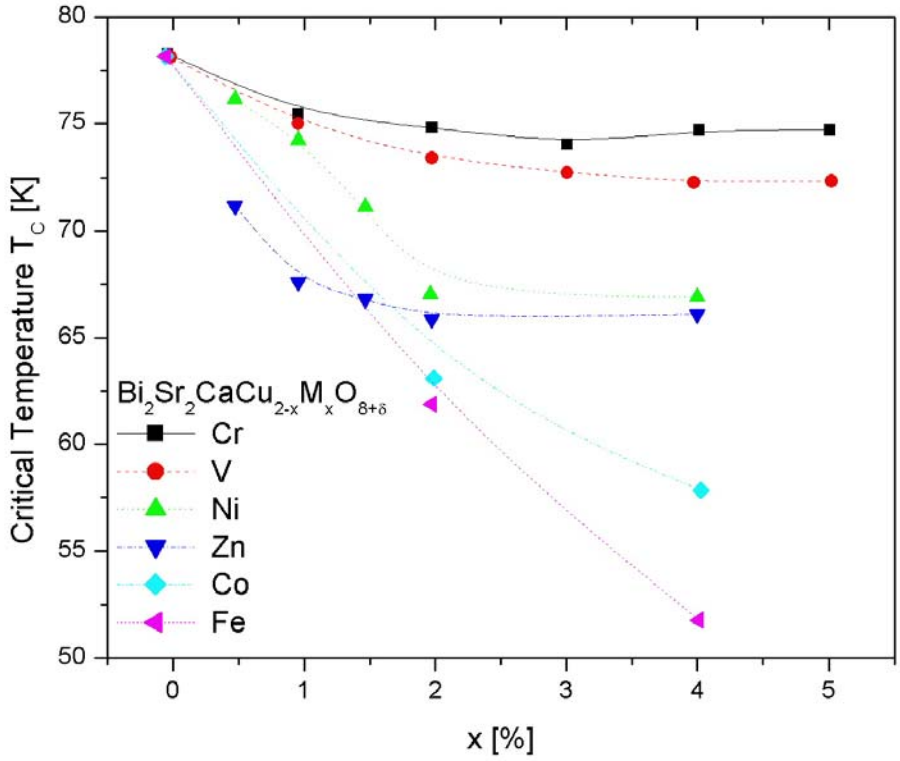

Figure 19. Critical temperature vs. nominal content of some 3d metals. [212, 228]

The largest critical temperature depressions are caused by Fe, Co and Ni, while V, Zn and Cr substitution have a less detrimental effect. The c-axis values decrease linearly with the increased dopant content. As previously noted single-phase material critical temperatures may vary, depending on the definition of the nominal composition. Different authors obtained single phase materials at substitution levels 10% for Fe (T_C = 38K) and Co (T_C = 40K), 2% for V (T_C = 78K),

1.5% for Ni (T_C = 65K) and 1% for Zn and Cr (T_C = 80K). [217, 216, 212, 228, 232, 233]

Contrary to established theoretical and experimental results for type I superconductors where the presence of magnetic impurities depresses T_c, J_c and H_c significantly, magnetization and resistivity measurements in high T_c superconductors showed different behavior. At lower substitution levels (less then 1%) of the 3d elements, an increase in critical current at higher temperatures and the shift of magnetic irreversibility lines towards higher values were observed while higher substitution levels (higher than 2%) led to rapid deterioration of all superconductivity properties, as in type I superconductors. [236, 243, 239, 261, 266, 265]

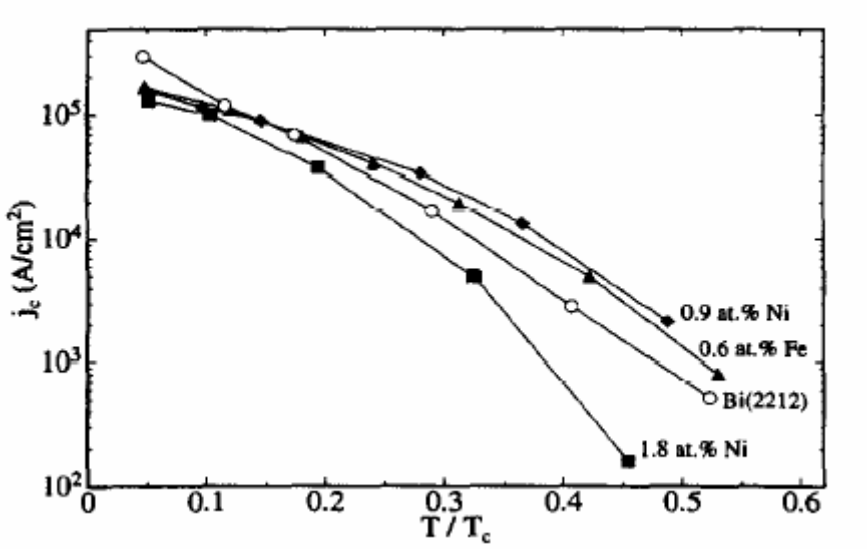

Figure 20. Critical current density in an applied field of 0.2 T versus the reduced temperature T/T_c for pure Bi-(2212) (◙) and Bi-(2212) doped with 0.6 at % Fe (▲), 0.9 at.% Ni (♦), and 1.8 at.% Ni (■). [236]

1.9 SYNTHESIS OF HIGH TEMPERATURE CU SUPERCONDUCTORS

Preparation routes of the polycrystalline superconductor synthesis can be broadly categorized into:

Solid state routes

Aqueous solution based routes

The main advantage of the solid-state route is the convenience of using off the shelf chemicals directly calcined to final products. Local variations in composition, carbon containing grain boundaries, and long reaction times are usually associated with this preparation procedure.

Aqueous solution based routes are more demanding with respect to the control of initial precursor, this is a multi step approach that usually gives superior quality of superconducting powder, based on the atomic scale mixing of initial precursors, higher reactivity, and thus lower synthesis temperatures

1.9.1 Solid State Route

Synthesis basically consists of mixing and grinding appropriate amounts of oxides, carbonates with intermittent calcinations steps that are performed under appropriate oxygen partial pressures and with subsequent annealing.

Solid state synthesis starting with nitrate (hydroxide) precursors has also been described. However, due to the highly hydroscopic nature of the initial raw materials, cation concentrations in the initial precursor mixture cannot be properly controlled. The literature largely describes the oxy-carbonate route of sample

preparation, however, the temperatures and oxygen partial pressures employed often differ. An overview of some of the synthesis conditions are given in the APPENDIX B and C. Synthesis routes for the YBCO and BSCCO systems vary. BSCCO material requires significantly higher repetition of grind–calcine steps, after each grinding step the temperature is increased - up to ~90% of the melting temperature (T_m) which has usually been determined by differential thermal analysis (DTA) and thermo gravimetric analysis (TGA). Higher complexity of BSCCO synthesis is substantiated upon looking at the quaternary phase diagram, having 16 to 20 four-phase equilibrium tetrahedra involving the Bi-2212 phase Figure 21 [92, 99, 129, 138]. Low melting eutectic and congruent melting phases require careful control over a wide range of temperatures and oxygen partial pressures.

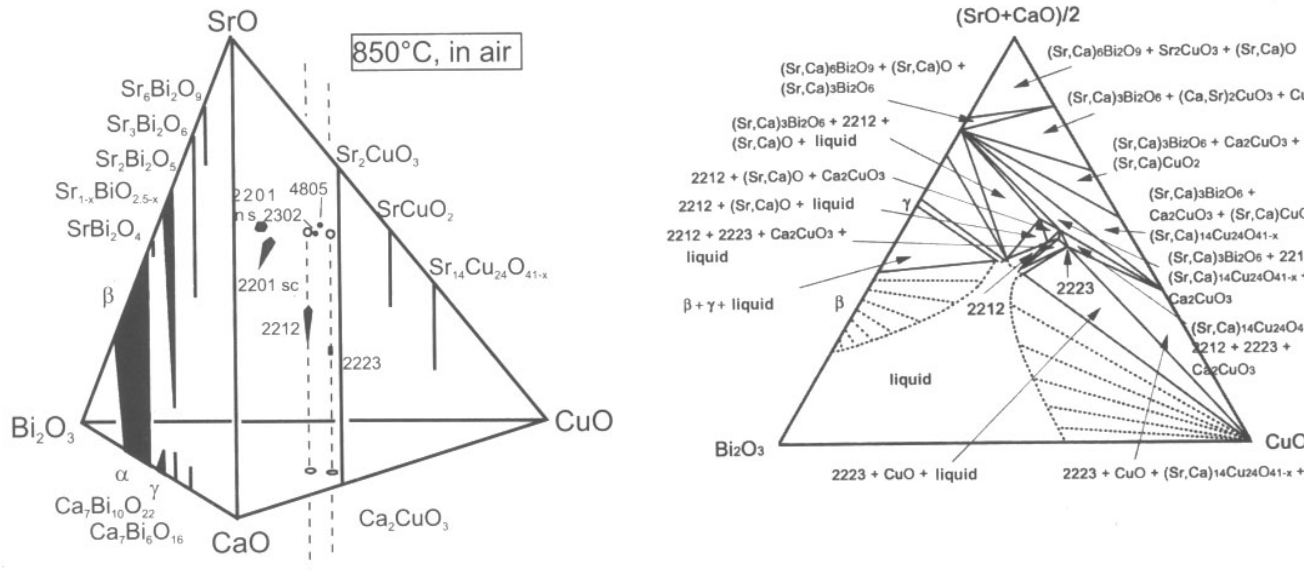

Figure 21 Quaternary phase diagram and pseudoternary section of the Bi-Sr-Ca-Cu-O at 850^{0}C in 21%O_2 according to Majewski [88,89,97,98,106,107,114-118127,128,136]

Decomposition of carbonates and formation of the Bi-2212 phase takes place at calcination temperatures ≥ 725^{0}C (depending on the oxygen partial pressure and stoichiometry). Though the formation of Bi-2212 occurs over the 725 - 850^{0}C temperature range, depending on the exact stoichiometry, reaction at these temperatures is sluggish. The powder mixture is generally exposed to an air environment (p_{O2} = 0.21). Several calcination-grinding steps are usually needed to improve both the homogeneity of the Bi-2212 phase and to reduce the carbon content that severely degrades properties of high-T_c superconductors. (Figure 22)

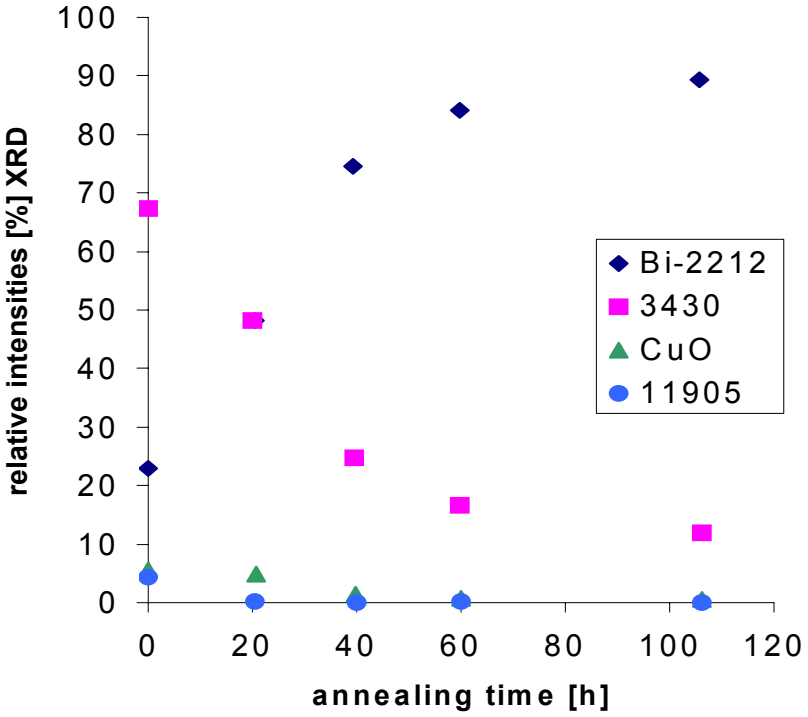

Figure 22. Development of the formation of the 2212 phase (XRD) as a function of the annealing time. ■ $Bi_3Sr_4Ca_3O$ (3430) ●$Bi_{11}Sr_9Cu_5O$ (11905) [92]

1.9.2 Aqueous Solution Based Routes

Preventing contamination of the raw material, allowing low reaction temperatures (due to the volatility of Bi, Tl and Pb cations) and assuring high yield of specific compositions requires processing that should be performed under stringent conditions. These conditions can only be assured by using highly reactive homogeneous, atomically mixed precursors, which are in the form of aqueous solution of metal salts.

The literature describes different routes of superconductor production that follows nitrate solution synthesis:

- Precipitation (hydroxides i.e. NH_4OH, NaOH or oxalates) followed by calcining.
- Formation of a gel followed by calcining
- Flash heating – pyrolisis
- Evaporation of water followed by calcining
- Freeze-drying
- Synthesis of nano-particles through microemulsion

1.9.2.1 Freeze-drying route

Freeze-drying represent a remarkable tool that provides the removal of solvent under controlled condition. By the removal of water, the homogeneity of the initial precursor solution is preserved as well as the atomic mixing of cations. Depending on the procedure by which the liquid precursor is frozen prior to freeze-drying, the final product particle size and shape can be controlled. The high level of

homogeneity allows the growth of fine-grained material at relatively lower calcination temperatures and shorter reaction times than other synthesis routes. Synthesis of mutually immiscible multi-component mixtures is also possible provided that they are dissolvable in a common solvent. Synthesis of oxides as well as metals and alloys had been reported. Tretyakov [288] has published review of conditions and applications associated with freeze-drying.

For the synthesis of perovskites, aqueous nitrate solutions are used as a rule. Owing to the use of nitrate precursors (obtained upon freeze-drying), superconducting materials are created from oxides rather than carbonates which avoids the problems associated with carbon. Our observation is that after only 5 minutes at 95% of the melting temperature Bi-2212 is formed. In principle the use of freeze-drying is a multi step process. The general procedure for obtaining fine powders might be explained relative to a simple flow sheet diagram (Figure 23) in the following way.

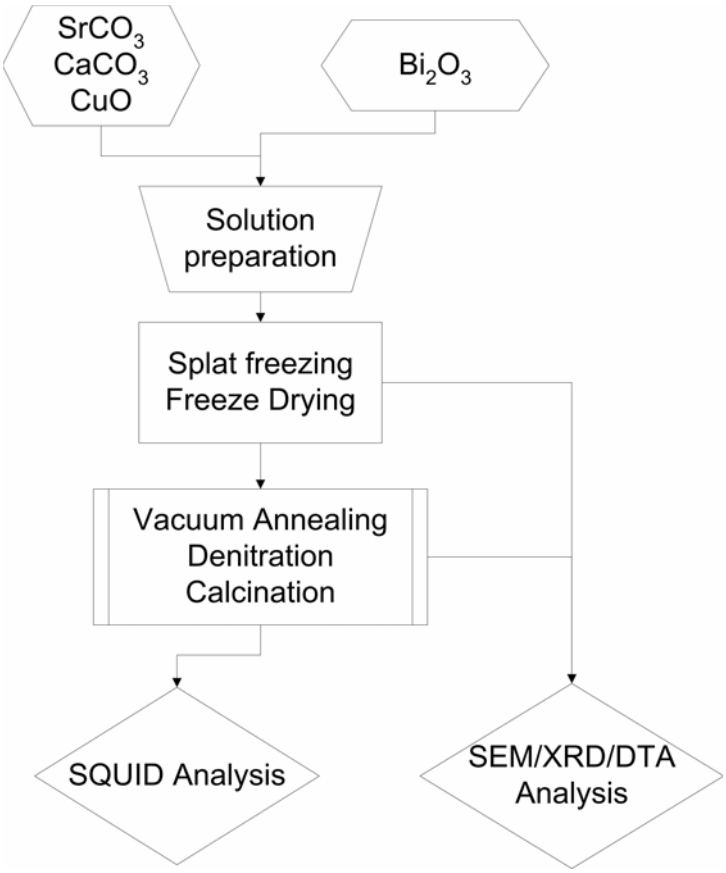

Figure 23 Flow sheet diagram of freeze drying process

Stoichiometric quantities of oxides and/or carbonates are dissolved in a water-nitric acid solution. During solution synthesis careful control over pH the value is required so that all of the material remains in solution without precipitation of hydroxides (i.e. $Bi(OH)_3$). The solution is rapidly frozen from solution preparation temperature (25 - 100^0C). The rapid freezing of the solution serves to preserve the cation mixing on the molecular level; it is therefore preferable to quench the solution rapidly so that amorphous ice is obtained. The rapid freezing step is usually performed through aerosol dispersion of solution into liquid nitrogen or through splat freezing. Creating an aerosol has the advantage of creating uniform, controllable

particle sizes, the drawback is formation an air film around the droplets preventing rapid solidification, as well as low yields. Splat freezing allows faster cooling rates and higher throughput but requires an additional step to pulverize the ice. After the removal of the water solvent through freeze-drying, chemically bound waters of hydration remain; i.e. $Ba(NO_3)_2 \cdot xH_2O$, $Cu(NO_3)_2 \cdot xH_2O$, etc. The waters of hydration need to be removed, since upon an increase of temperature, during the denitration step they inadvertently lead to “melting” of nitrates and demixing (phase separation). To remove chemically bound water and stabilize the precursor the powders are placed into a vacuum furnace and slowly heated to a temperature determined by DTA - TGA (~150 - 200°C for the YBCO, BSCCO system). During drying, the color of the freeze - dried powder changes from pale blue to pale green corresponding to the dehydration reaction, $Cu(NO_3)_2 \cdot xH_2O \rightarrow Cu(NO_3)_2 + Cu(OH)_2$. At this point the precursor preparation is complete. Further steps are similar to the solid-state route; precursor materials can be peletized and flash heated at 80 - 95% of the melting temperature, leading to simultaneous denitration and calcining into a final product. A second possibility is to first denitrate the precursor material at appropriate temperature, (for copper perovskites ~ 600°C) and than peletize and calcine. The use of this approach, implemented through this research, alleviated the removal of fine fraction created during the denitration step which can subsequently be swept away by the flowing gas atmosphere.

Table 2. Freeze-drying synthesis route of Cu based superconducting powders

Initial precursor	Applied technique	Calcination Time[h]/temperature [C]	Atmosphere	Results	Reference
Nitrates	Freeze-drying of aqueous solution	Thermal decomposition by flash heating to 850C followed by isothermal annealing	20-22% O_2	Single Phase uniform size 2212 powder with high surface area for studies of oxygen stoichiometry	Krishnaraj 1994,1995 [282, 283]
Nitrates	Freeze-drying of aqueous solution	Air dehydratation at 200C thermal decomposition 12h/ 800C Calcination 40-240h / 805-860 C	20-53% O_2	Pb-Free ceramics synthesis and studies	M'Hamdi and Lacour 1992, 1993 [284, 285]

2.0 RESEARCH

The main consideration in any iso or aliovalent substitutional study is the definition of a starting or reference composition, the matrix that is to be used for the future studies. Comparison of the literature reports shows that even when exactly the same composition is used for the starting precursor, the final stoichiometry varies significantly depending on the synthesis route. Additionally, though Bi-2212 currently represents a generic designation for the 85-94K superconductor it can represent any composition within the solid solution region or even a mixture with some of the 20 surrounding phases and not just stoichiometric composition. (Figure 9, Figure 12 and Figure 21)

This study investigated properties influencing flux pinning. In order to obtain controlled sample stoichiometry, the initial emphasis focused on the synthesis of Bi - 2212 superconductors. One of the goals of the study was to investigate to what extent different synthesis methods influence superconducting properties of the polycrystalline and single crystal materials. The goal was to create a well defined matrix that could be used for the substitution studies elucidating the often-conflicting literature reports.

The second part of the study was the investigation of the correlation between pinning and structure properties in Bi-2212 superconductors as a function of cation substitution, second phase doping, and oxygen annealing experiments.

Occupational modulation is one of the defining characteristics of cuprate superconductors. Superconductivity in strontium cuprate superconductors obtained at high pressures (6GPa, 1000˚C, T_c=110K [286]) ($SrCuO_2$, $(Sr_{1-x}Ca_x)CuO_2$ etc) is intimately related to incommensurate modulation. Although the modulation is apparent in all bismuth cuprates, only small number of publications have attempted to relate modulation and pinning properties. This study identified influence of substitution effects on both structure properties and pinning.

Upon definition of the starting stoichiometry (matrix), this study focused on the following:

1. Influence of intrinsic cation non-stoichiometry on the structure and pinning properties in Bi-2212
2. Influence of Ca site rare earth doping on the structure and pinning properties
3. Influence of the concentration of oxygen vacancies (through different annealing schedules) on structure

This study identified the influence of the pinning effects, and compared the results with point defect simulation calculations. Point defects, formed as a result of cation substitution or doping, intrinsic nonstoichiometry or oxygen annealing (formation of oxygen vacancies or interstitials) are of the length scale of individual fluxoids and could contribute to enhancement of pinning. Point defects, especially if they are coupled, are thought to effectively pin flux lines. Although most experiments focused on polycrystalline materials, influence of high temperature annealing on single crystal samples was also investigated.

2.1 SYNTHESIS OF BSCCO SUPERCONDUCTORS

Although the ideal material, on the basis of measurement and interpretation, for the determination of pinning properties in superconducting materials is a single crystal, single crystalline samples are not available. Synthesis of single crystal specimens with controlled and well-defined stoichiometries is an unachievable task. Single crystal stoichiometry will inadvertently change even if the same composition of starting materials is used. Incongruent melting, oxygen partial pressure variation and high reactivity of the melt are some of the factors responsible for variation in single crystal stoichiometries. In addition, phase diagram even after more than twenty years since discovery is not fully presented.

Synthesis of superconductors through the use of aqueous solutions is capable of mixing all of the starting materials on the atomic level, with a high level of accuracy and precision, which is the main prerequisite for the investigation of the influence of doping. Contrary to solid state techniques that require high temperatures and long synthesis times, solution based techniques require a significantly shorter time. Several solution techniques were investigated to determine if the synthesis procedure influences the superconducting properties (T_c, H_{irr}…). The research mainly focused on the freeze-drying procedure and its optimization. Influence of different freezing processes of nitrate solution, as well as calcination of final products were inestigated.

2.2 PROCESSING

2.2.1 Polycrystalline sample synthesis

To better understand the properties of superconducting materials as a function of processing conditions, XRD patterns and DTA scans of $Bi_2Sr_2CaCu_2O_x$ synthesized by several methods were compared. The critical temperatures were determined using magnetic measurements.

A single nitrate master solution of stoichiometric $Bi_2Sr_2CaCu_2O_x$ (Bi-2212) was prepared using reagent grade Bi_2O_3, $SrCO_3$, $CaCO_3$ and CuO dissolved in a nitric acid-deionized water mixture in the Bi:Sr:Ca:Cu molar ratio 2:2:1:2. The pH value was adjusted to prevent back melting during freeze-drying. The initial solution was divided in five parts:

1. Freeze-drying: Two parts of solution were freeze-dried; one part was splat quenched onto a Teflon coated copper block while the other was sprayed as an aerosol into the liquid nitrogen.
2. Evaporation: The nitrate solution was evaporated using a laboratory rotary evaporator.
3. Oxalate coprecipitation: The nitrate solution was mixed with oxalic acid and the precipitation was induced by adjusting the pH value to 3 with ammonium hydroxide (NH_4OH).
4. Sol-gel synthesis: The nitrate solution was mixed with citric acid and ethylene glycol. NH_4OH is used to adjust the pH value. The gelation occurred at 80^0C and exothermic decomposition at ~200^0C.

Upon the completion of the first processing step, nitrate powders obtained by different methods were denitrated at 600^0C and sintered at appropriate temperatures determined by DTA in a 7% oxygen atmosphere. Oxalate powder was obtained after washing with deionized water; annealing and calcinations were performed as

determined by DTA. To investigate the influence of one step synthesis (without denitration) two grams of freeze-dried material were converted to Bi-2212 by pressing the pellets and flash heating.

Figure 24 presents the DTA comparison of materials obtained upon completion of the first part of the processing experiments. It can be seen that except for the freeze-dried material the samples show additional endothermic events, indicating formation of phases other than Bi-2212. Material obtained by the sol-gel route has a similar shape of the endothermic peak, which is further supported after evaluation of the XRD patterns.

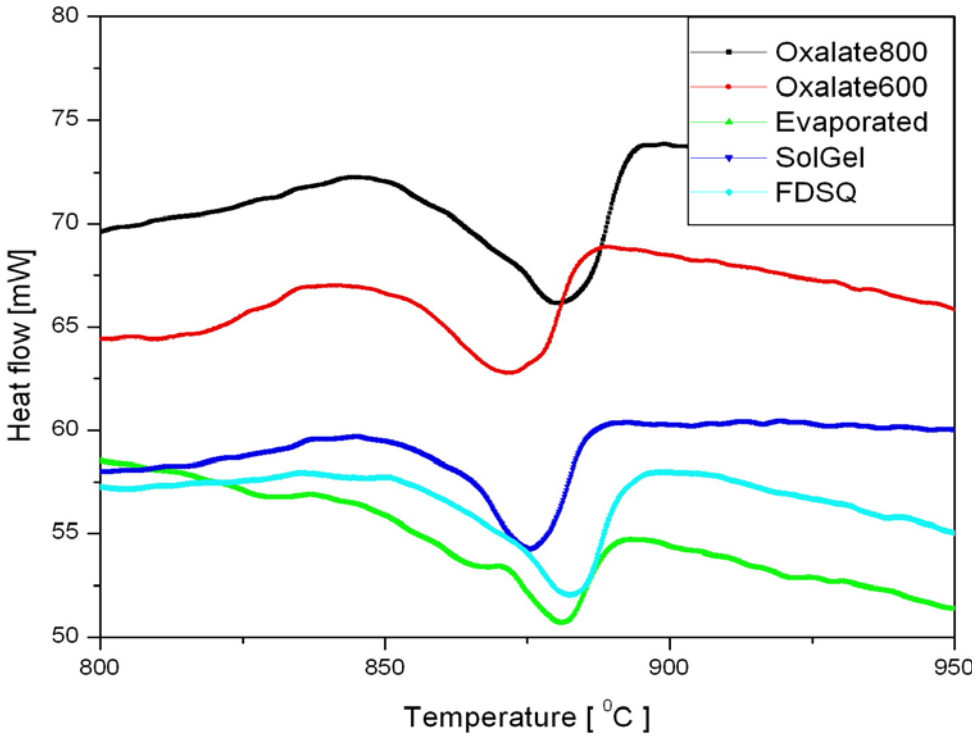

Figure 24. DTA of Bi-2212 samples obtained by different preparation routes (freeze drying, sol-gel, evaporation from the nitrate solution and oxalate route). Same oxygen partial pressure (7%) and heat rate used 10 ˚C/min

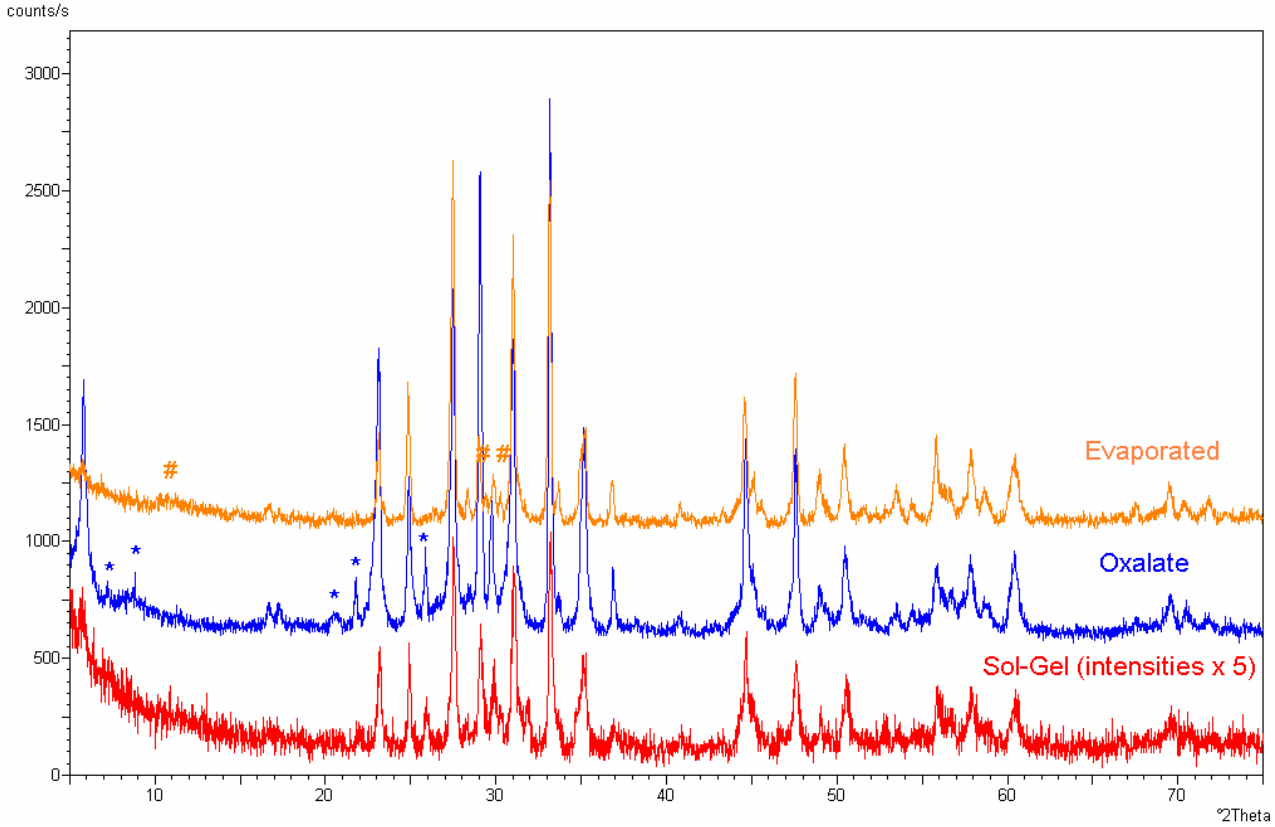

Figure 25. XRD patterns of materials obtained through different synthesis procedures * and # indicate impurity phases present.

XRD patterns presented in Figure 25 show the presence of impurity phases and confirm the interpretation of the results from the DTA. The XRD pattern of the sol-gel obtained sample does not show the presence of impurity phases. It should be noted, however, that the intensities of the sol-gel sample are multiplied five times. Better crystallinity was obtained only after extended annealing (4 days).

Based on the XRD and DTA results, further research used the freeze-drying method of sample preparation. Phase pure samples (to the limit of the x-ray diffractometer) were obtained in a 7% oxygen atmosphere. The XRD scans of samples produced by freeze-drying for different annealing atmospheres are shown

in Figure 29 - 29. Freeze-drying sample synthesis route proved to produce samples of superior quality in a consistent and repeatable manner.

Initially thirty samples of different cation stoichiometries were synthesized via the freeze-drying method, and calcined in 21% or 7% Oxygen. The ratio of the superconducting 2212 phase versus bordering phases was determined via XRD measurements, which allowed mapping the field where the 2212 solid solution exists (Figure 26). My results indicate that the volume where 2212 might be obtained can be extended to higher bismuth contents of the solid solution.

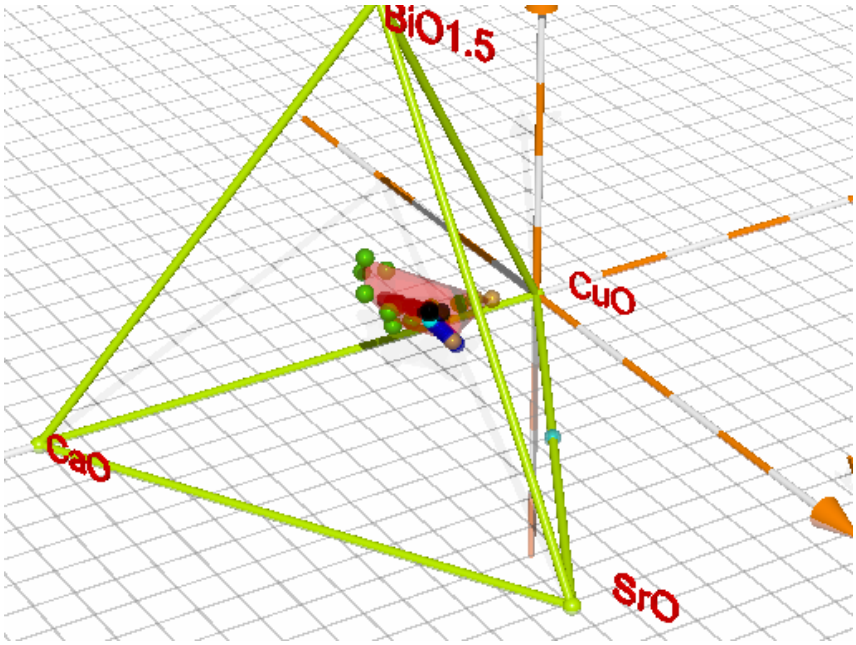

Figure 26 Pseudo-Quaternary phase diagram $BiO_{1.5}$-SrO-CuO-CaO illustrating solid solution region of Bi-2212. Green spheres represent the 30 synthesized compositions at 830^0C 21%O_2, blue spheres represent synthesized Bi:Sr:Ca:Cu = 2:2+x:Ca:Cu+x ratio with x = 0-0.9 in 7% O2 established to be phase pure

2.2.2 Single crystal sample synthesis

Single crystalline material usually represents the sample of choice for the analysis of structural and electrical properties. However incongruent melting and a wide range of solid solubility in the Bi-2212 system does not allow precise control of stoichiometry. To understand the influence of single crystal preparation on structure properties, and compare consistency of structure analysis techniques (XRD, TEM) several single crystal synthesis routes were used. Single crystals were obtained using the self-flux and alkali flux method with either pre-calcined or raw charges.

Single crystal samples were made in alumina crucibles by heating to 1000° C in 21% oxygen atmosphere 20° C/h soaking at that temperature for 10h and than slowly cooling 1.5° C/h to 800° C. Single crystals of [001] orientation grew perpendicular to the crucible bottom in the case of raw charge. When a precalcined charge was used the [001] crystals grew both perpendicular and parallel to the bottom of the crucible. However, only a small portion of the crystals (< 5%) were parallel to the bottom of the crucible and appeared on the top of the solidified melt. Upon extraction of a portion of the crystals from the crucible no contamination from the crucible was observed using EDX. Small needle like crystals (2 x 0.5 x 0.2 mm) obtained through the alkali flux method developed on the side of the crucible. Even after multiple washing with 100° C water, alkali flux residue was still noticeable by using BSE-SEM (Figure 27). The results of different single crystal synthesis techniques are presented in the Table 3.

Table 3. Influence of single crystal preparation procedure on the size of single crystals and the type of defects

	Self Flux		Alkali Flux
	Precalcined	Raw	Precalcined
Size	3 x 1 x 0.1 mm	2 x 1 x 0.1 mm	5 x 0.2 x 0.1mm
Defects	(SrCa)CuO2, 2201	(SrCa)CuO2, 2201	(SrCa)CuO2, 2201, Bi2O3

The largest single crystals were obtained using pre-calcined charges (superconductors) of the stoichiometric composition. Single crystals obtained from the raw materials (oxides, carbonates) of stoichiometric composition were the easiest to extract from the crucible and therefore used for the annealing study.

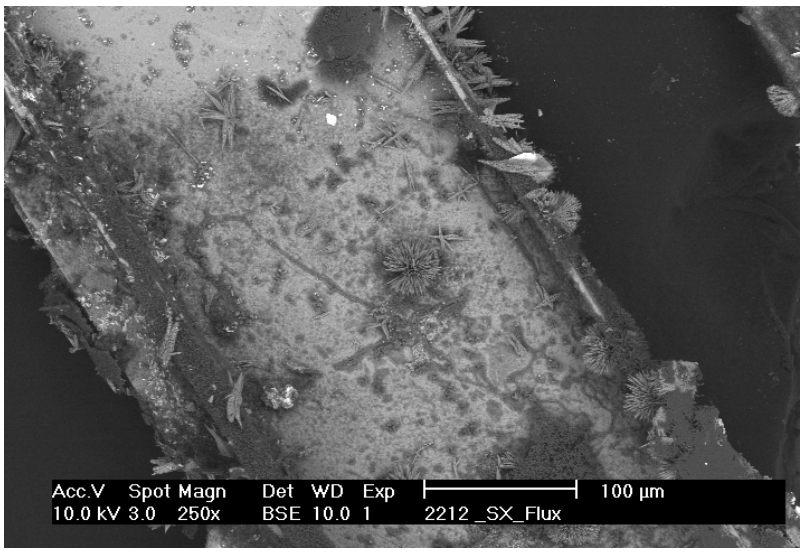

Figure 27 Typical crystal extracted from the alkali flux, (Sr, Ca)CuO_2 impurities and remaining flux are observable on the surface even after repeated washing with 100˚ C water

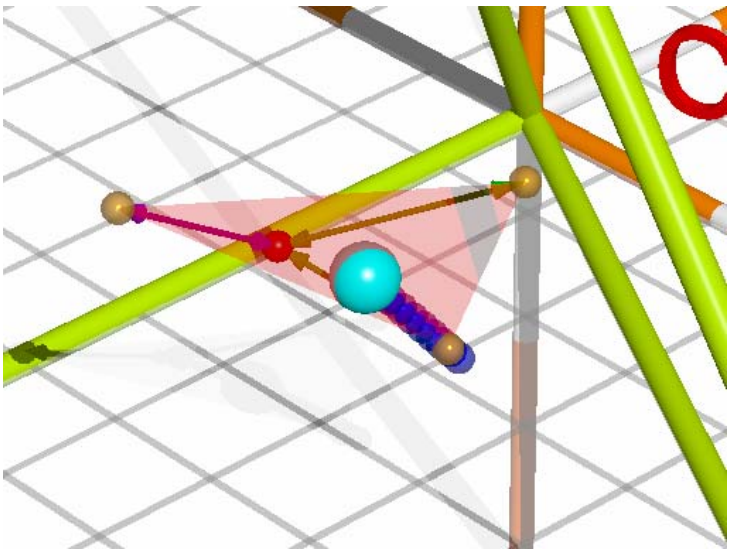

Figure 28 Detail of the Figure 26 showing three compositions (yellow spheres) from which the single crystals analyzed by the SEM were made. Light blue sphere marks the average composition for that vertex.

Detail of the Figure 26 showing three compositions (yellow spheres) from which the three analyzed single crystals were made is given in Figure 28. Light blue sphere marks the average composition for that vertex, and dark blue spheres show compositions of polycrystalline samples obtained through freeze-drying. The red sphere represents the average composition of the phase field where Bi-2212 is stable.

2.3 RESULTS AND DISCUSSION

The main method of structural analysis during the research was by using XRD analysis. The XRD powder pattern presented in Figure 29 illustrates one of the patterns obtained upon 8h annealing in a 7% oxygen atmosphere, without regrinding. It was determined that it was phase pure Bi-2212 to the experimental limit of our powder diffractometer (highly parallel and monochromated beam produces lattice parameter resolution of 0.01%). Initial attempts to synthesize phase pure Bi-2212 corresponding to the published compositions [282, 283] failed. Only after lowering the oxygen partial pressure was it possible to synthesize material without secondary phases. It was determined that the phase purity of Bi-2212 is in intimate relationship with the annealing atmosphere. Figure 30 and Figure 31 show the XRD patterns of material annealed in 21% and 100% oxygen atmosphere, respectively. Appropriate melting temperatures as a function of oxygen partial pressure determined using DTA are given in Figure 32. It can be seen that the additional peaks (later identified as $Bi_2Sr_2Cu_1O$ / $Bi_{17}Sr_{16}Cu_{12}O$ phase) appear in both XRD patterns of samples annealed in 21% and 100% oxygen atmospheres. This supports previous findings that stoichiometric Bi-2212 cannot be obtained in air. DTA scans show the shifting of the melting point towards lower temperatures with the lowering of the oxygen partial pressure in the annealing atmosphere.

To determine the effects of the addition of secondary phases on the critical current, $SrCuO_2$ was added to the Bi-2212. This was achieved through dissolving oxides/carbonates in Bi:Sr:Ca:Cu = 2 : 2+x : Ca : Cu+x ratio with x = 0, 0.1, 0.2, 0.3,

0.4, 0.6. The solution was subsequently processed through freeze-drying. The resulting material was analyzed by using XRD, SEM, DTA, TGA and SQUID/VSM.

$SrCuO_2$ grown under ambient conditions has a plate-like morphology similar to the Bi-2212 system. $SrCuO_2$ has an orthorhombic unit cell (a = 3.913, b = 3.573, c = 16.331 Å) that consists of CuO planes inserted between double Sr and O layers, where Cu cations are square-coordinated by four oxygen anions. Square coordinate Cu-O units are linked together by sharing edges and form double copper chains. These double chains, stretching along the c-axis, are considered magnetically as a quasi-one-dimensional (1D) antiferomagnetic chain.

If the 2212 diffraction patterns are compared to the $SrCuO_2$ diffraction pattern (Figure 33 and Figure 29) obtained through the same freeze-drying process, no minor phases associated with $SrCuO_2$ could be detected in the Bi-2212 matrix. Additionally no Bi-2201 phases could be detected by using either XRD or SEM analysis

Figure 35 - Figure 38. Micrographs shown in Figure 35 through Figure 38 represent surface and the cross section of the undoped and doped samples after pressing and sintering. The grain size does not change with increasing doping level and other phases cannot be detected by using EDX.

All of the powder diffraction analyses were performed at $T_{room}=20^0$ C on 10mg of reacted material using a low background sample holder and the Philips XPERT system. The Bi-2212 XRD patterns were matched to pcdpf 41-0317 and later refined using JANA 2000 software. It is worth mentioning that while the melting temperature

of Bi-2212 did not appreciably differ from the range reported in the literature, $SrCuO_2$ synthesized via freeze-drying melts at temperatures 300^0C lower than reported.

Although it was expected that the added $SrCuO_2$ would form a precipitate, even after the addition of 40 mole % of $SrCuO_2$ to stoichiometric Bi-2212 no additional diffraction lines could be detected. This may indicate that $SrCuO_2$ incorporates within the Bi-2212 and modifies the crystal structure [290] by changing the lattice parameters and modulation vector. This is further supported by a decrease in critical temperature as a function of $SrCuO_2$ addition. The other explanation could be that inherent defect composition and defect density changes. If we assume that the stoichiometric Bi-2212 is the reference material that is optimally doped, that is it has the highest T_C, the defect structure using Kroger-Vink notation can be written as:

$$2\delta\ SrCuO_2 \xrightarrow{Bi_2Sr_2Ca\ Cu_2O_{8.20}} 2\delta\ Sr'_{Bi} + 2\delta\ Cu^{\bullet}_{Cu} + \delta\ V^{//}_{Ca} + 2\delta\ O^{x}_{O} + 4\delta\ V^{\bullet\bullet}_{O}$$

or

$$\delta\ SrCuO_2 \xrightarrow{Bi_2Sr_2Ca\ Cu_2O_{8.20}} \delta\ Sr^{\bullet\bullet}_{i} + \delta\ Cu^{\bullet\bullet}_{i} + 2\delta\ V^{///}_{Bi} + \delta\ V^{//}_{Ca} + 2\delta\ V^{\bullet\bullet}_{O}$$ or

$$\delta\ SrCuO_2 \xrightarrow{Bi_2Sr_2Ca\ Cu_2O_{8.20}} \delta\ Sr^{x}_{Sr} + \delta\ Cu^{x}_{Cu} + 2\delta\ V^{///}_{Bi} + \delta\ V^{//}_{Ca} + 4\delta\ V^{\bullet\bullet}_{O}$$

The set of equations describing the possible defect reactions is not exhausted with the previous three possibilities; both cations (Sr, Cu) can occupy any of the other cation sites [112]. The above reactions use Kroger – Vink methodology $Sr^{/}_{Bi}$ represent the Sr ion on the Bi site, the defect has one negative charge since the Sr^{2+} on Bi^{3+}, similarly Cu^{3+} on Cu^{2+} has one positive charge $Cu^{\cdot}_{Cu}$. From the first reaction, simultaneous increase in defect concentration on both Sr and Cu sites leads to increase in oxygen vacancy concentration. Though all considered defects are

charged species, together they form a neutral defect cluster. This concept will be revisited in next chapters discussing computational study using general utility lattice package (GULP).

A possibility exists that due to atomic mixing of $SrCuO_2$ and Bi-2212, $SrCuO_2$ forms as a submicron size precipitate that is mixed with the parent Bi-2212. If $SrCuO_2$ formed the precipitate 40% $SrCuO_2$ addition would cause either additional lines to be present in the XRD pattern or since there is an overlap between the Bi-2212 and $SrCuO_2$ there would be extended broadening of the peaks. However, this was not observed neither by XRD or SEM analysis. Full XRD structural analysis is presented in 2.4.2.

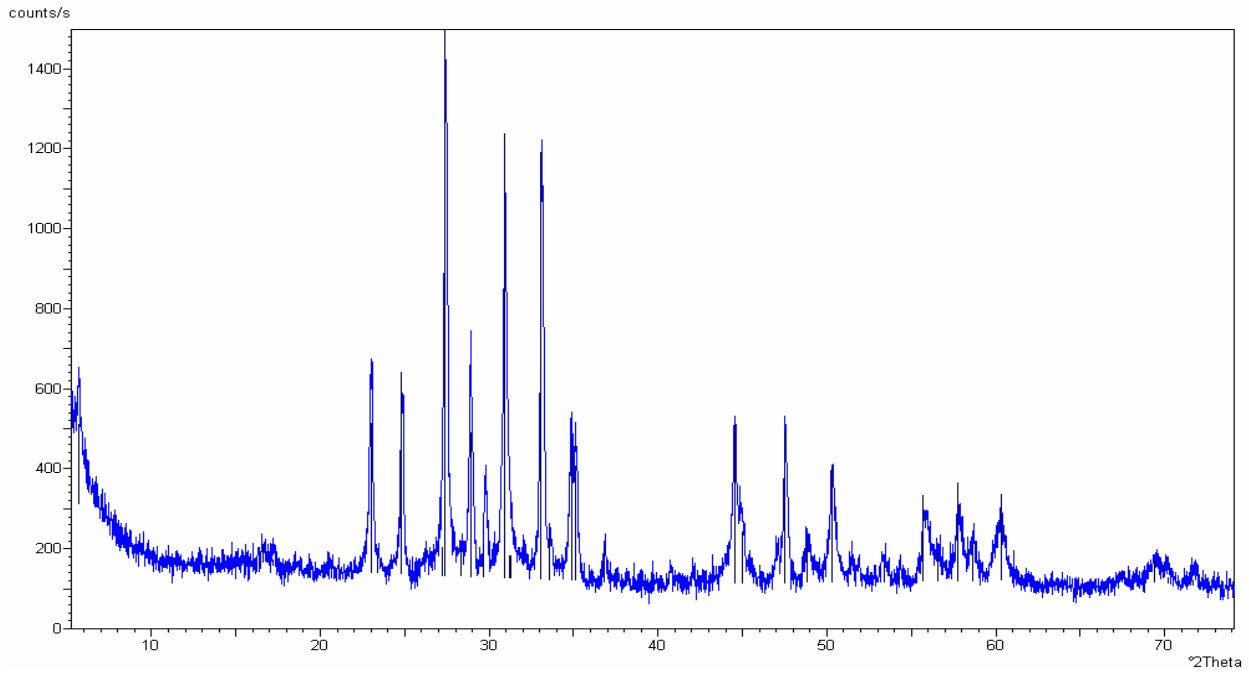

Figure 29. $Bi_2Sr_2CaCu_2O_{8+\delta}$ synthesized via freeze-drying in 7% O_2 atmosphere patterns were matched to pcdpf(41-0317).

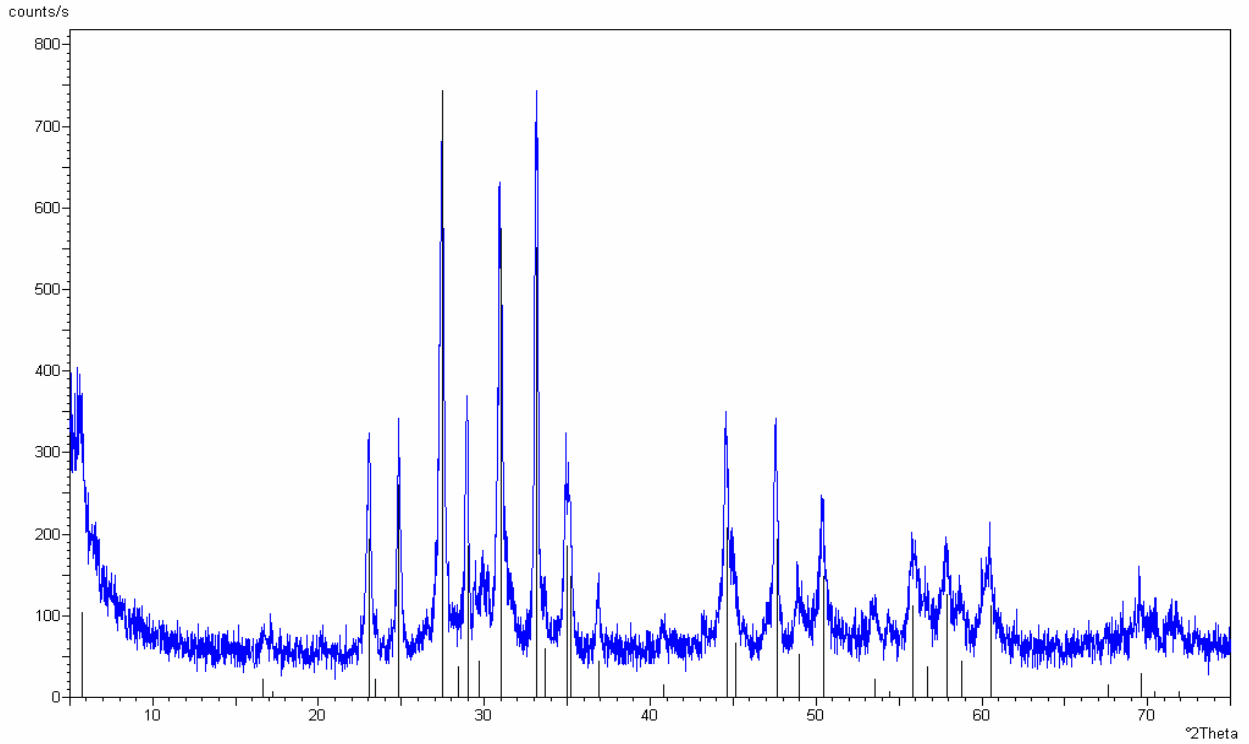

Figure 30. $Bi_2Sr_2CaCu_2O_{8+\delta}$ synthesized via freeze-drying in 21% O_2 atmosphere. Black lines correspond to pcdpf (41-0317).

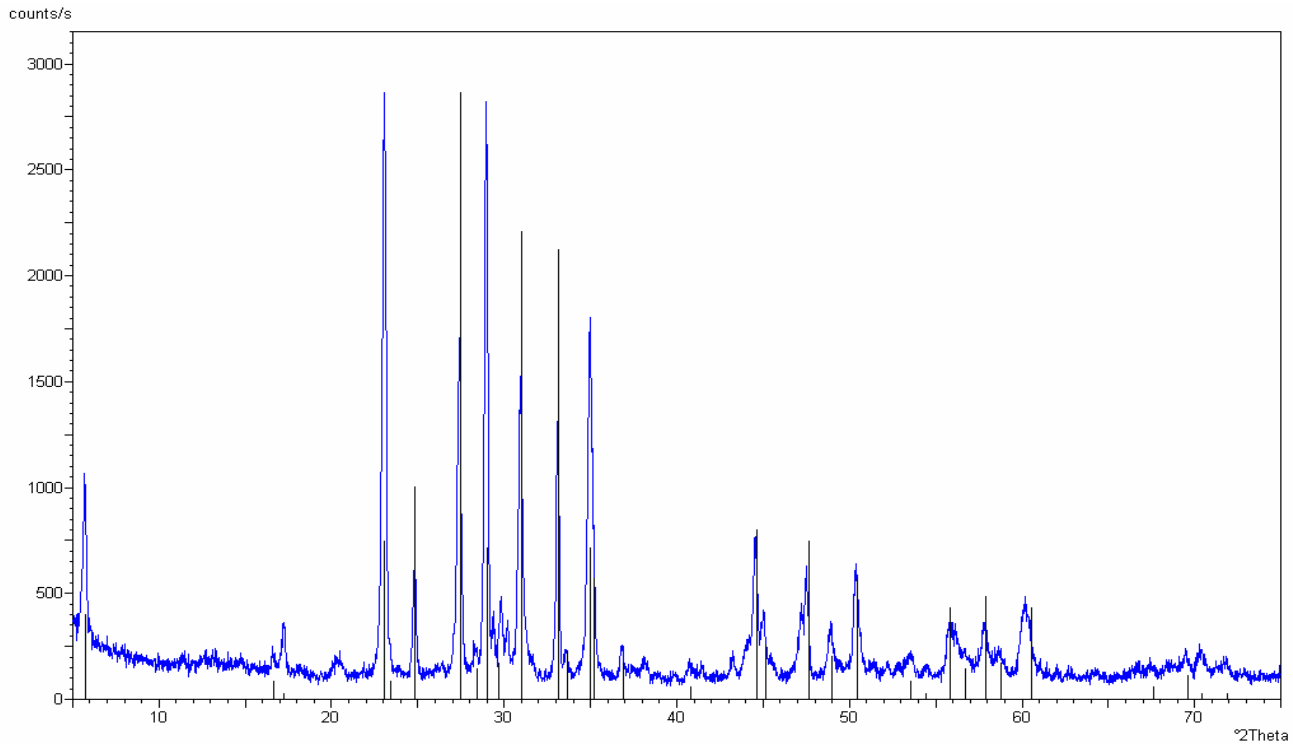

Figure 31. $Bi_2Sr_2CaCu_2O_{8+\delta}$ synthesized via freeze-drying in 100% O_2 atmosphere. Black lines correspond to pcdpf (41-0317).

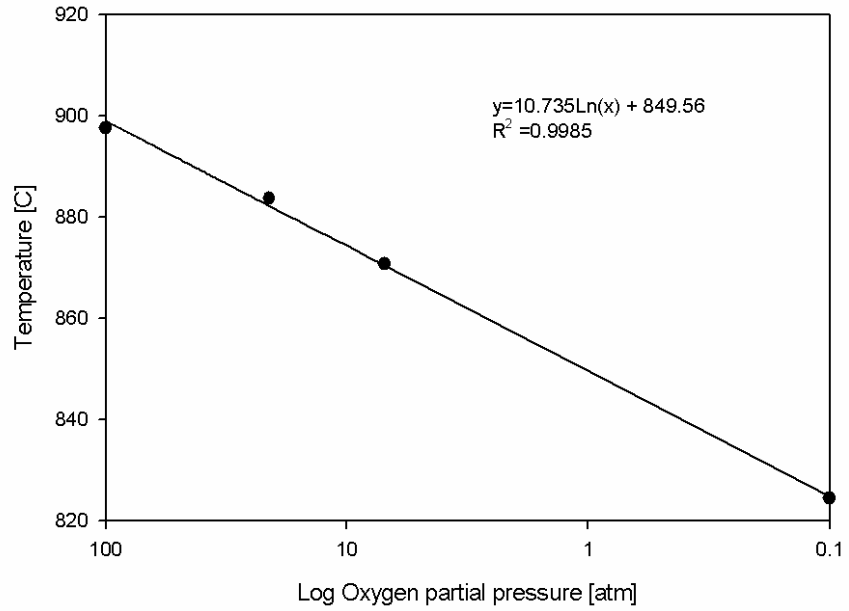

Figure 32. Melting point as a function of oxygen partial pressure; measured by DTA

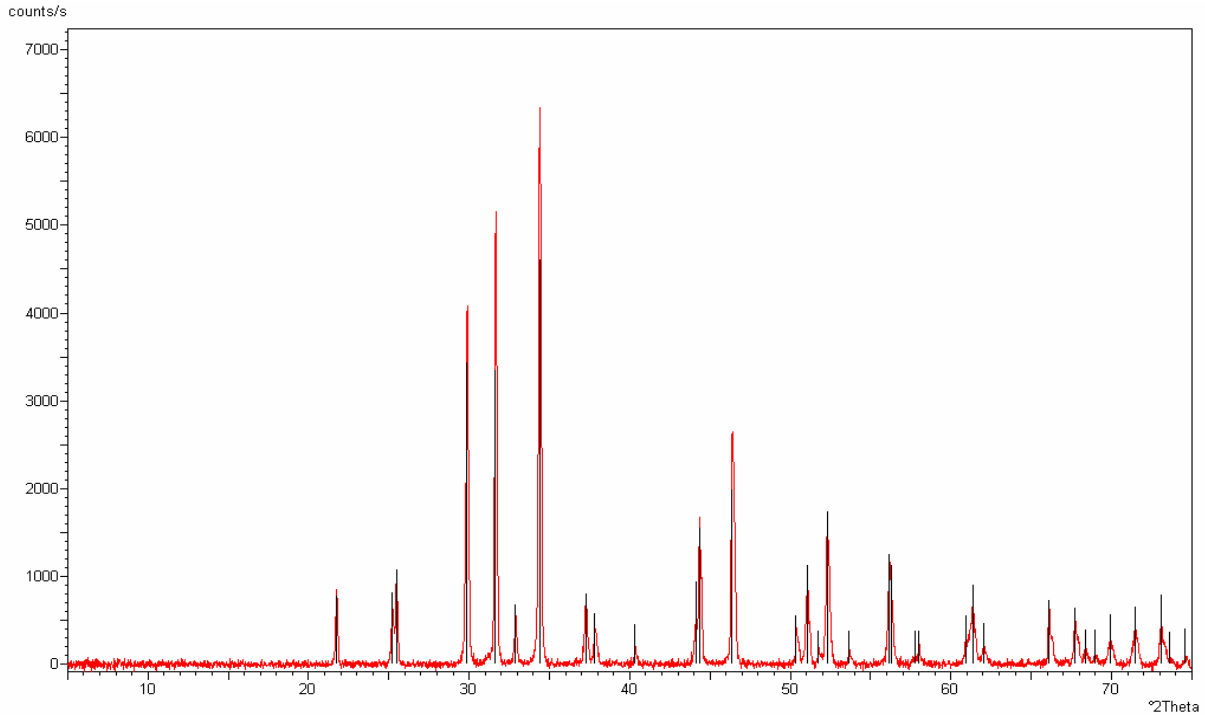

Figure 33. $SrCuO_2$ XRD powder pattern. Black lines correspond to pcpdf 39-1492

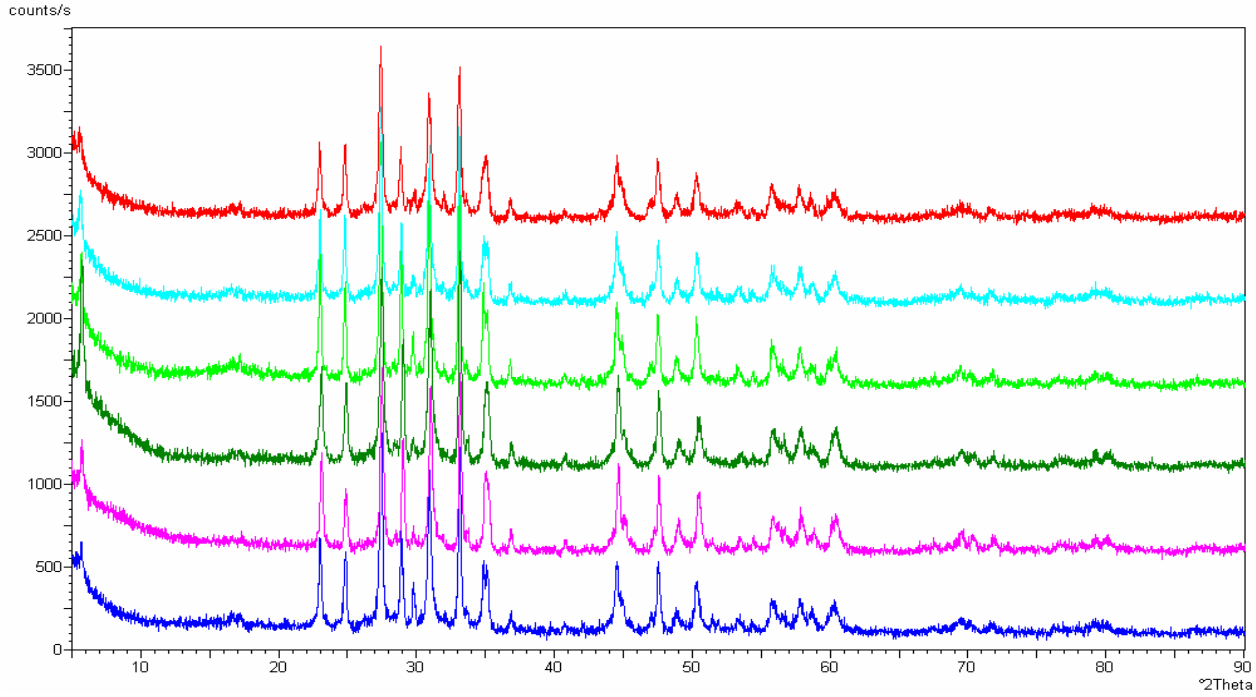

Figure 34. Overall diffraction patterns starting from the bottom: 2.0; 2.001; 2.01; 2.1; 2.2; 2.3;

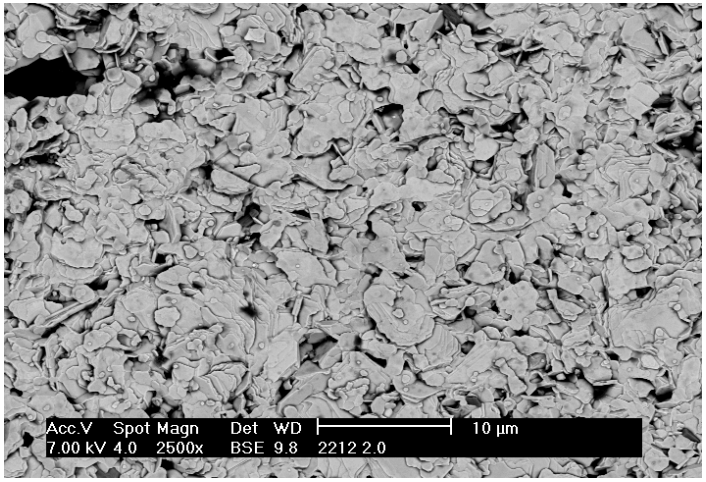

Figure 35 Top surface Bi-2212 undoped

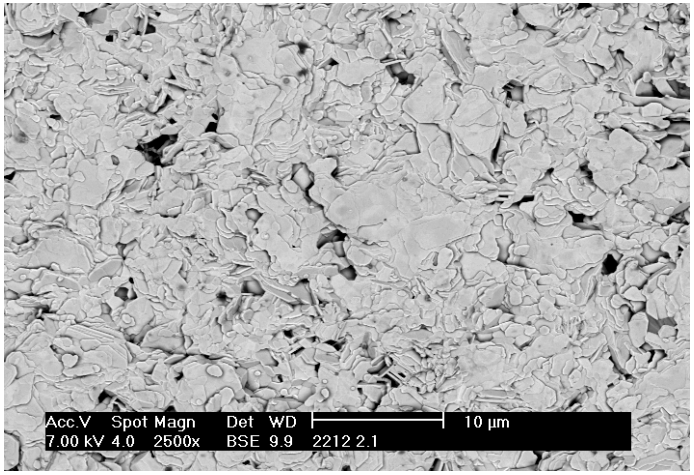

Figure 36 Top surface Bi-2212 0.1% $SrCuO_2$

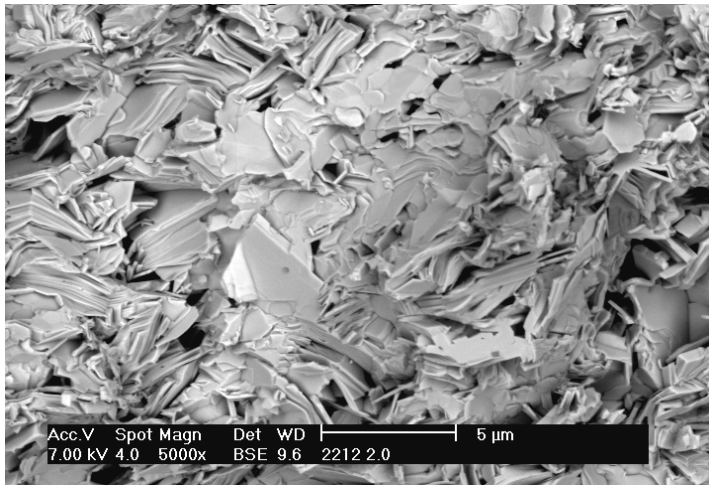

Figure 37 Cross section Bi-2212 undoped

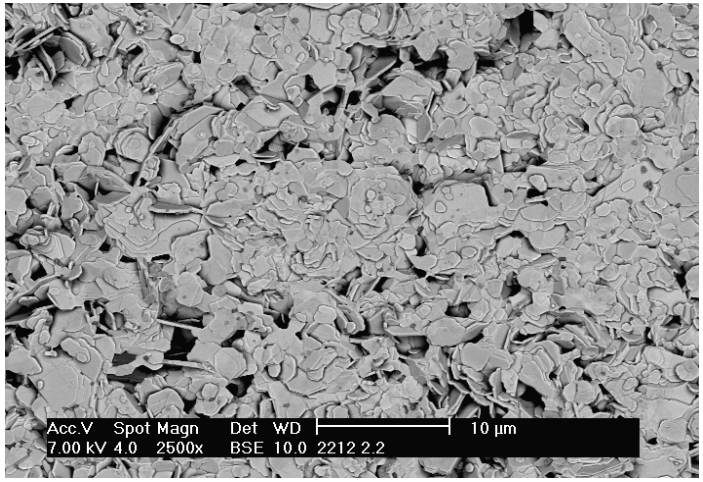

Figure 38 Top surface Bi-2212 0.2% $SrCuO_2$

2.4 PINNING PROPERTIES STUDY

Not only is vortex pinning in high temperature superconductors essential from a practical point of view, understanding the vortex-pin interaction is a scientific challenge. The main problem inhibiting the practical application, since the discovery of superconductors has been the inability of the material to effectively pin the flux vortices. Current transport through the Type II superconductor in the mixed state exerts a Lorentz force on the magnetic flux vortices, unless these lie parallel to the current flow. If under the influence of this force the vortices move (perpendicular to the current flow), then dissipation will occur which is manifested as electrical resistance. Pinning forces created by isolated defects in the material oppose the motion of the flux lines and increase the critical current. Aside from intrinsic pinning centers, artificial pinning centers have been introduced and developed to increase the critical current, ranging from oxygen annealing to introduce oxygen vacancies or interstitials, cation substitution, dispersal of small non-superconducting second phases, and the creation of columnar defects by proton, neutron, or heavy ion irradiation. Unfortunately, unlike the relatively straightforward determination of T_C, there still does not exist a standard for the determination of pinning energies. The values obtained vary depending on the analysis method, and the model used. The problem is further complicated due to the differences in behavior of vortices in different types of cuprate superconductors, i.e. while pinning energies decrease with an increase of oxygen content in YBCO type superconductors [49] the energy apparently increases in the BSCCO superconductors [47, 48]. Theoretical research

supports the findings in the YBCO systems which suggest that the introduction of randomly distributed point defects “softens” the flux lattice and allows depining at lower fields and temperatures.

Both theoretical and experimental findings in all cuprate superconducting materials show that the introduction of columnar defects increases the pinning. This can be explained with a comparison between the dislocation pinning and vortex pinning. Vortex formation requires energy, which is contained in the circulating currents flowing around the vortex core. Pinning the flux vortex lowers its free energy in a superconductor. It can be seen that the vortex line energy is directly proportional to the length of the flux vortex. As vortices begin to penetrate superconductor from the lower critical field H_{c1} the vortex formation energy ε can be estimated. Each flux line carries one flux quanta, which requires energy:

$$\Delta E_F = n\varepsilon LA$$

L – length of the sample, A – area of the sample

At the same time the gain in the magnetic expulsion energy can be represented as:

$$\Delta E_M = H_{c1}\Delta MV = H_{c1}\frac{n\phi}{\mu_0}LA$$

∆M – change in magnetization of the sample; V – sample volume

When the vortex formation energy is equal to the expulsion energy (i.e. at B_{c1}):

$$\Delta E_M = \Delta E_F \Rightarrow n\varepsilon LA = H_{c1}\frac{n\phi}{\mu_0}LA$$

so that the energy of the flux vortex is:

$$\varepsilon = H_{c1}\frac{\phi}{\mu_0}$$

When the flux vortex is pinned by the columnar defect (dislocation, ion track etc) of the length *l* the free energy of the system will be lower by:

$$\Delta E = \varepsilon\, l$$

Then the force required to depin the vortex from the defect is related to the pinning energy by:

$$F_p = \frac{\Delta E}{\delta} = \frac{\varepsilon\, l}{\delta}$$

where *δ* represents the distance that the vortex must be displaced from the pinning site. Equating the Lorentz force to the pinning force and assuming that only a segment of the vortex is being pinned, the fraction of the pinned vortex might be calculated as:

$$F_L = F_p \rightarrow J_c \phi \frac{l}{c} = \frac{\varepsilon\, l_p}{\delta}$$

$$\frac{l_p}{l} = J_c \phi \frac{\delta}{\varepsilon\, c}$$

If the core pinning is assumed, the energy gain per unit length in the line defect is represented by:

$$\varepsilon_c = \frac{H_c^2}{8\pi} \pi \xi_{ab}^2 = \frac{\phi^2}{64\pi^2 \lambda_{ab}^2}$$

Influence of point disorder is however poorly understood.

2.4.1 Influence of $SrCuO_2$ addition on the superconducting properties

Measurements of the field-cooled and zero field cooled magnetization dependence on temperature, M(T), for the samples with various amounts of "$SrCuO_2$", are presented in Figure 39. When field-cooled at 10 Oe, the samples exhibit a two-step transition. The onset of superconductivity has a range Tc = 84-95 K depending on the amount of "$SrCuO_2$" added. The maximum critical temperature of 95K corresponds to the optimally doped material (see Figure 15). Oxygen content determined from TGA indicated an oxygen content of 8.17 which did not appreciably change with "$SrCuO_2$" additions. The subsequent decrease in critical temperature is consistent with the incorporation of $SrCuO_2$ within the Bi-2212 crystal structure.

Figure 40 shows magnetic hysteresis curves of pressed and sintered $Bi_2Sr_2CaCu_2O_{8.17}$. At all temperatures the M–H curves are asymmetric, which might be due to the interaction between bulk and surface pinning effects that are also observed in other high-T_c superconductors. Although bulk pinning is generally accepted as being dominant at low temperatures, the asymmetry in magnetization curves could support the existence of surface barriers. The magnetization data were analyzed using the critical current density calculated by the Bean model (289). It is readily observable from Figure 41 that the 0.1% $SrCuO_2$ addition increases the critical current density three fold. This is also evident at all temperatures at which magnetization measurements were performed. In addition to the previous samples, two samples having 0.01% and 0.001% $SrCuO_2$ addition were synthesized, after the initial 0.1 – 0.6 samples had been investigated, to possibly further clarify the influence of $SrCuO_2$ additions. Magnetic measurements (performed using vibrating

sample magnetometer VSM) showed that the sample having the 0.001% $SrCuO_2$ addition exhibits the higher critical current density.

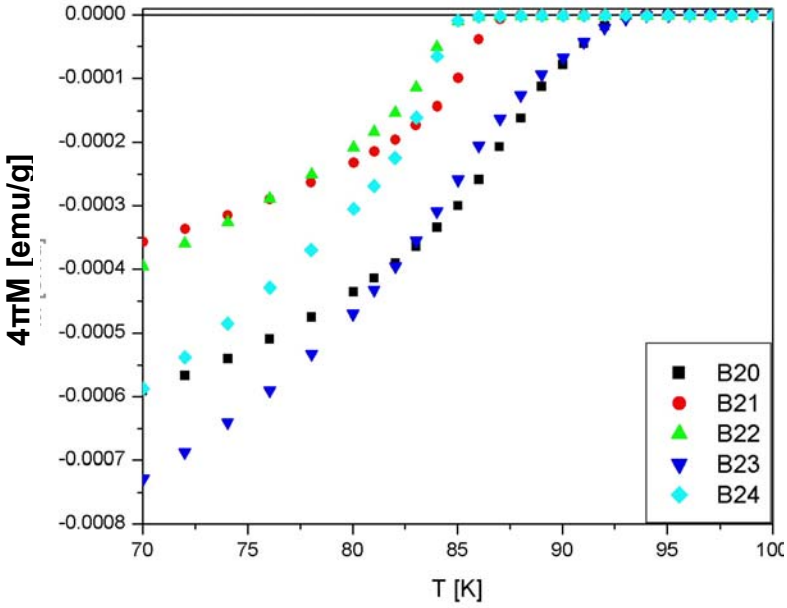

Figure 39 Magnetization – temperature curves as a function of $SrCuO_2$ doping level under H = 10 Oe; ▪ 0 mol% $SrCuO_2$ ●10 mol% $SrCuO_2$ ▲ 20 mol% $SrCuO_2$ ▼30 mol% $SrCuO_2$ ♦ 40 mol% $SrCuO_2$

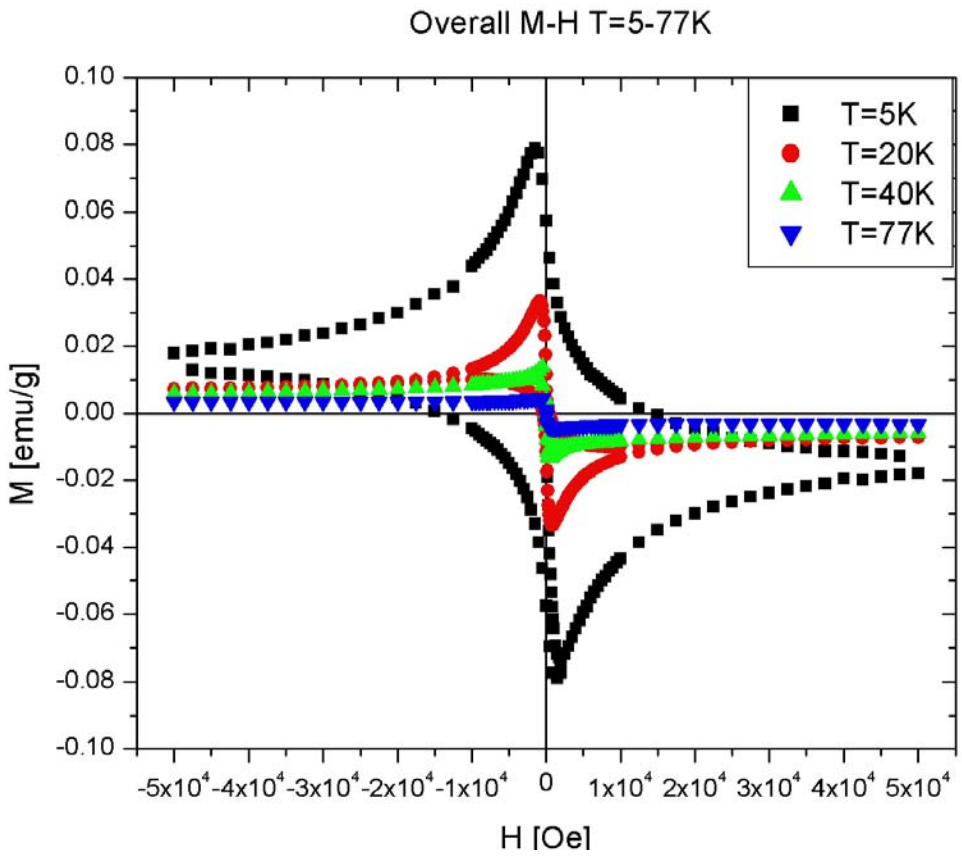

Figure 40 Overall magnetic hysteresis curves 4 - 77K for the undoped sample

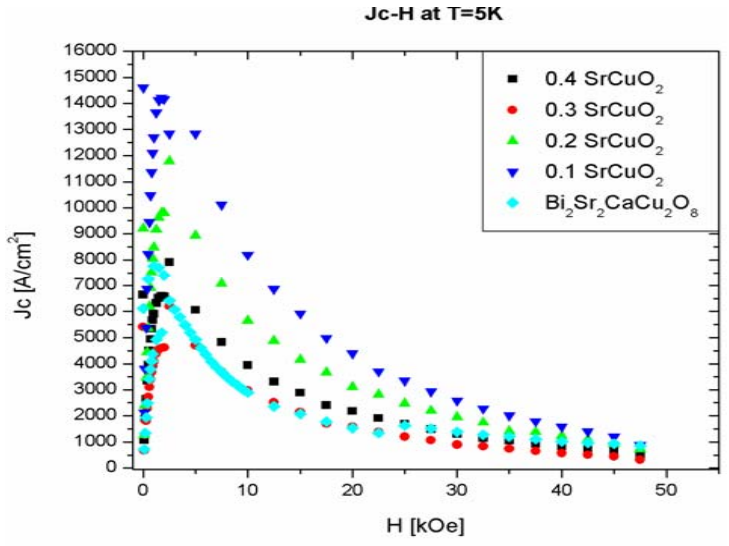

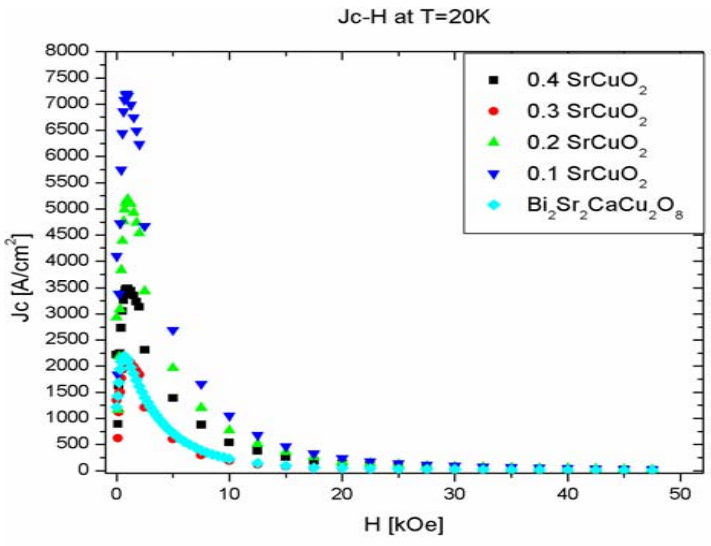

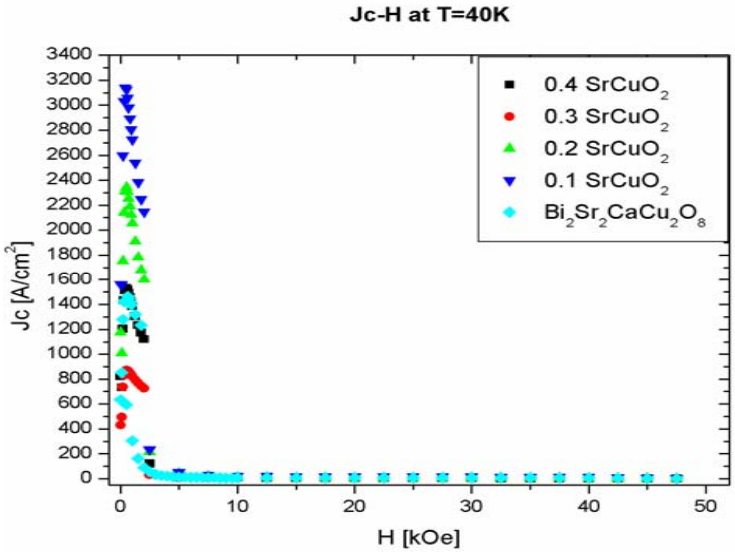

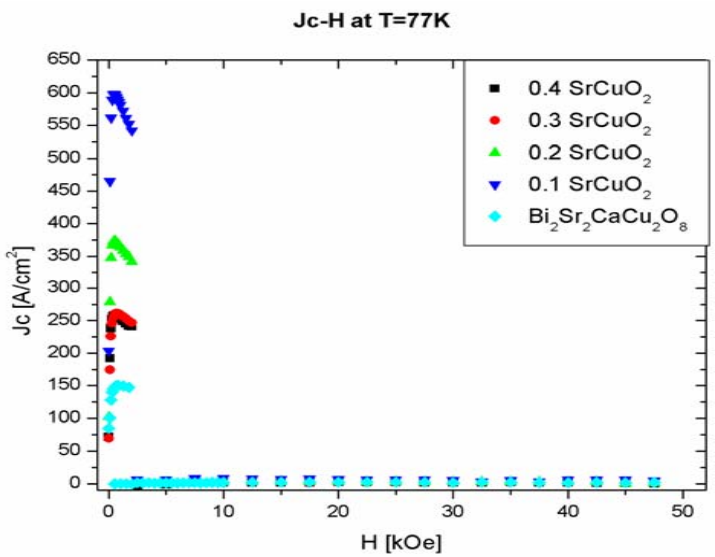

Figure 41 J_C-H curves for different doping levels

2.4.2 Influence of $SrCuO_2$ addition - XPS analysis

In addition to the previous analysis, polycrystalline $Bi_2Sr_{2+x}CaCu_{2+x}O_{8+\delta}$ ($xSrCuO_2$) was studied by X-ray photoelectron spectroscopy (XPS), to determine the cation and oxygen oxidation states. XPS spectra for each substitution level indicate that the main oxidation states for Bi and Cu are +3 and +2, respectively.

The deconvoluted Bi $4f_{7/2}$ - $4f_{5/2}$ spectra with binding energies of 158.5 eV and 165 eV shown in Figure 43 are consistent with the 3+ oxidation state of bismuth previously published for Bi_2X_3 (X=O, S, Se, Te) compounds [41]. Measured binding energies are smaller than previously reported for nonconducting Bi compounds, but agree well with other XPS results on Bi-2212. Each spectrum is comprised of $4f_{7/2}$ and $4f_{5/2}$ spin-orbit components, and neither show broadening at higher binding energies indicating purity of the samples. The assumption of Bi in a state between 3+ and 5+ has remained controversial for some time. Comparison of reported Bi_2X_3 XPS peak shapes shows that the Bi is in the 3+ state. However, the increase of coordination of Bi ions (i.e. by additional oxygen insertion) may be the cause of the reported increase in Bi valence, rather than the lowering of conduction electron density. Insulating Bi-O planes might lower the Josephson coupling between the Cu-O planes, and contribute to flux lattice melting at lower fields and temperatures. As previously noted, structural studies of Bi-2212 point to the possible presence of extra oxygen within or near the Bi-O planes and indicate this layer is a charge reservoir. As can be seen, higher levels of $SrCuO_2$ additions do not change either the shape of the peaks or the binding energies.

The best fit of the Cu 2p main peak was obtained by using two components, one at a low binding energy (LBE) of 933 eV, the other at a HBE of 935 eV. Complex satellite Cu2p signal characteristic is a signature of the 2+ oxidation state within cuprate superconductors. The intensity of the satellite peak is approximately 40-45% of the main peak for p-type superconductors. All the $Cu2p_{3/2}$ spectra exhibit the main component that is associated with the $2p3d^{10}L$ final state accompanied by a satellite associated with multiple splitting of the $2p3d^{9}$ final state. In this case 2p denotes a core hole state and L represents charge transfer from oxygen to the Cu 2+ ions. The ratio of the intensities of the satellite to the main peak (Cu $2p_{3/2}$) does not seem to be influenced by the level of $SrCuO_2$ addition. The best fit of the main peak was obtained by using two components, one at a low binding energy (LBE) of 933 eV, the other at a HBE of 935 eV.

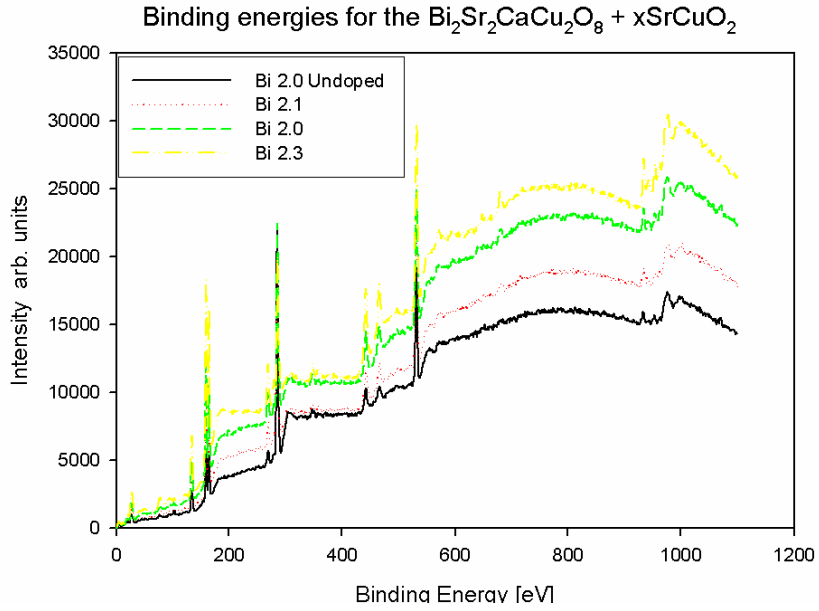

Figure 42 Survey spectra of the $Bi_2Sr_{2+x}CaCu_{2+x}O_{8+\delta}$ ($xSrCuO_2$ x = 0 - 0.4)

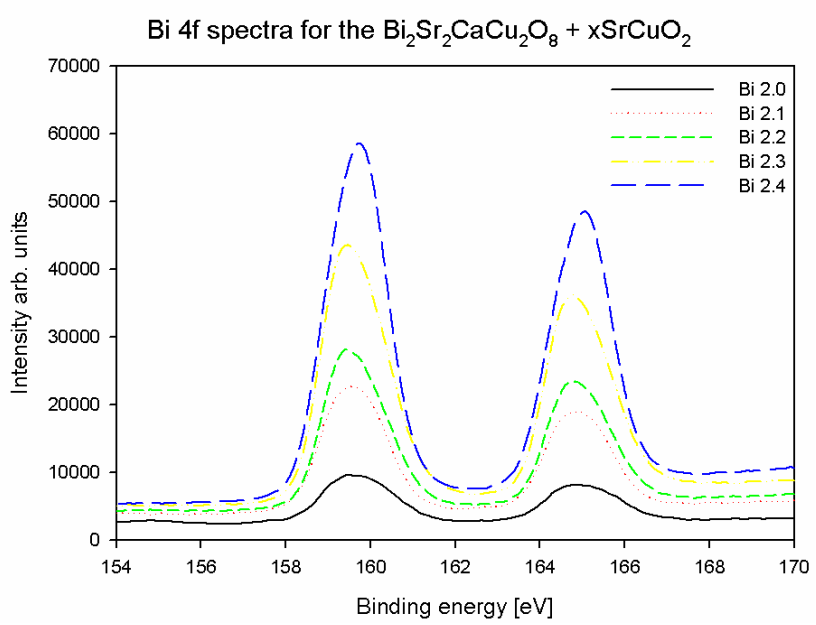

Figure 43 Bi 4f spectra of $Bi_2Sr_{2+x}CaCu_{2+x}O_{8+\delta}$ ($xSrCuO_2$ x = 0 - 0.4)

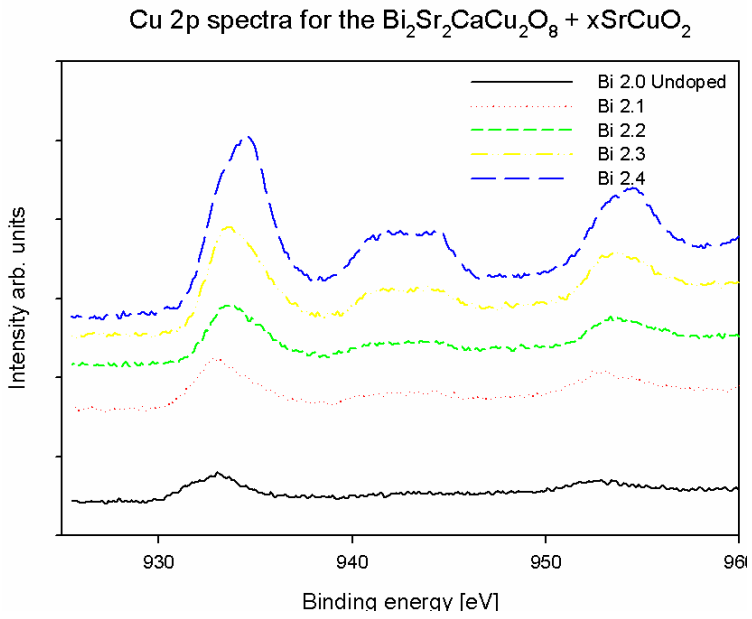

Figure 44 Cu 2p spectra of $Bi_2Sr_{2+x}CaCu_{2+x}O_{8+\delta}$ ($xSrCuO_2$ x = 0 - 0.4)

2.4.3 Influence of $SrCuO_2$ addition on structure

Although the reports of incommensurate structures in Bi-2212 are not consistent the diferences can be attributed to the solid solution behavior and intrinsic relation to the oxygen partial pressure during the synthesis. Features such as: dislocation entanglements, twins, anti phase boundaries and satellite reflections that are usually described as a sign of loss of the classical 3d translation symmetry in modulated crystals have been observed. The atoms from cell to cell change their basic structural parameters such as occupancies or positions. Since the changes are not random, they can be described by periodic modulation functions. To determine the influence of $SrCuO_2$ additions on lattice parameters and modulation vector and possibly explain the observed increase in critical current density further XRD and TEM investigations were performed. TEM analysis was attempted to determine if additional features (stacking faults, twins, dislocations) are present, that can help explain the increase in the pinning properties.

Analysis of both polycrystalline and single crystal structures were performed on a JEOL 200CX transmission electron microscope. To prevent the possibility of ion bombardment changing the modulation, samples were prepared by dispersing polycrystalline (single crystals) on a copper grid, covered with a holey carbon film. The difficulty of performing characterization using powdered samples is illustrated with several micrographs. Bright field micrographs show one of the electron transparent areas. Diffraction patterns are representative of the thin sections in the sample. Several diffraction spots used to make dark field micrographs demonstrate how the thin area is composed of crystals having different orientations.

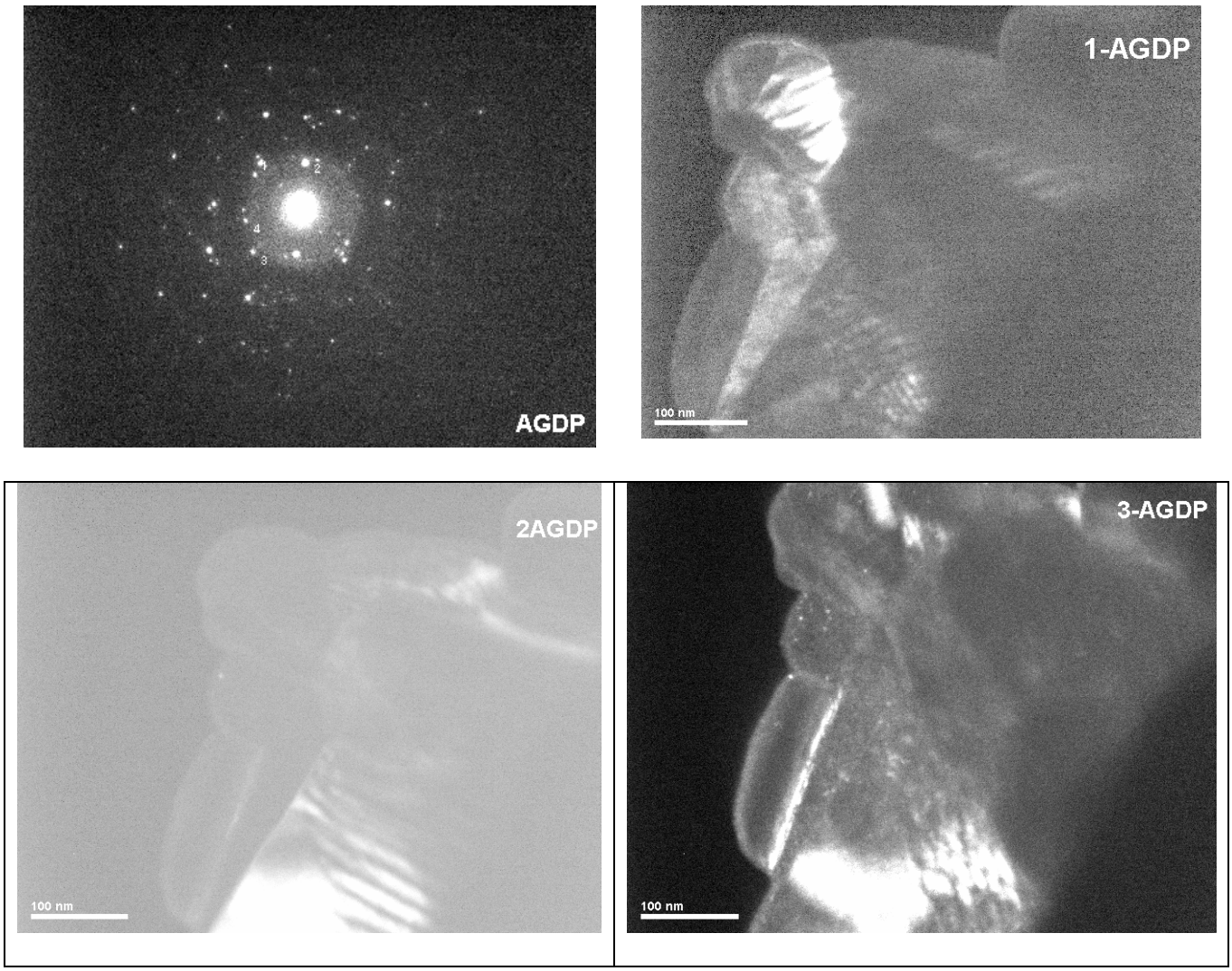

Figure 45 Series of TEM micrographs obtained from the dispersed polycrystalline sample. AGDP diffraction pattern of one transparent area. 1-3 AGDP dark field images using spots 1-3 from the AGDP illustrating that the thin area is assembled of crystals having different orientations.

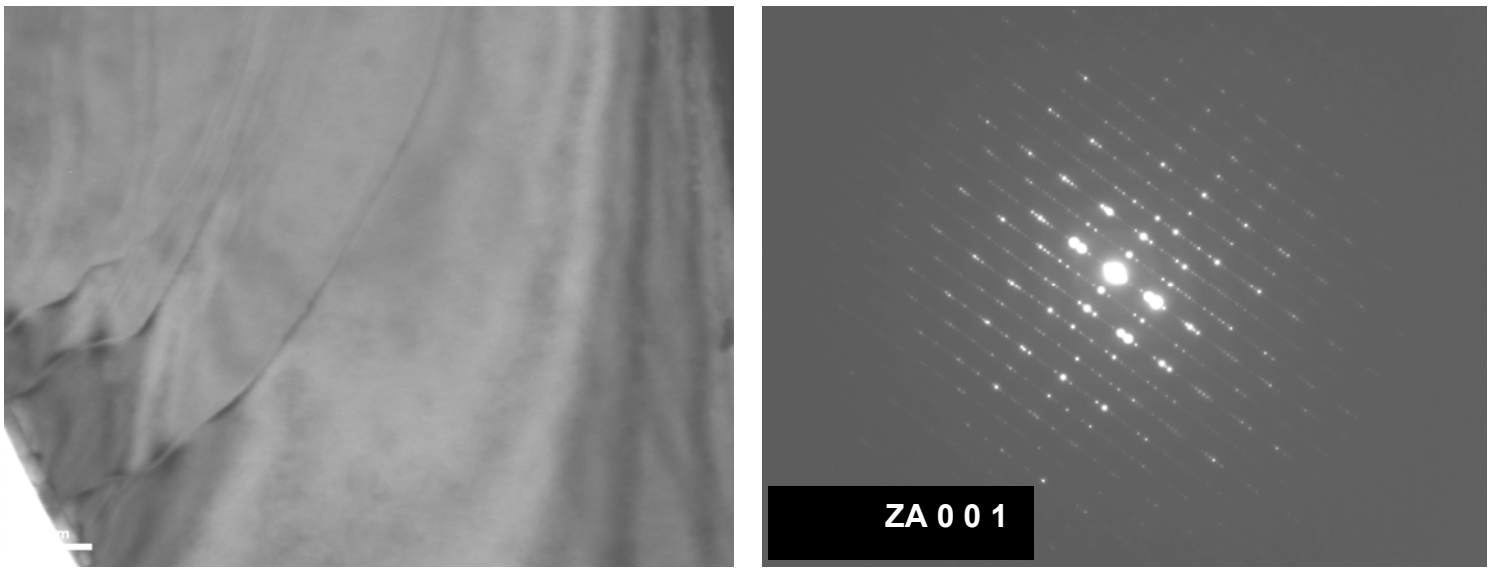

Figure 46 Bright field micrograph and corresponding diffraction pattern of a single crystal sample. Additional satellite reflections corresponding to modulation are visible in the diffraction pattern.

Crystal lattice parameters a = 5.44 Å, b = 5.37 Å as well as lattice modulation q = 0.2b were determined from selected area diffraction patterns with a 001 zone axis Figure 46 show bright field micrograph and accompanying SAD pattern. Upon determination of a, b lattice parameters and the modulation vector, single crystal samples were ground and analyzed using XRD and the JANA2000 software package, to compare results of XRD Rietveld refinement and electron diffraction. Refinement pertaining to a, b, c and the modulation vector was subsequently performed on the $SrCuO_2$ added samples as well as Nd_{Ca} substituted samples.

Lattice parameters can be extracted from the experimental powder XRD pattern by using the standard least squares method, which only pertains to the determination of lattice parameters and not the modulation vector. It is possible to determine modulation vector using a reciprocal map obtained through Q scan XRD

(ω-2θ), but this requires sufficiently large single crystalline samples. From the observation that the ω-2θ scans show only (00l) peaks it can be concluded that the Bi2212 is c-axis oriented. The c lattice parameters of the obtained phases in the examined samples were determined from the angular position of the (00l) peaks in the ω-2θ scans. The satellite peaks stem from a superstructure along the b-axis, due to incommensurate modulation of the metal ion positions. The periodicty of the superstructure is 4.5b-5b (0.2-0.22 b*). Reciprocal space maps of the single crystal obtained from raw charge are shown in Figure 47 and Figure 48. The maps show the main peak 0020 and the surrounding satellite peaks, stemming from the lattice modulation. Reciprocal map of the as cleaved crystal surface is shown in the Figure 47. It can be readily seen that the Ar annealing contributes to “smearing” of the both main peak and the satellite reflections. The observed “smearing” can be interpreted as interlayer disordering, and the sign of nonuniform oxygen removal from the lattice.

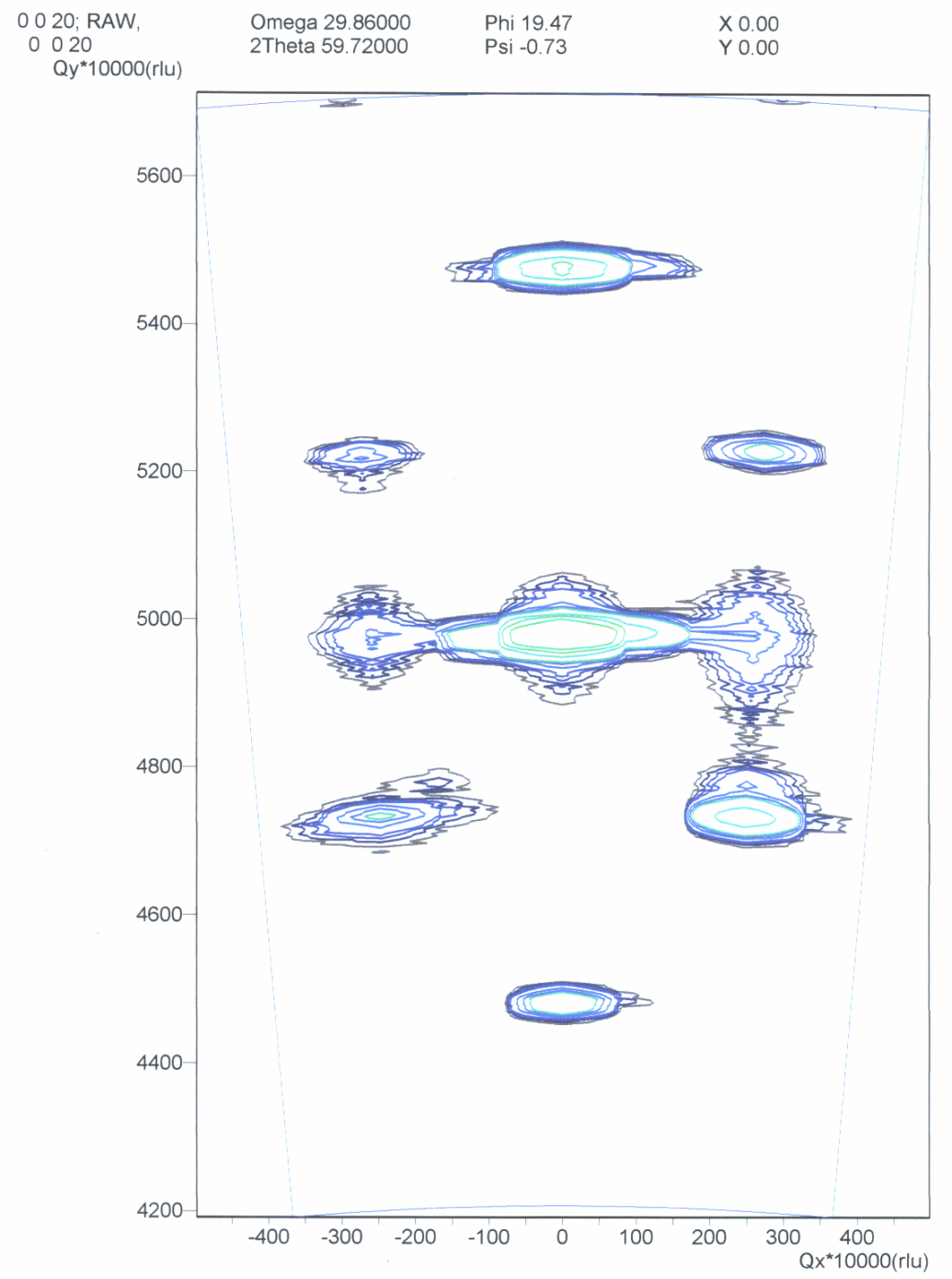

Figure 47 Reciprocal space map of the (0 0 20) peak. Single crystal Bi-2212 P_{O2} (21%), as cleaved.

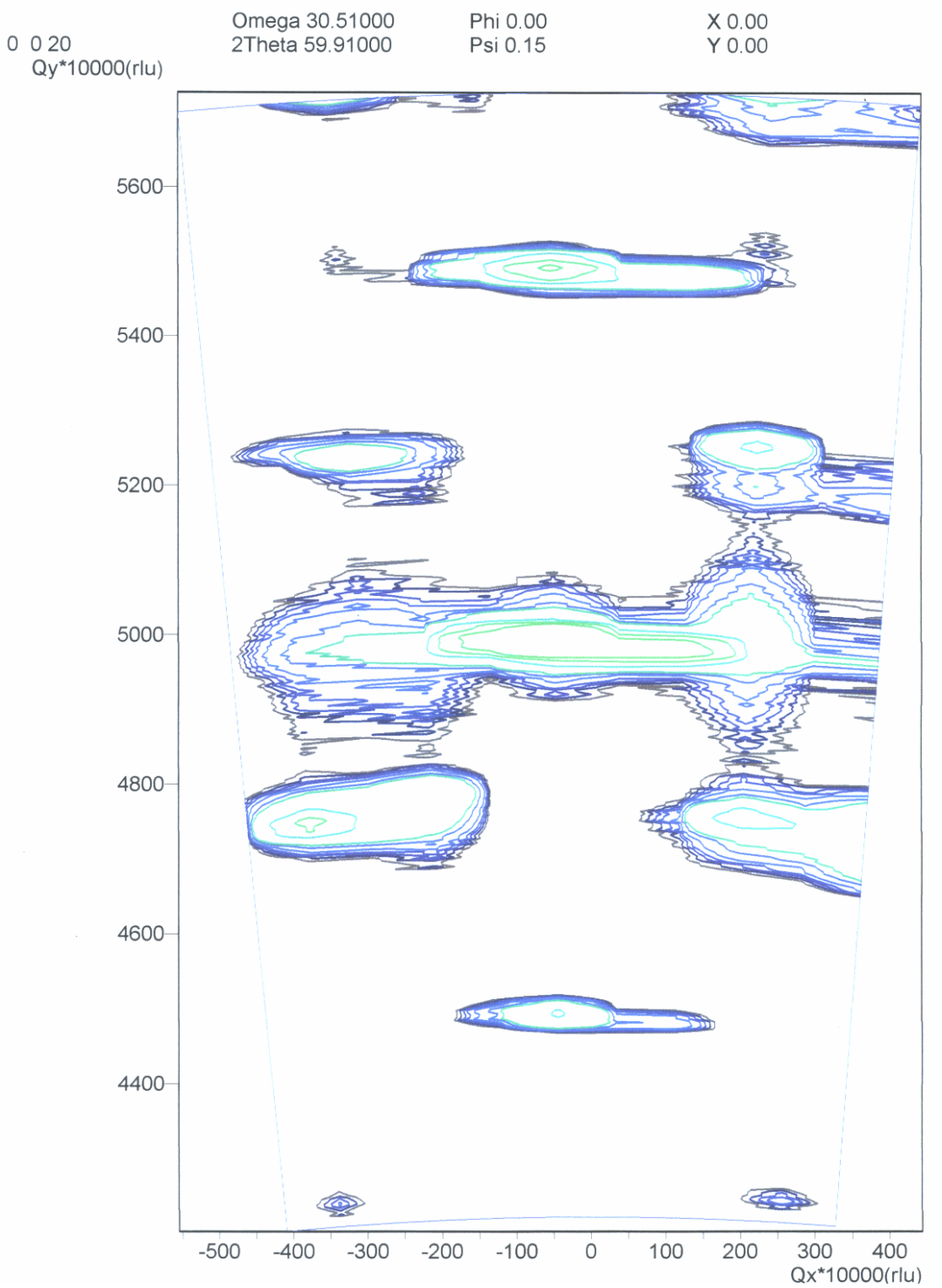

Figure 48 Reciprocal space map of the (0 0 20) peak. Single crystal Bi-2212 annealed in pure Ar (99.999%) 780 ˚C, as cleaved.

The use of Rietveld analysis is the predominate method of the unknown structure determination, and had played important role in elucidating the structure of high temperature superconductors. Though primarily meant to be used for neutron diffraction analysis, Rietveld analysis was also adopted for XRD analysis. The Rietveld method is based on the comparison and adjustment of calculated pattern to the experimental pattern (θ - 2θ). The diffraction pattern is calculated from a series of structural parameters (space group, cell parameters, atomic coordinates etc) to which peak shape and width parameters (background, Lorentz polarization correction, etc) are added. The calculated pattern is than compared to the observed data. Parameters are readjusted by a least-square process until the best fit is obtained, such that the difference between the measured and calculated pattern is minimized. Within the framework of the “proper” Rietveld structure refinement method, intensities of the Bragg peaks in a powder diffraction pattern are estimated within certain constraints - unit cell symmetry and crystallographic space group. However, several spin-off Rietveld techniques had recently been developed that take into account entire pattern.

Detail of the XRD pattern and the fit obtained is show in Figure 49, black lines in the second row represent the calculated positions of fundamental reflections based on the Bbmb (Bb2b) space group (66), and the green lines represent the modulation. The third raw represents the difference between calculated and the experimental values.

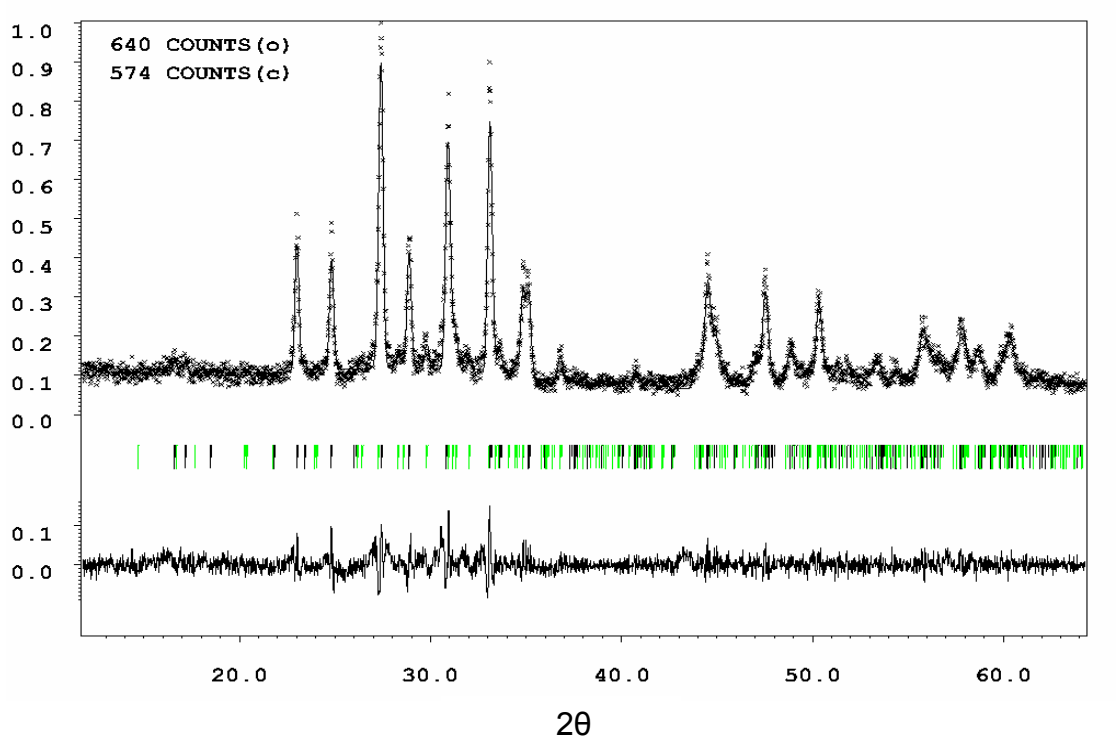

Figure 49 Determination of lattice parameters and modulation vector using Rietveld refinement software JANA 2000

The changes in lattice parameters a, b, c and the modulation vector q as a function of $SrCuO_2$ addition are shown in Figure 50. Addition of $SrCuO_2$ contributes to the sharp decrease of the a and c lattice parameters and the increase in b lattice parameter and the modulation vector.

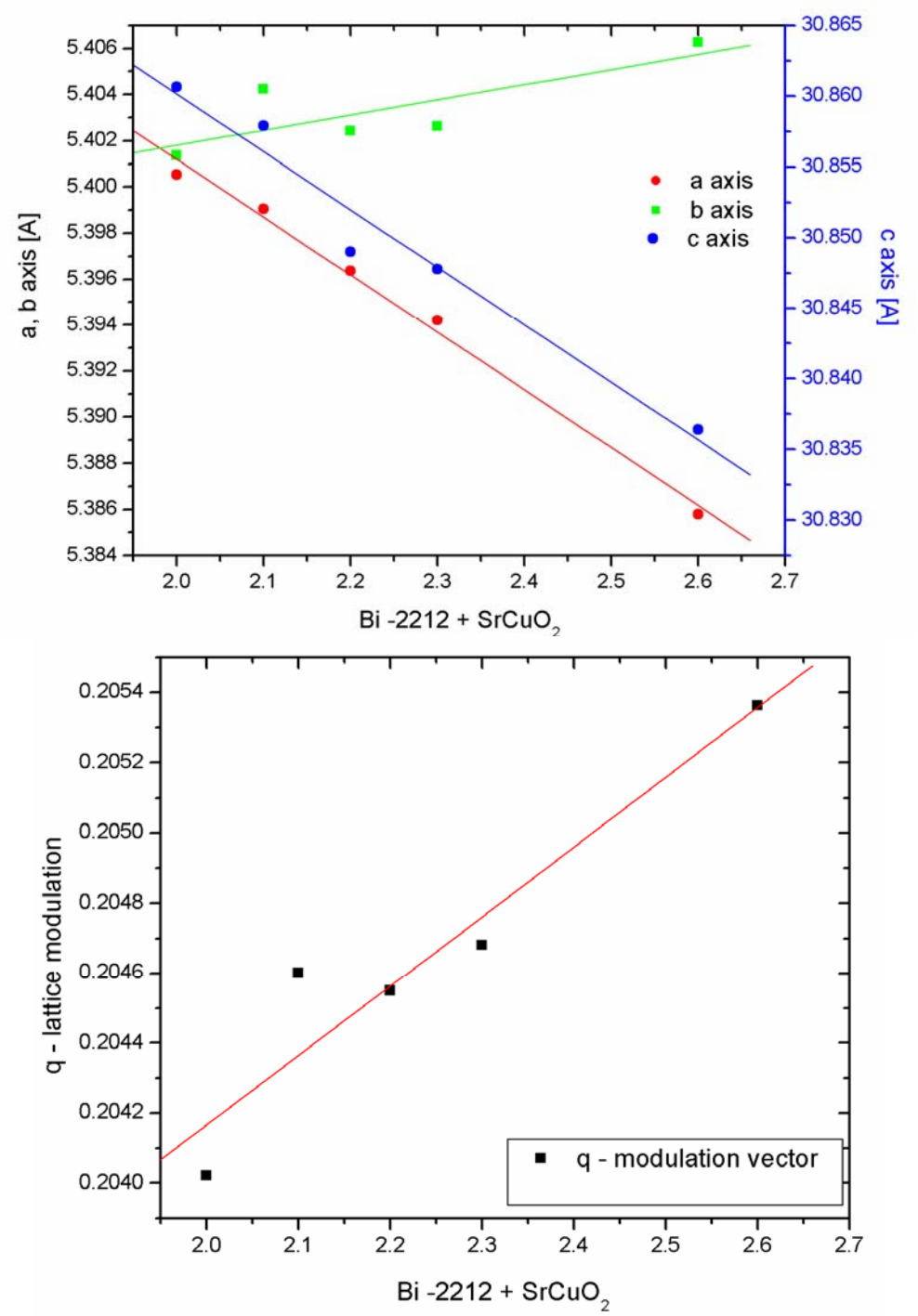

Figure 50 Lattice parameters a, b, c and lattice modulation vector q as a function of the $SrCuO_2$ added to Bi-2212, as determined by JANA 2000 Rietveld software. The lines represent linear fit to the data.

2.4.4 Influence of $Nd^{\bullet}_{Ca}$ substitution on the superconducting properties

To evaluate influence of the rare earth substitution on the pinning and structural properties of the Bi-2212 superconductors calcium cations were substituted by neodymium (Nd). Calcium cations occupy equivalent sites in the lattice as yttrium in YBCO materials. And though favorable pinning properties had been reported when Nd substitutes for Y, and several studies report increase in critical temperature in Bi-2212 materials, no systematic study with regard to the pinning was reported.

Measurements of the field-cooled and zero field cooled magnetization dependence on temperature, M(T), for the samples with various amounts of Nd substituted for Ca, are presented in Figure 51. The onset of superconductivity has a range Tc = 84-95K depending on the Nd substitution level. The maximum critical temperature as in the previous case of $SrCuO_2$ addition is 95K and corresponds to the optimally doped material see Figure 15, the critical temperature decreases with the increased substitution level. The subsequent systematic decrease in critical temperature could be attributed to overdoping induced by incorporation of additional oxygen necessary for the charge compensation within the Bi-2212 crystal structure. This observation disagrees with previous studies, however it should be noted that the starting critical temperature those studies is T_C=74-85K which is well below optimal value.

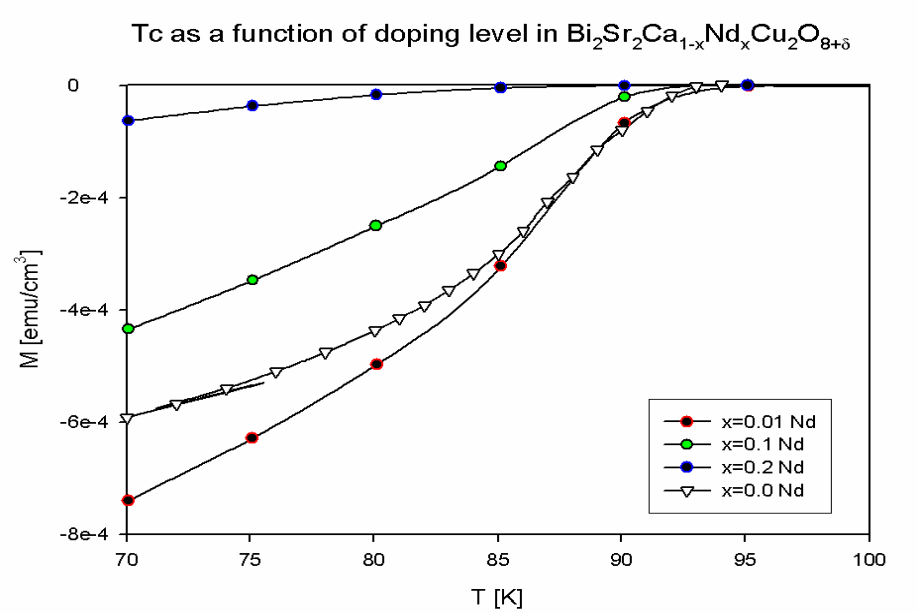

Figure 51 Magnetization – temperature curves as a function of Nd substitution under H = 10 Oe; ▪ 0 mol% Nd_{ca} ●10 mol% Nd_{ca} ▲ 20 mol% Nd_{ca} ▼30 mol% Nd_{ca}

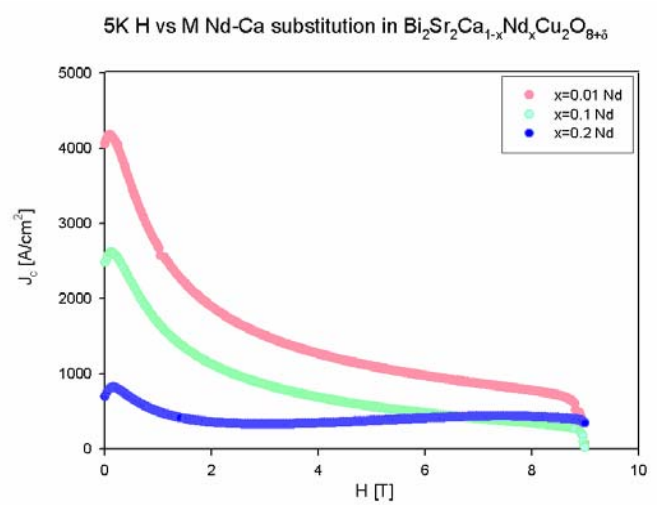

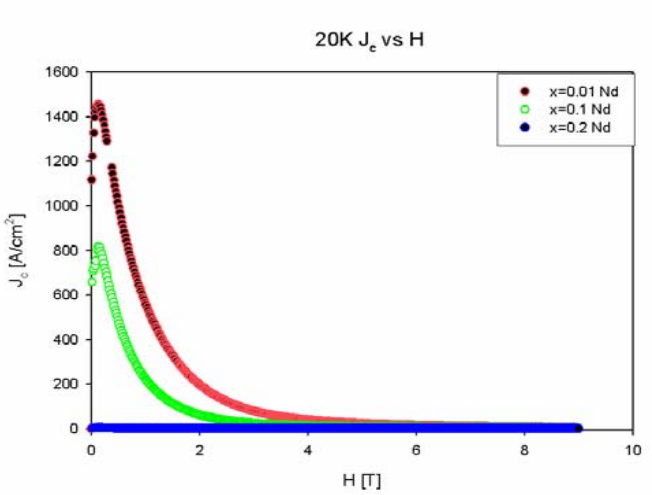

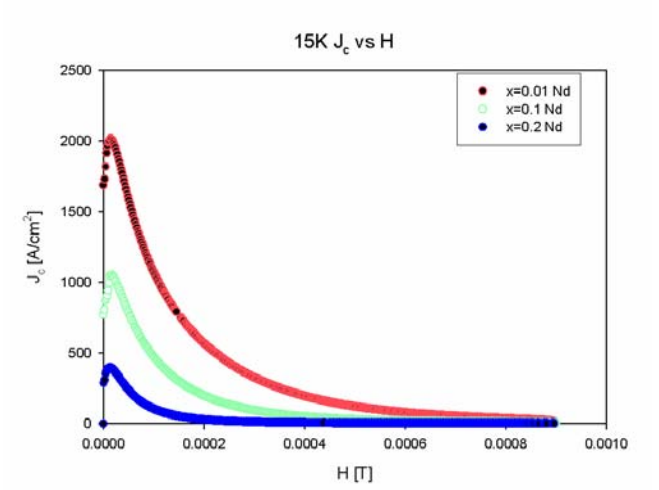

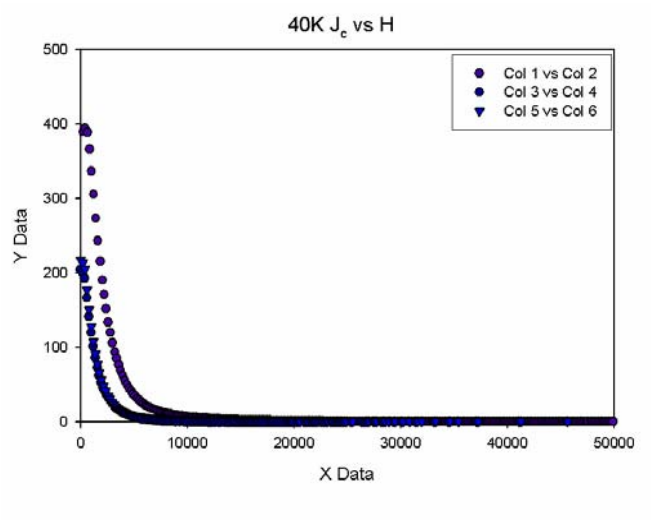

Figure 52 J_C-H curves for different Nd_{Ca} substitution levels

2.4.5 Defect energy calculation

Molecular modeling and simulation represent one of the important techniques in condensed matter physics, chemistry and materials science. Although idea of molecular modeling is not new, the recent increases of computer processor speed has allowed modeling of complex systems. Empirical models, utilizing pair potential functions (Lennard-Jones, Morse, Buckingham etc.) that describe interactions between pairs of atom (ions) are intended to model physical properties of materials. The lattice is described in terms of effective potentials interactions and consist of long and short-range Coulombic forces. Structure, energy, mechanical and electric properties of perfect and imperfect crystals can be calculated as well as dynamic properties under various conditions. The caveat, however, is prior accurate determination of interatomic potentials, whether in molecular mechanics or quantum mechanical simulations.

Pair potentials generally consist of two terms accounting for the short range and long range interactions. Interaction between two atoms are described as attractive at large separations, but strongly repulsive at close range. Expressions for the electrostatic interactions follow a Coulomb law, which is always attractive for partial charges of opposite sign and always repulsive for partial charges of equal sign.

The most commonly used interatomic potential functions are based on ether the Lennard – Jones, or Buckingham potential [66, 67]:

$$\Phi_i(r) = -\frac{A}{r^6} + \frac{B}{r^n}$$

where A and B represent constants, $\frac{A}{r^6}$ represent attractive interaction and $\frac{B}{r^n}$ with n=12 repulsive part, r is the distance between the pair of atoms. Lennard - Jones potentials are usually used to simulate noble gases (Ar, Ne, Xe etc) and to make initial qualitative estimates.

The Buckingham potential, was developed using the Born-Mayer [66] potential, and is expressed as:

$$\Phi_i(r) = Ae^{\frac{r}{\rho}} - \frac{B}{r^6}$$

Parameters A, B and ρ represent constants and are fitted for each type of interparticle interaction. The first term represents repulsive interaction between the pair of ions, and the value of A is mainly governed by ionic radius, ρ is the repulsive range. The second term represents the attractive term where B relates to the van der Waals interactions. These interatomic potentials are empirical, that is, the parameters describing the interactions are fitted to the experimentally known properties (lattice constants, elastic constants, etc) until the smallest deviation is observed. One of the important aspects of the fitted potentials is that they are conceived as interchangeable between different types of materials (Sr-O potential can be used in calculations of SrO, $SrTiO_3$). Lennard-Jones and Buckingham potentials used in empirical models also account for polarization by incorporating a shell model [68] where ions are considered to consist of a charged core where the entire mass of the ion is located and a massless charged shell coupled by a spring force constant, k. The sum of the core and shell charge is equal to the formal charge of the ion. The ion polarizability can be expressed as:

$$\alpha = \frac{1}{4\pi\varepsilon}\left(\frac{Y^2}{k}\right)$$

Lattice modeling begins with simulation of a perfect lattice; lattice energy is minimized with respect to the unit cell lattice vectors and ion positions taking into account volume or pressure at which the simulations are performed. Upon establishing the minimum in energy of the lattice, defects are introduced and the lattice is allowed to relax. The effect is confined to a short distance from the defect, which is allowed by the use of a Mott-Littleton approach when calculating defect energies. The premise of the Mott–Littleton approach is division of the crystal into two concentric spherical regions. In the central region surrounding the defect, the introduction of defect imposes large changes in the surrounding lattice. Lattice relaxation within region I is treated through precise energy minimization in which the positions of all atoms within the region are adjusted by applying interatomic potentials until all atoms are in equilibrium. The importance of region size selection is presented for the region I in Figure 53 for the case of vacancies on oxygen sites in YBCO. It can be seen that the selection of region I strongly influences calculated defect energies and that the regions size should be adjusted to allow minimum of the defect energies irrespective of the increase of computation intensiveness. It can also be seen that the increase in region I size leads to treatment of a high number of ions, and though computational time is increased to hours, it is still significantly lower than if the ab-initio method was applied for the same number of particles.

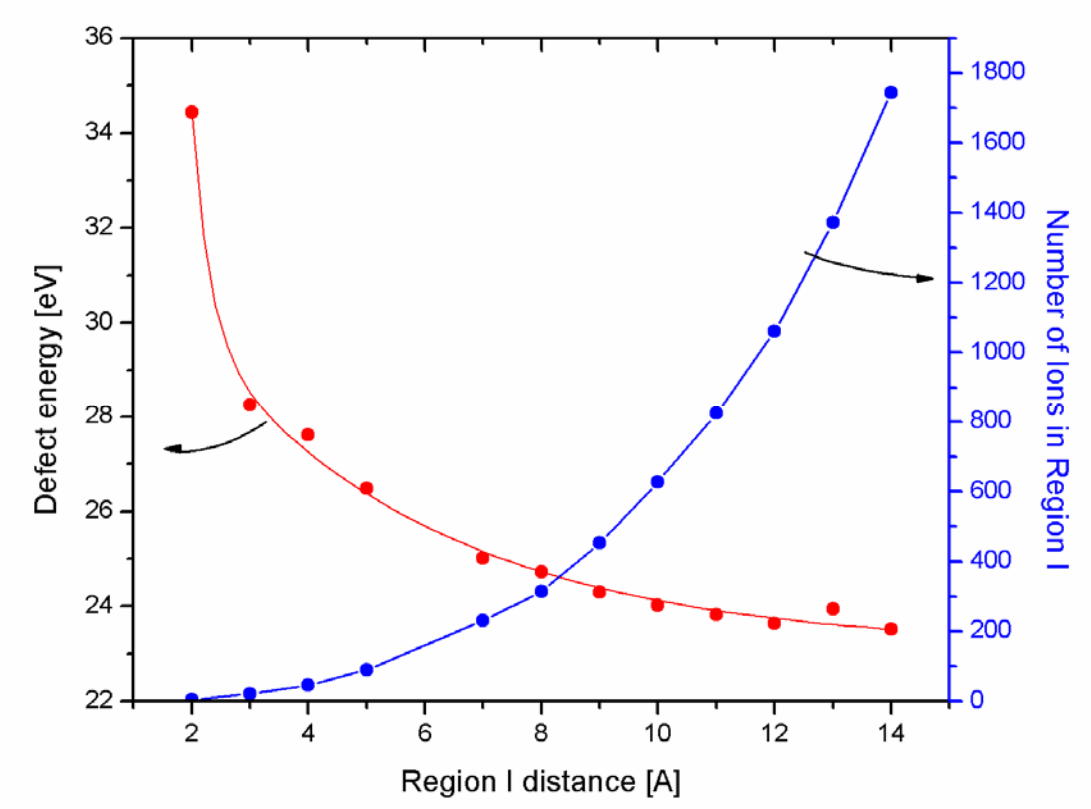

Figure 53 Influence of region I size on defect energies, number of ions used in calculation as a function of region I size. Calculated for the $V^{\bullet\bullet}_{O}$ in YBCO using GULP.

The second region represents the interface between the “defected” region I and the continuum. The influence of defect on ions in this region is negligible and while explicit calculations are performed in region I the calculations are more approximate in the II region.

As previously discussed, crystal defects in superconducting materials can pin flux vortices. Although accurate experimental determination of point defect energies in ionic materials is very difficult, if not impossible task. Empirical models can determine qualitative representation of processes and final states.

2.4.5.1 Defect chemistry and properties in $YBa_2Cu_3O_{6+x}$ (x=0-1) and $Bi_2Sr_2CaCu_2O_{8+\delta}$

Atomistic simulation has been applied to different superconducting materials and defect energies in La_2CuO_4, $YBa_2Cu_3O_{6+x}$ and $YBa_2Cu_4O_{8+x}$ [51-62] have been calculated. Several transferable empirical pair-potential models in the YBCO system have been developed by Baetzold [51-57] that show good correlation between calculated and experimental structural and bulk properties. The calculation of defect energies and bulk properties is repeated for a new set of potentials developed by Baetzold [58] using a general utility lattice program (GULP)[64]. For a zone I radius of 10Å and zone II of 24Å the calculated lattice energy is –260.10 eV, total monopole-monopole contribution (Coulomb energy) is -290.31 eV, and the remainder is contributed by interionic potential energy 30.20 eV (short range interionic repulsion). An example of the GULP input-output files is given in the appendix for the case of initial lattice energy and bulk properties calculation. The summary of calculated values for lattice energy, lattice parameters, interionic distances, elastic constants etc. is given in Table 4 where experimentally determined properties are also shown for comparison. Experimental values shown were obtained for single-phase polycrystalline samples at 10K using neutron diffraction, bond lengths and lattice parameters were refined by Rietveld refinement. The basic defect energies are given in

Table 5. Defect energies are described as energy needed to remove the ion from the bulk to the infinity.

Table 4 Calculated and experimentally obtained bond lengths and lattice parameters for YBCO

	Calculated	***F. Beech [69]***	***Jorgensen [70]***
Y-O	***2.394***	***2.386***	***2.376***
Y-O	***2.402***	***2.407***	***2.4038***
Ba-O	***2.957***	***2.883***	***2.866***
Ba-O	***2.944***	***2.964***	***2.9806***
Ba-O	***2.894***	***2.944***	***2.9573***
Ba-O	***2.734***	***2.74***	***2.7345***
Cu(1)-O	***1.940***	***1.94***	***1.9406***
Cu(1)-O	***1.834***	***1.847***	***1.8596***
Cu(2)-O	***1.925***	***1.926***	***1.9258***
Cu(2)-O	***1.944***	***1.957***	***1.9599***
Cu(2)-O	***2.298***	***2.299***	***2.2676***
a [A]	***3.823***	***3.8174***	***3.81196***
b [A]	***3.851***	***3.8804***	***3.8813***
c [A]	***11.706***	***11.652***	***11.64028***
V [A^3]	***172.3***	***172.6015***	***172.222***

Table 5 Calculated defect formation energies for $YBa_2Cu_3O_{7-x}$

Defect	Final energy [eV]	Defect	Final energy [eV]
V_Y	54.49	V_{Ba}-Ba_{i_2}	19.46
V_{Ba}	18.99	V_{Cu}-$Cu_{\_1}$	-14.06
V_{Cu1}	26.49	V_{Cu}-$Cu_{\_2}$	-15.71
V_{Cu2}	28.49	V_{Cu1}-$Cu_{\_1}$	11.22
V_{O1}	20.56	V_{Cu1}-$Cu_{\_2}$	-248.86
V_{O2}	20.93	V_O-O_{i_1}	-2.14
V_{O3}	18.04	V_O-O_{i_2}	0.00
V_{O4}	18.43	V_{O1}-O_{i_1}	DNC
Y_{i_1}	DNC	V_{O1}-O_{i_2}	0.84
Y_{i_2}	-23.83	V_{Os}-Os_{i_1}	-1.18
Ba_{i_2}	4.95	V_{Os}-Os_{i_2}	0.46
Ba_{i_1}	0.02	V_{Os1}-Os_{i_1}	-1.09
Cu_{i_1}	-14.06	V_{Os1}-Os_{i_2}	0.72
Cu_{i_2}	-15.71	VBa-Bai_1	19.46
O_{i_1}	-16.45	V_Y-Y_{i_2}	15.08
O_{i_2}	-10.48		
Os_{i_1}	-14.11		
Os_{i_2}	-13.98		
V_Y-Y_{i_1}	DNC		

Several implications of the calculated defect energies are readily observable. Vacancy formation energies on the cation sublattice are much higher than on the anion sublattice, in particular formation of $V_Y^{\bullet\bullet\bullet}$ is highly unlikely. On the anion sublattice, the lowest vacancy formation energies are observed on the O-3 sites. Interstitial ions can be placed at O-5 (0.5 0 0) and O-6 (0 0.5 0) sites it can be seen that while the lowest oxygen interstitial formation energies are observed on O-5 sites, converse is true for cation interstitial formation. It must be noted that the elastic or bulk modulus increases as the compressibility or deformability of the material decreases. The bulk modulus represents the measure of resistance of a material to deformation, computational substitution studies may be use as a guide, in which direction synthesis should go, particularly in the case of YBCO. It can be seen that though superconducting properties stay the same for isovalent rare earth – Y substitution, bulk modulii significantly change.

For the case of $Bi_2Sr_2CaCu_2O_{8+\delta}$ pair potential parameters were adopted with Baetzold's help from the work of Kovaleva et al [71]. The model was originally derived by Prade [72] based on the Tarascon [25] proposed tetragonal crystal structure. Although Tarascon's structural model assumes a idealized tetragonal crystal structure, and does not account for the occupational modulation, the pair potential parameters provide good qualitative description. Upon relaxation of the crystal structure equilibrium metal oxygen bond lengths were extracted and are given in Table 6. The experimentally determined bond lengths are presented and the difference shown. Vacancy formation energies as well as interstitial formation energies were calculated. Oxygen interstitial positions were considered to be at I_{O4}

(0.5 0.0 0.25) lying between Bi-O3 planes, considered to be the source of modulation in BSCCO materials and I_{O5} (0.5 0.5 0.0), which is in the center between Ca ions.

Table 6 Calculated and experimentally obtained bond lengths and lattice parameters for $Bi_2Sr_2CaCu_2O_{8+\delta}$

	Tarascon	***GULP***	***Difference***
Ca-O	***2.525***	***2.555***	***0.03***
Sr-O	***2.565***	***2.557***	***0.01***
Sr-O	***2.742***	***2.845***	***0.10***
Sr-O	***2.911***	***2.991***	***0.08***
Bi-O	***2.227***	***2.007***	***0.22***
Bi-O	***2.711***	***2.772***	***0.06***
Bi-O	***2.9711***	***2.827***	***0.14***
Cu-O	***1.911***	***1.992***	***0.08***
Cu-O	***2.168***	***1.816***	***0.35***
a	***3.814***	***3.949***	***0.14***
b	***3.814***	***3.949***	***0.14***
c	***30.52***	***29.61***	***0.91***

Table 7 Calculated defect formation energies for $Bi_2Sr_2CaCu_2O_{8+\delta}$

Defect	*Defect Energy [eV]*
VBi	***28.74***
VSr	***14.85***
VCa	***43.94***
VCu	***8.00***
VO1	***12.79***
VO2	***22.99***
VO3	***22.32***
IO5	***-2.57***
Sr-Cu	***16.61***
Cu-Sr	***11.53***
Sr-Ca	***-16.11***
Cu-Ca	***11.52***

It can be seen from Table 7 that oxygen interstitials are associated with the lowest defect energies and that the formation of oxygen interstitials on site I-5 that is between the Bi-O planes is the most favorable. This is in agreement with experimental findings that attribute origin of modulation to the interstitial positions between Bi-O planes. It can also be seen that the formation energies of Sr_{Ca} on sites are lower than Sr_{Cu} on sites which was also confirmed experimentally.

If the reference state of $Bi_2Sr_2CaCu_2O_{8+\delta}$ is defined to be $\delta = 0$, based on its p-type conduction and inability to form stable compound at $\delta < 0$, oxygen incorporation would lead to formation of interstitial sites.

Universal defect model for the YBCO [73] and BSCCO type superconductors for the oxygen incorporation, desorption :

$$\frac{1}{2}O_2 + V_i = O_i'' + 2h^{\bullet} \qquad K_{ox} = \frac{[O_i'']p^2}{P_{O_2}^{\frac{1}{2}}}$$

$$O_i'' + 2h^{\bullet} = O_i' + h^{\bullet} = O_i^x \qquad K_1 = \frac{[O_i^{/}]\ p}{[O_i^x]} \qquad K_2 = \frac{[O_i^x]}{P_{O_2}^{\frac{1}{2}}}$$

$$0 = e + h \qquad K_i = np$$

Zone I

$$[O_i' - V_i] = const$$

$$[O_i'] = [V_O^{\bullet}]$$

$$[O_i^x] = P_{O_2}^{\frac{1}{2}} \frac{1}{K_2}$$

$$\log[O_i^x] \propto \frac{1}{2}\log P_{O_2}$$

$$p = \frac{K_1[O_i^x]}{[O_i^{/}]} = \frac{K_1 K_2 P_{O_2}^{\frac{1}{2}}}{[O_i^{/}]} = K_p P_{O_2}^{\frac{1}{2}}$$

$$\log p \propto \frac{1}{2}\log P_{O_2}$$

$$n = \frac{K_i}{K_p P_{O_2}^{\frac{1}{2}}} = \frac{K_n}{P_{O_2}^{\frac{1}{2}}}$$

$$\log n \propto -\frac{1}{2}\log P_{O_2}$$

$$[O_i''] = \frac{K_{ox}}{p^2} P_{O_2}^{\frac{1}{2}} = \frac{K_{ox}}{\left(K_p P_{O_2}^{\frac{1}{2}}\right)^2} P_{O_2}^{\frac{1}{2}} = \frac{K_{ox}}{K_p^2} P_{O_2}^{-\frac{1}{2}}$$

$$\log[O_i''] \propto -\frac{1}{2}\log P_{O_2}$$

$$[O_i''] = P_{O_2}^{\frac{1}{2}} \frac{K_5}{p^2} = P_{O_2}^{\frac{1}{2}} \frac{K_5}{P_{O_2} K_p^2} = \frac{1}{P_{O_2}^{\frac{1}{2}}} \frac{K_5}{K_p^2} = \frac{1}{P_{O_2}^{\frac{1}{2}}} K_6$$

$$\log[O_i''] \propto -\frac{1}{2}\log P_{O_2}$$

ZONE II

$$[O_i'] = h^{\bullet}$$

$$\left[O_i^x\right] = P_{O_2}^{\frac{1}{2}} \frac{1}{K_2}$$

$$\log\left[O_i^x\right] \propto \frac{1}{2}\log P_{O_2}$$

$$K_1 = \frac{\left[O_i^{/}\right] p}{\left[O_i^x\right]} = \frac{\left[O_i^{/}\right]^2}{\left[O_i^x\right]} = \frac{\left[O_i^{/}\right]^2}{K_2 P_{O_2}^{\frac{1}{2}}}$$

$$\left[O_i'\right] = \sqrt{K_1 K_2}\, P_{O_2}^{\frac{1}{4}}$$

$$\log\left[O_i'\right] \propto \frac{1}{4}\log P_{O_2}$$

$$p = \frac{K_1\left[O_i^x\right]}{\left[O_i^{/}\right]} = \frac{K_1 P_{O_2}^{\frac{1}{2}}}{p} = \frac{K_1}{p} P_{O_2}^{\frac{1}{2}}$$

$$\log p \propto \frac{1}{4}\log P_{O_2}$$

$$\log n \propto -\frac{1}{4}\log P_{O_2}$$

$$\left[O_i''\right] = \frac{K_{ox}}{p^2} P_{O_2}^{\frac{1}{2}} = \frac{K_{ox}}{\left(K_1 P_{O_2}^{\frac{1}{2}}\right)} P_{O_2}^{\frac{1}{2}} = \frac{K_{ox}}{K_1} P_{O_2}^{0} \propto const$$

Defect Type	***Zone***	
	I	***II***
	$[O_i'] = [V_O^{\bullet}]$	$[O_i'] = h^{\bullet}$
n	***-1/2***	***-1/4***
p	***1/2***	***1/4***
$[O_i^x]$	***1/2***	***1/2***
$[O_i']$	***0 (const)***	***1/4***
$[O_i'']$	***-1/2***	***0 (const)***

Consequently substitution of lower valence state ions will increase charge density and vice versa.

i.e. $2sCaO + \frac{s}{2}O_2 \xrightarrow{YBa_2Cu_3O_{6+x}} 2sCa_Y^{/} + 2sh^{\bullet} + 3sO_O^x + 2sV_{Cu}^{//} + 2sV_O^{\bullet\bullet}$

i.e. $zY_2O_3 + \frac{3z}{2}O_2 \xrightarrow{YBa_2Cu_3O_{6+x}} 2zY_{Ba}^{\bullet} + zO_i^{//} + 2zO_O^x + 2zV_{Cu}^{//} + \frac{z}{2}V_O^{\bullet\bullet}$

conversely case of $Bi_2Sr_2CaCu_2O_{8+\delta}$:

$zBi_2O_3 + \frac{z}{2}O_2 \xrightarrow{Bi_2Sr_2CaCu_2O_{8+\delta}} 2zBi_{Sr}^{\bullet} + zO_i^{//} + 2zO_O^x + 2zV_{Cu}^{//} + \frac{z}{2}V_O^{\bullet\bullet}$

$2sPbO + \frac{s}{2}O_2 \xrightarrow{Bi_2Sr_2CaCu_2O_{8+\delta}} 2sPb_{Bi}^{/} + 2sh^{\bullet} + 3sO_O^x + 2sV_{Cu}^{//} + sV_O^{\bullet\bullet}$

Additional oxygen is introduced in the structure through oxygenation, oxygen than occupies interstitial ion sites in the crystal and produces holes for charge neutrality.

2.5 CONCLUSIONS

Phase pure Bi-2212 polycrystalline superconductors were synthesized from a stoichiometric precursor with T_c = 94K without post annealing. The extent of solid solution for the Bi-2212 phase depends intimately on the synthesis conditions, the use of freeze-drying and calcining in 7% oxygen atmosphere allows creation of the phase pure material. Calcination in atmospheres with higher oxygen partial pressure (21%, 100%) did not produce phase pure samples, furthermore annealing at higher oxygen partial pressures leads to decomposition of the Bi-2212 phase.

The effect of $SrCuO_2$ additions on the critical current density and microstructure of Bi-2212 compound were determined. The X-ray diffraction patterns showed that the formation of Bi-2212 is not influenced by the presence of "$SrCuO_2$" additions in the precursor solution, i.e. no additional peaks belonging to second phases were detected. It was also demonstrated that an increase of $SrCuO_2$ content does not appreciably change the Bi-2212 grain size or form a glassy phases around individual grains. It was observed from the XRD results that the lattice and modulation parameters change with the introduction of $SrCuO_2$, i.e. a and c lattice parameters decreasing and b and modulation vector increasing as a function of $SrCuO_2$ addition.

The critical temperatures determined by SQUID magnetometry show dependence of the "$SrCuO_2$" addition level, an increase of added $SrCuO_2$ lowers the critical temperature and broadens the transition. Magnetization measurements indicate that $SrCuO_2$ additions are incorporated into the structure of the Bi2212

phase. Intergranular critical current density, J_c, determined by the Bean model shows increased sensitivity to the "$SrCuO_2$" content. The maximum supercurrent density $J_c(0)$ = 30 kA/cm^2 was observed in the sample containing an addition of 0.001 mole % of $SrCuO_2$.

The effect of Nd substitution on Ca sites was quantified in terms of critical current density, lattice parameters and critical temperature for $Bi_2Sr_2Ca_{1-x}Nd_xCu_2O_{8+\delta}$ (x = 0–4). It was observed that both the critical temperature and critical current density drop precipitously as a function of Nd substitution. Though these observations are in conflict with recent and earlier published data, it should be noted that comparisons were made with respect to optimally doped samples which can be deduced from the high reported critical temperatures of T_c=94K. The observed decrease in critical temperature is consistent with overdoping of the parent phase, as more Nd is being substituted for Ca, more oxygen interstitials are being introduced in and consequently more electron holes are being generated which leads to overdoping of the optimally doped material.

Finally, a universal defect model for oxygen incorporation in cuprate superconductors is proposed. It had been shown through defect energy calculation that formation of defect complexes of aliovalent cation substitution coupled with oxygen interstitial formation leads to the lowest defect energies. Appropriate Brower diagrams were calculated and presented.

APPENDIX A

SYNTHESIS

Freeze-drying

$Bi_2Sr_2CaCu_2O_x$ (Bi-2212), $SrCuO_2$, and $Bi_2Sr_{2+y}CaCu_{2+y}O_x$ (y=0.001-0.6) samples were prepared by a freeze-drying procedure, i.e. reagent grade Bi_2O_3, $SrCO_3$, $CaCO_3$ and CuO were dissolved in nitric acid-deionized water mixture in the appropriate molar ratio. The pH value was adjusted to prevent back melting during freeze drying, the light blue solutions were subsequently splat-frozen onto a Teflon coated copper block pre-cooled to liquid nitrogen temperature (77K). The pale blue slush was homogenized with homogenizer and freeze-dried for 3 days in an Edwards commercial freeze-drier starting with a temperature – 40^0C and pressure 0.001 mbar with slow increase in temperature over three days to 40^0C. The resulting green-blue powder was then quickly transferred to vacuum oven where the water of hydration was removed by heating the powder to 130^0C in approximately 15 mmHg low vacuum and flowing argon. The green powder was analyzed by X-ray diffraction (XRD) and scanning electron microscopy (SEM) as well as differential thermal analysis (DTA) for each sample composition in order to determine proper annealing and sintering cycles. It was established that denitration should be performed at

600^0C in 100% O_2 followed by flash heating above 800^0C in 7%O_2. Phase pure 2212 samples were obtained after five hours as determined by XRD and SEM.

Magnetic characterization of the samples was performed with a commercial SQUID-magnetometer Quantum Design MPMS II. Measurements were performed using a 3-cm scan length in order to keep samples in a homogeneous magnetic field.

APPENDIX B

Solid state preparation route conditions

Initial powders	Calcination Time [h]/Temperature[C]	Atmosphere	Reference
Bi_2O_3, $SrCO_3$, $CaCO_3$, CuO	3 x 12 / 820		269
Bi_2O_3, $SrCO_3$, $CaCO_3$, CuO	3 / 800-850	air	270, 271
Bi_2O_3, $Sr(NO_3)_2$, CaO, CuO	3 x 24 / 800-850	air	4272
Bi_2O_3, $SrCO_3$, $CaCO_3$, CuO	32-109 / 840-860 8 / 840-860	air air	273
Bi_2O_3, $SrCO_3$, $CaCO_3$, CuO	2 x 18 / 820 2 / 865		274
Bi_2O_3, $SrCO_3$, $CaCO_3$, CuO	2 x 24 / 750 / 800 66 / 820 174 / 850	air	275
Bi_2O_3, $SrCO_3$, $CaCO_3$, CuO	2 x 12 / 780 / 810 70 / 820	air air	276
Bi_2O_3, $SrCO_3$, $CaCO_3$, CuO	$\leq$ 24 / 700-830 $\leq$ 7 x 48 / 800-870 $\leq$ 7 days / 830	air	277
Bi_2O_3, $SrCO_3$, $CaCO_3$, CuO Nitrates			
	2 x 3 / 125 / 450 3 x 12 / 750-850 890 12 / 850	air air 21% O_2/N_2	279
Bi_2O_3, $SrCO_3$, $CaCO_3$, CuO	24 / 750 48 / 800 24 / 60 / 850	air	280
	15 / 670	N_2	
$Bi(OH)_3$, $Ca(OH)_2$ $Cu(OH)_2$, $Sr_2Cu(OH)_6$	4-10 / 700-800	2% O_2 in Ar	281

APPENDIX C

In this appendix, an example of the General Utility Lattice Program input and output files is given. These commands were used for the computer simulations presented in 2.4.4, and can serve as a template for future computational study using GULP. As discussed in 2.4.4 perfect crystal lattices (i.e. lattices which do not contain any defects) are initially simulated, upon which the lattice is removed from equilibrium by virtue of introducing a defect (vacancy, interstitial, complex defect). The lattice is allowed to relax, equilibrium energy is recalculated, the difference between the defective and perfect lattice representing the energy of a defect.

Sample GULP input files for simulation of perfect and defective lattice (V_Y) is given below:

conp opti defe comp phonon torsion

title

YBa2Cu3O7 potential developed 9-11-04 (Note: atoms labelled Os are O's at sites 1 and 4)

end

cell

3.8174 3.8804 11.65200 90.0 90.0 90.0 1 1 1 1 1 1

fract 26

```
Ba   core  0.5        0.50     -0.18540     -7.1173     1 1 1
Ba   shel  0.5        0.50     -0.18540      9.1173     1 1 1
Ba   core  0.5        0.50      0.18540     -7.1173     1 1 1
Ba   shel  0.5        0.50      0.18540      9.1173     1 1 1
Cu   core  0.0        0.00      0.35590      0.0        1 1 1
Cu   shel  0.0        0.00      0.35590      2.0        1 1 1
Cu   core  0.0        0.00     -0.35590      0.0        1 1 1
Cu   shel  0.0        0.00     -0.35590      2.0        1 1 1
Cu   core  0.0        0.00      0.0          0.0        1 1 1
Cu   shel  0.0        0.00      0.0          2.0        1 1 1
Y    core  0.5        0.50      0.5          0.0        1 1 1
Y    shel  0.5        0.50      0.5          3.00       1 1 1
Os   core  0.0        0.50      0.0          1.590933   1 1 1
Os  shel   0.0        0.50      0.0         -3.2576     1 1 1
Os  core   0.0        0.0      -0.158500     1.590933   1 1 1
Os  shel   0.0        0.0      -0.158500    -3.2576     1 1 1
Os  core   0.0        0.0       0.158500     1.590933   1 1 1
Os  shel   0.0        0.0       0.158500    -3.2576     1 1 1
O   core   0.0        0.50      0.377800     1.2576     1 1 1
O   shel   0.0        0.50      0.377800    -3.2576     1 1 1
O   core   0.0        0.50     -0.377800     1.2576     1 1 1
O   shel   0.0        0.50     -0.377800    -3.2576     1 1 1
O   core   0.5        0.0       0.377700     1.2576     1 1 1
```

```
O   shel    0.5          0.0          0.377700       -3.2576      1 1 1
O   core    0.5          0.0         -0.377700        1.2576      1 1 1
O   shel    0.5          0.0         -0.377700       -3.2576      1 1 1
centre fract   0.51 0.51 0.51
vacancy  fract 0.50  0.5  0.50
maxcycle 210
mode2a  4
size    8.00   21.00
species   1
library library.lib
```

Library of potentials used in this case is given below:

```
species
buck
O     shel Cu    shel     716.47       0.32698     0.00  0.0 20.0
buck
O     shel O     shel    22764.0       0.149        75.00  0.0 20.0
buck
O     shel Ba    shel     1671.37      0.359280    0.00  0.0 20.0
buck
O     shel Y     shel     1041.53      0.37129     0.00  0.0 20.0
buck
Cu    shel Ba    shel   11552.4        0.29373     0.00  0.0 20.0
```

buck

Os shel Ba shel 1366.19 0.34806 0.00 0.0 20.0

buck

Os shel Cu shel 5469.58 0.22432 0.00 0.0 20.0

buck

O shel Os shel 22764.0 0.1490 75.00 0.0 20.0

buck

Os shel Os shel 22764.0 0.1490 75.00 0.0 20.0

buck

Ba shel Ba shel 2663.7 0.2558 0.00 0.0 20.0

buck

O shel Ca shel 1228.9 0.3372 0.00 0.0 20.0

buck

Os shel Ca shel 1228.9 0.337200 0.00 0.0 20.0

spring

Ba 426.1

spring

Y 999999.

spring

Cu 999999.

spring

O 49.8

spring

Os 100.

Oxygen and barium polarisability was simulated by splitting the total charge of i.e. oxygen ion (-2.0) into a positive core (charge +1.590933 for the case of Os or +1.2576 for other oxygen ions) and a negative shell (charge –3.2576). Core and shell are linked by a spring, with spring constant *k*, as explained in the text.

APPENDIX D

VB MACRO

```
'Subroutine to split continuous data file into 5 sections.

Sub B_Split_Data()



Dim Volume
Dim TStr
Dim CSR 'CSR = Current Row in the original data set
Dim CSC 'CSR = Current column in the original data set
Dim ZRs(4) As Double 'Array containing the row numbers of all zeros.
Dim MaxMinV(3) As Double 'Values of max and mins.

Dim COR 'Current output row
Dim COC 'Current output column
Dim OutStartRow 'Row number to begin placing separated data.
Dim OutStartClm 'Column number to begin placing separated data.

Dim SgnChng As Boolean  'True if there is a change of sign instead of a 0.
Dim Found0 As Boolean   'True is a zero is found.

OutStartClm = 6
OutStartRow = 2

'Get volume
Volume = CDbl(InputBox("Enter volume", "Volume", 1))

'Finding the starting point
TStr = Cells(35, 1).Value
If InStr(1, TStr, "TIME", vbTextCompare) > 0 Then
  CSR = 2
  CSC = 2
Else
  CSR = 2
  CSC = 3
End If

CSR = CLng(InputBox("Enter start row of data.", "Start Row", CSR))
CSC = CLng(InputBox("Enter column for field.", "Field Column", CSC))
```

```
'Find the row numbers for the zeros. Loop down through the rows until
'a zero is found but, if the next value is 0 don't stop.
Do While Cells(CSR + 1, CSC).Value = 0
  CSR = CSR + 1
Loop
'This is the place to begin.
ZRs(0) = CSR

'The next step is to look for the next zero or change of sign and find the maximum value within ‘that range. Start by initializing array values.
MaxMinV(1) = 0

'This time we look for the next zero or change of sign. If there is a zero immediately following that ‘one we have to find the last consecutive zero for the next starting point. If no zero is encountered ‘the position should be set so the split data contains the point opposite the split so it can be used ‘for interpolation.
SgnChng = False
Found0 = False
Do
  CSR = CSR + 1
  'Check for maximum value
  If MaxMinV(1) < Cells(CSR, CSC).Value Then MaxMinV(1) = Cells(CSR, CSC).Value
  'Check for sign change
  If Cells(CSR, CSC).Value * Cells(CSR + 1, CSC).Value < 0 Then SgnChng = True
  'Check for 0
  If Cells(CSR, CSC).Value = 0 Then Found0 = True
Loop Until (SgnChng) Or (Found0)
If SgnChng Then
  'If there is just a change of sign, increment CSR so the split data will contain the point on the ‘other side of the change of sign for interpolation.
  CSR = CSR + 1
  'This is the place to begin when spliting the data for set 2.
  ZRs(1) = CSR
  'Set the starting point for set 3 back 1, for interpolation point.
  ZRs(2) = CSR - 1
Else
  'This is the place to begin when spliting the data for set 2.
  ZRs(1) = CSR
  'Check to see if we need to skip extra zeros for the set 3 starting point.
  Do While Cells(CSR + 1, CSC).Value = 0
    CSR = CSR + 1
  Loop
  'Set the starting point for set 3.
  ZRs(2) = CSR
End If

'The next step is to look for the next zero and find the maximum value within that range. Start by ‘initializing array values.
MaxMinV(2) = 0

SgnChng = False
Found0 = False
Do
  CSR = CSR + 1
  'Check for maximum value
  If MaxMinV(2) > Cells(CSR, CSC).Value Then MaxMinV(2) = Cells(CSR, CSC).Value
```

```
  'Check for sign change
  If Cells(CSR, CSC).Value * Cells(CSR + 1, CSC).Value < 0 Then SgnChng = True
  'Check for 0
  If Cells(CSR, CSC).Value = 0 Then Found0 = True
Loop Until (SgnChng) Or (Found0)
If SgnChng Then
  'If there is just a change of sign, increment CSR so the split data will contain the point on the ‘other
side of the change of sign for interpolation.
  CSR = CSR + 1
  'This is the place to begin when spliting the data for set 4.
  ZRs(3) = CSR
  'Set the starting point for set 5 back 1, for interpolation point.
  ZRs(4) = CSR - 1
Else
  'This is the place to begin when spliting the data for set 4.
  ZRs(3) = CSR
  'Check to see if we need to skip extra zeros for the set 5 starting point.
  Do While Cells(CSR + 1, CSC).Value = 0
    CSR = CSR + 1
  Loop
  'Set the starting point for set 5.
  ZRs(4) = CSR
End If

'Find the last maximum value
MaxMinV(3) = 0
Do
  CSR = CSR + 1
  'Check for maximum value
  If MaxMinV(3) < Cells(CSR, CSC).Value Then MaxMinV(3) = Cells(CSR, CSC).Value
Loop While Cells(CSR, CSC).Value > 0

'Time to split up the data
'Section 1
CSR = ZRs(0) - 1
COR = OutStartRow
COC = OutStartClm
Cells(1, COC).Value = 0
Cells(COR, COC).Value = "Field (1)"
Cells(COR, COC + 2).Value = "Mag. (1)"
Do
  CSR = CSR + 1
  COR = COR + 1
  Cells(1, COC).Value = Cells(1, COC).Value + 1
  Cells(COR, COC).Value = Cells(CSR, CSC).Value
  Cells(COR, COC + 1).Value = Cells(CSR, CSC + 1).Value / Volume
Loop Until Cells(CSR, CSC).Value >= MaxMinV(1)

'Section 2
'Reverse order
CSR = ZRs(1) + 1
COR = OutStartRow
COC = COC + 2
Cells(1, COC).Value = 0
Cells(COR, COC).Value = "Field (2)"
Cells(COR, COC + 1).Value = "Mag. (2)"
```

```
Do
  CSR = CSR - 1
  COR = COR + 1
  Cells(1, COC).Value = Cells(1, COC).Value + 1
  Cells(COR, COC).Value = Cells(CSR, CSC).Value
  Cells(COR, COC + 1).Value = Cells(CSR, CSC + 1).Value / Volume
Loop Until Cells(CSR, CSC).Value >= MaxMinV(1)

'Section 3
CSR = ZRs(2) - 1
COR = OutStartRow
COC = COC + 2
Cells(1, COC).Value = 0
Cells(COR, COC).Value = "Field (3)"
Cells(COR, COC + 1).Value = "Mag. (3)"
Do
  CSR = CSR + 1
  COR = COR + 1
  Cells(1, COC).Value = Cells(1, COC).Value + 1
  Cells(COR, COC).Value = Cells(CSR, CSC).Value
  Cells(COR, COC + 1).Value = Cells(CSR, CSC + 1).Value / Volume
Loop Until Cells(CSR, CSC).Value <= MaxMinV(2)

'Section 4
'Reverse order
CSR = ZRs(3) + 1
COR = OutStartRow
COC = COC + 2
Cells(1, COC).Value = 0
Cells(COR, COC).Value = "Field (4)"
Cells(COR, COC + 1).Value = "Mag. (4)"
Do
  CSR = CSR - 1
  COR = COR + 1
  Cells(1, COC).Value = Cells(1, COC).Value + 1
  Cells(COR, COC).Value = Cells(CSR, CSC).Value
  Cells(COR, COC + 1).Value = Cells(CSR, CSC + 1).Value / Volume
Loop Until Cells(CSR, CSC).Value <= MaxMinV(2)

'Section 5
CSR = ZRs(4) - 1
COR = OutStartRow
COC = COC + 2
Cells(1, COC).Value = 0
Cells(COR, COC).Value = "Field (5)"
Cells(COR, COC + 1).Value = "Mag. (5)"
Do
  CSR = CSR + 1
  COR = COR + 1
  Cells(1, COC).Value = Cells(1, COC).Value + 1
  Cells(COR, COC).Value = Cells(CSR, CSC).Value
  Cells(COR, COC + 1).Value = Cells(CSR, CSC + 1).Value / Volume
Loop Until Cells(CSR, CSC).Value >= MaxMinV(3)

End Sub
```

```
'Subroutine to perform interpolation of data for 4th and 5th
' data series (positive and negative sides of the hysteresis loop.
' The routine uses the field values from the 2nd and 3rd data sets
' as the field for the interpolation of the other sets.
Sub C_Interp_Data()

Dim RefFieldRow   'Row number in reference field column
Dim RefLastRow    'Last row for reference field
Dim RefFieldClm   'Column number for reference field
Dim IntFieldRow   'Row number in interpoled data field column
Dim IntLastRow    'Last row for interpoled data field
Dim IntFieldClm   'Column number for interpoled data field

Dim COC           'Current output column

'Initialize values for 2nd and 4th sets.
RefFieldRow = 2
RefFieldClm = 8
IntFieldRow = RefFieldRow + 2
IntFieldClm = 14
COC = 17

'Calculate last rows
RefLastRow = Cells(1, RefFieldClm).Value + RefFieldRow + 1
IntLastRow = Cells(1, IntFieldClm).Value + IntFieldRow - 1

'Write column headings
Cells(RefFieldRow, COC).Value = "Field (2)"
Cells(RefFieldRow, COC + 1).Value = "Mag. (2)"
Cells(RefFieldRow, COC + 2).Value = "Interp. (5)"
Cells(RefFieldRow, COC + 3).Value = "Diff. (2,5)"
Cells(RefFieldRow, COC + 4).Value = "Sum (2,5)"
RefFieldRow = RefFieldRow + 1

'Copy 0 field values before attempting interpolation.
If Cells(RefFieldRow, IntFieldClm).Value = 0 Then
  Cells(RefFieldRow, COC).Value _
    = Cells(RefFieldRow, RefFieldClm).Value
  Cells(RefFieldRow, COC + 1).Value _
    = Cells(RefFieldRow, RefFieldClm + 1).Value
  Cells(RefFieldRow, COC + 2).Value _
    = Cells(RefFieldRow, IntFieldClm + 1).Value
  Cells(RefFieldRow, COC + 3).Value _
    = Cells(RefFieldRow, COC + 1).Value _
    - Cells(RefFieldRow, COC + 2).Value
  Cells(RefFieldRow, COC + 4).Value _
    = Cells(RefFieldRow, COC + 1).Value _
    + Cells(RefFieldRow, COC + 2).Value
'Else
'  RefFieldRow = RefFieldRow + 1
'  IntFieldRow = RefFieldRow + 1
End If

RefFieldRow = RefFieldRow + 1
```

```
'Find interpolated values from interpolation data set.
Do
  'Increment row number of data set to interpolate until the current
  ' field value in the interp. set is >= to the reference field.
  Do _
  While (Cells(RefFieldRow, RefFieldClm).Value _
      > Cells(IntFieldRow, IntFieldClm).Value) _
  And (IntFieldRow < IntLastRow)
    IntFieldRow = IntFieldRow + 1
  Loop
  'Check to see if the current interp. field is the same as the
  ' reference field. If it is just copy the value to the new set.
  If Cells(RefFieldRow, RefFieldClm).Value _
   = Cells(IntFieldRow, IntFieldClm).Value _
  Then
    Cells(RefFieldRow, COC + 2).Value _
      = Cells(IntFieldRow, IntFieldClm + 1).Value
  Else
    'Check to see if the last field value for the interpolation set
    ' is greater than or equal to the last field value for the reference
    ' set. This will prevent a non-sensical value at the end.
    If (Cells(RefFieldRow, RefFieldClm).Value _
      < Cells(IntFieldRow, IntFieldClm).Value) _
    Then
      'Linear interpolation
      Cells(RefFieldRow, COC + 2).Value _
        = Cells(IntFieldRow - 1, IntFieldClm + 1).Value _
        + (Cells(RefFieldRow, RefFieldClm).Value _
         - Cells(IntFieldRow - 1, IntFieldClm).Value) _
        / (Cells(IntFieldRow, IntFieldClm).Value _
         - Cells(IntFieldRow - 1, IntFieldClm).Value) _
        * (Cells(IntFieldRow, IntFieldClm + 1).Value _
         - Cells(IntFieldRow - 1, IntFieldClm + 1).Value)
    End If
  End If
  'Copy reference field value and mag. values to output columns.
  ' Calculate sum and difference.
  If (Cells(RefFieldRow, RefFieldClm).Value _
    <= Cells(IntFieldRow, IntFieldClm).Value) _
  Then
    Cells(RefFieldRow, COC).Value _
      = Cells(RefFieldRow, RefFieldClm).Value
    Cells(RefFieldRow, COC + 1).Value _
      = Cells(RefFieldRow, RefFieldClm + 1).Value
    Cells(RefFieldRow, COC + 3).Value _
      = Cells(RefFieldRow, COC + 1).Value _
      - Cells(RefFieldRow, COC + 2).Value
    Cells(RefFieldRow, COC + 4).Value _
      = Cells(RefFieldRow, COC + 1).Value _
      + Cells(RefFieldRow, COC + 2).Value
  End If

  'Increment reference row number to check next point.
  RefFieldRow = RefFieldRow + 1
Loop _
Until (RefFieldRow >= RefLastRow) Or (IntFieldRow >= IntLastRow)
```

```
'Initialize values for 3rd and 4th sets.
RefFieldRow = 2
RefFieldClm = 10
IntFieldRow = RefFieldRow + 2
IntFieldClm = 12
COC = 22

'Calculate last rows
RefLastRow = Cells(1, RefFieldClm).Value + RefFieldRow + 1
IntLastRow = Cells(1, IntFieldClm).Value + IntFieldRow - 1

'Write column headings
Cells(RefFieldRow, COC).Value = "Field (3)"
Cells(RefFieldRow, COC + 1).Value = "Mag. (3)"
Cells(RefFieldRow, COC + 2).Value = "Interp. (4)"
Cells(RefFieldRow, COC + 3).Value = "Diff. (3,4)"
Cells(RefFieldRow, COC + 4).Value = "Sum (3,4)"
RefFieldRow = RefFieldRow + 1

'Copy 0 field values before attempting interpolation.
If Cells(RefFieldRow, IntFieldClm).Value = 0 Then
  Cells(RefFieldRow, COC).Value _
    = Cells(RefFieldRow, RefFieldClm).Value
  Cells(RefFieldRow, COC + 1).Value _
    = Cells(RefFieldRow, RefFieldClm + 1).Value
  Cells(RefFieldRow, COC + 2).Value _
    = Cells(RefFieldRow, IntFieldClm + 1).Value
  Cells(RefFieldRow, COC + 3).Value _
    = Cells(RefFieldRow, COC + 1).Value _
    - Cells(RefFieldRow, COC + 2).Value
  Cells(RefFieldRow, COC + 4).Value _
    = Cells(RefFieldRow, COC + 1).Value _
    + Cells(RefFieldRow, COC + 2).Value
'Else
'  RefFieldRow = RefFieldRow + 1
'  IntFieldRow = RefFieldRow + 1
End If

RefFieldRow = RefFieldRow + 1

'Find interpolated values from interpolation data set.
Do
  'Increment row number of data set to interpolate until the current
  ' field value in the interp. set is >= to the reference field.
  Do _
  While (-Cells(RefFieldRow, RefFieldClm).Value _
      > -Cells(IntFieldRow, IntFieldClm).Value) _
  And (IntFieldRow < IntLastRow)
    IntFieldRow = IntFieldRow + 1
  Loop
  'Check to see if the current interp. field is the same as the
  ' reference field. If it is just copy the value to the new set.
  If Cells(RefFieldRow, RefFieldClm).Value _
   = Cells(IntFieldRow, IntFieldClm).Value _
  Then
```

```
    Cells(RefFieldRow, COC + 2).Value _
      = Cells(IntFieldRow, IntFieldClm + 1).Value
  Else
    'Check to see if the last field value for the interpolation set
    ' is greater than or equal to the last field value for the reference
    ' set. This will prevent a non-sensical value at the end.
    If (-Cells(RefFieldRow, RefFieldClm).Value _
      < -Cells(IntFieldRow, IntFieldClm).Value) _
    Then
      'Linear interpolation
      Cells(RefFieldRow, COC + 2).Value _
        = Cells(IntFieldRow - 1, IntFieldClm + 1).Value _
        + (Cells(RefFieldRow, RefFieldClm).Value _
         - Cells(IntFieldRow - 1, IntFieldClm).Value) _
        / (Cells(IntFieldRow, IntFieldClm).Value _
         - Cells(IntFieldRow - 1, IntFieldClm).Value) _
        * (Cells(IntFieldRow, IntFieldClm + 1).Value _
         - Cells(IntFieldRow - 1, IntFieldClm + 1).Value)
    End If
  End If
  'Copy reference field value and mag. values to output columns.
  If (-Cells(RefFieldRow, RefFieldClm).Value _
   <= -Cells(IntFieldRow, IntFieldClm).Value) _
  Then
    Cells(RefFieldRow, COC).Value _
      = Cells(RefFieldRow, RefFieldClm).Value
    Cells(RefFieldRow, COC + 1).Value _
      = Cells(RefFieldRow, RefFieldClm + 1).Value
    Cells(RefFieldRow, COC + 3).Value _
      = Cells(RefFieldRow, COC + 1).Value _
      - Cells(RefFieldRow, COC + 2).Value
    Cells(RefFieldRow, COC + 4).Value _
      = Cells(RefFieldRow, COC + 1).Value _
      + Cells(RefFieldRow, COC + 2).Value
  End If

  'Increment reference row number to check next point.
  RefFieldRow = RefFieldRow + 1
Loop _
Until (RefFieldRow >= RefLastRow) Or (IntFieldRow >= IntLastRow)

End Sub
```

REFERENCES

1. A.C. Rose Innes and E.H. Rhoderick; Introduction to superconductivity; pergamon (1978)

2. Michael Tinkham; Introduction to superconductivity; Dover Publications (2004)

3. P.G. De Gennes; Superconductivity of Metals and alloys; W.A. Benjamin, INC. (1966)

4. V.V. Schmidt; The Physics of Superconductors; Springer (1997)

5. Charles Kittel; Introduction to Solid State Physics; John Wiley and Sons (1986)

6. Heike Kamerlingh Onnes; Investigations into the properties of substances at low temperatures, which have led, amongst other things, to the preparation of liquid helium; *Nobel Lecture, December 11, 1913;* Also at http://www.nobel.se/physics/laureates/1913/onnes-lecture.html

7. W. Meissner, R. Ochsenfeld "Ein neuer Effekt bei Eintritt der Supraleitfahigkeit" Die naturwissenschaften 21 (1933) 787

8. Gorter, C. J.; Casimir, H. Superconductivity. I. Physica (The Hague) (1934), 1 306-20.

9. London, F.; London, H. Superconduction. and diamagnetism. Physica (The Hague) (1935), 2 341-54.

10. Pippard, A. B. An experimental and theoretical study of the relation between magnetic field and current in a superconductor. Proc. Roy. Soc. (London) (1953),

11. Pippard, A. B. The surface impedance of superconductors and normal metals at high frequencies. V. Analysis of experimental results for superconducting tin. Proc. Roy. Soc. (London) (1950)

12. David R. Nelson; Defect and Geometry in Condensed Matter Physics; Cambridge University Press (2002)

13. J.M.S. Skakle (1998) “Crystal Chemistry and doping of YBCO-123 and related superconductors” Materials Science and engineering 823 1-40

14. Valo J., Leskela M (1997)"Studies on preparation and substitution of YBa2Cu4O8.” Studies of High Temperature Superconductors, 25 135-183

15. Michel, C., M. Hervieu, et al. (1987). "Superconductivity in the bismuth strontium copper oxide system." Zeitschrift fuer Physik B: Condensed Matter 68(4): 421-3.

16. Michel, C., J. Provost, et al. (1987). "Introduction of bismuth into the high Tc superconductor lanthanum strontium copper oxide (La2-xSrxCuO4-y)." Zeitschrift fuer Physik B: Condensed Matter 68(4): 417-19.

17. Maeda, H., Y. Tanaka, et al. (1988). "A new high-Tc oxide superconductor without a rare earth element." Japanese Journal of Applied Physics, Part 2: Letters 27(2): L209-L210.

18. Bordet, P., J. J. Capponi, et al. (1988). "A note on the symmetry and Bi valence of the superconductor Bi2Sr2Ca1Cu2O8." Physica C: Superconductivity 156(1): 189-192.

19. Gao, Y., P. Lee, et al. (1988). "The incommensurate modulation of the 2212 bismuth-strontium-calcium-copper-oxygen superconductor." Science (Washington, DC, United States) 241(4868): 954-6.

20. Lin, J. J., E. L. Benitez, et al. (1988). "Superconducting properties of single-crystal bismuth strontium calcium copper oxide (Bi2Sr2CaCu2O8+y)." Physical Review B: Condensed Matter and Materials Physics 38(7): 5095-7.

21. Subramanian, M. A., C. C. Torardi, et al. (1988). "New oxide superconductors." Physica C: Superconductivity 153-155(Part 1): 608-612.

22. Subramanian, M. A., C. C. Torardi, et al. (1988). "New oxide superconductors." Physica C: Superconductivity and Its Applications (Amsterdam, Netherlands) 153-155(Pt. 1): 608-12.

23. Sunshine, S. A., T. Siegrist, et al. (1988). "Structure and physical properties of single crystals of the 84-K superconductor bismuth strontium calcium copper oxide (Bi2.2Sr2Ca0.8Cu2O8+d)." Physical Review B: Condensed Matter and Materials Physics 38(1): 893-6.

24. Tarascon, J. M., P. Barboux, et al. (1988). "Preparation, structure and properties of the high Tc Bi-based and Y-based cuprates." Physica C: Superconductivity 153-155(Part 1): 566-571.

25. Tarascon, J. M., Y. Le Page, et al. (1988). "Crystal substructure and physical properties of the superconducting phase bismuth strontium calcium copper

oxide (Bi4(Sr,Ca)6Cu4O16+x)." Physical Review B: Condensed Matter and Materials Physics 37(16): 9382-9.

26. Torrance, J. B., Y. Tokura, et al. (1988). "New class of high Tc structures: Intergrowth of multiple copper oxide perovskite-like layers with double sheets of BiO." Solid State Communications 66(7): 703-706.

27. Von Schnering, H. G., L. Walz, et al. (1988). "Structure of the superconducting bismuth strontium calcium copper oxides (Bi2(Sr1-xCax)2CuO8-d and Bi2(Sr1-yCay)3Cu2O10-d, 0 ? x ? 0.3 and 0.16 ? y ? 0.33)." Angewandte Chemie 100(4): 604-7.

28. Zandbergen, H. W., W. A. Groen, et al. (1988). "Models for the modulation in A2B2CanCu1+nO6+2n, A, B=Bi, Sr OR Tl, Ba and n=0, 1, 2." Physica C: Superconductivity 156(3): 325-354.

29. Gladyshevskii, R. E. and R. Flukiger (1996). "Modulated structure of Bi2Sr2CaCu2O8+[bold delta], a high-Tc superconductor with monoclinic symmetry." Acta Crystallographica Section B 52(1): 38-53.

30. Elly Brouns and J. W. Visser (1964). “An anomaly in the crystal structure of Na2CO3” Acta Crystallographica 17: 614

31. P.M. de Wolff, A.Janner and T.Janssen (1983). “Bravais classes for incommensurate crystal phases” Acta Crystallographica Section A 39: 658-666

32. Dehling, (1927) *Z.Kristallogr., 65,* 615-631.

33. Bourges P. ”The spin excitation spectrum in superconducting $YBa_2Cu_3O_{6.85}$” Science Vol 288, Issue 5469,p 1234

34. Hinkov, V. “Two-dimensional geometry of spin excitations in the high-transition- temperature superconductor YBa2Cu3O6+x”, Nature, (2004). Vol. 430, p650

35. Akiji Yamamoto, Mitsuko Onoda, Eiji Takayama-Muromachi, and Fujio Izumi “ Rietveld analysis of the modulated structure in the superconducting oxide” (1990) Phys Rev B 42, 4228;

36. J. W. Heaton and A. C. Rose-Innes (1964) “Critical currents of a superconductor of the second kind” Cryogenics 4 (2) pp 85-89

37. Jorge G. Ossandon; (1991) “Magnetization of the Effects of Oxygen Deficiency δ on the superconductive properties of aligned YBCO materials” PhD Thesis; The university of Tennessee, Knoxville

38. G. Blatter, M. V. Feigel'man, V. B. Geshkenbein, A. I. Larkin, V. M. Vinokur (1994), “Vortices in high-temperature superconductors” *Rev. Mod. Phys.* **66** p. 1125.

39. M. E. McHenry and R. A. Sutton (1994). “Flux Pinning and Dissipation in High Temperature Oxide Superconductors” invited review (150 pages). *Progress in Materials Science* 38, 159,

40. Campbell, A. M., and J. E. Evetts (2001) “Flux vortices and transport currents in type II superconductors” Advances In Physics, Volume: 50 Number: 8 Page: 1249 – 1449

41. Thomas P. DEBIES and J. Wayne RABALAIS (1977) “X ray photoelectron spectra and electronic structure of Bi_2X_3 (X= O, S, Se, Te)” Chemical Physics (20) pp 277-283

42. Brandt, E. H. (1995). "The flux-line lattice in superconductors." Reports on Progress in Physics 58(11): 1465-594.

43. Senoussi, S. (1992) “Review of the critical current densities and magnetic irreversibilities in high-Tc superconductors” Journal de Physique III, 2, 7, 1041-1258

44. John R. Clem (1991) “Two-dimensional vortices in a stack of thin superconducting films: A model for high-temperature superconducting multilayers” Phys. Rev. B 43, 7837–7846

45. Charles P. Poole (2000) “Handbook of superconductivity” Academic Press

46. W. Gerhäuser, G. Ries, H. W. Neumüller, W. Schmidt, O. Eibl, Saemann–Ischenko, and S. Klaumünzer (1992) “ Flux line pinning in Bi-2212 crystals: interplay of intrinsic 2D behavior and irradiation-induced columnar defects” Phys. Rev. Lett 68 879-882

47. Kes, P. H. (1991). "Flux pinning and creep in high temperature superconductors." Physica C: Superconductivity 185-189(Part 1): 288-291.

48. Li, T. W., A. A. Menovsky, et al. (1996). "Flux pinning in Bi-2212 single crystals with various oxygen contents." Physica C: Superconductivity 257(1-2): 179-186.

49. Theuss, H. and H. Kronmueller (1991). "The influence of a point defect structure on the magnetic properties of yttrium barium copper oxide (YBa2Cu3O7-d) polycrystals." Physica C: Superconductivity and Its Applications (Amsterdam, Netherlands) 177(1-3): 253-61.

50. Yadin Y. Goldschmidt (1997) “Phase transitions of the flux-line lattice in high-temperature superconductors with weak columnar and point disorder” Phys. Rev. B. 56 2800-2808

51. Baetzold, R. C. (1988). "Atomistic simulation of ionic and electronic defects in yttrium barium copper oxide (YBa2Cu2O7)." Physical Review B: Condensed Matter and Materials Physics 38(16-A): 11304-12.

52. Baetzold, R. C. (1989). "Electronic calculations of large copper oxide clusters." Inorganic Chemistry 28(4): 640-4.

53. Baetzold, R. C. (1990). "Atomistic study of defects in yttrium barium copper oxide (YBa2Cu3O7)." Physical Review B: Condensed Matter and Materials Physics 42(1-A): 56-66.

54. Baetzold, R. C. (1991). "Computations of point defect energies in yttrium barium copper oxide (YBa2Cu3O6.5)." Physica C: Superconductivity and Its Applications (Amsterdam, Netherlands) 181(4-6): 252-60.

55. Baetzold, R. C., R. Grimes, et al. (1993). "Computational study of hole species in models of the cuprate superconductors." Journal of Physics and Chemistry of Solids 54(7): 793-800.

56. Baetzold, R. C. (1994). "Classical and quantum simulations of yttrium cuprate properties." Molecular Simulation 12(2): 77-87.

57. Baetzold, R. C. and J. Mir (1994). "A computational model for growth of (100) SrTiO3 and (001) YBa2Cu3O7 oxide films." Journal of Crystal Growth 135(1-2): 145-53.

58. Baetzold, R. C. Private communication

59. Islam, M. S. and R. C. Baetzold (1989). "Atomistic simulation of dopant substitution in yttrium barium copper oxide (YBa2Cu3O7)." Physical Review B: Condensed Matter and Materials Physics 40(16): 10926-35.

60. Islam, M. S. and R. C. Baetzold (1994). "Atomistic mechanisms of oxygen diffusion in YBa2Cu3O7-x and YBa2Cu4O8." Journal of Materials Chemistry 4(2): 299-303.

61. Islam, M. S. (1994). "Dopant effects in the 1-2-3 superconductor." Molecular Simulation 12(2): 101-13.

62. Islam, M. S. and R. C. Baetzold (1994). "Atomistic mechanisms of oxygen diffusion in YBa2Cu3O7-x and YBa2Cu4O8." Journal of Materials Chemistry 4(2): 299-303.

63. Moseev, N. V. (1995) “Atomic modeling of point defects in Bi2Sr2CaCu2O8.” Fizika Tverdogo Tela (Sankt-Peterburg) 37(5), 1531-5.

64. GULP - a computer program for the symmetry adapted simulation of solids, J.D. Gale, *JCS Faraday Trans.,* 93, 629 (1997)

65. The General Utility Lattice Program, J.D. Gale and A.L. Rohl, *Mol. Simul.*, **29**, 291 (2003)

66. Buckingham R.A. (1938). “The Classical equation of state for gaseous helium, neon and argon“ Proceedings of the Royal Society of London A 168 pp 264-283

67. Lennard Jones J.E. (1924) “On the determination of Molecular fields –II From equation of state of a gas” Proceedings of The Royal Society of London A106 463-477; ibid 709-719

68. Dick B.G,Overhauser A. W. (1958) “Theory of Dielectric constant for alkalihalide crystals” Physical Review 112 pp 90-103

69. F. Beech, S Miraglia, A. Santoro, R.S. Roth (1987) “Neutron study of the crystal structure and vacancy distribution in the superconductor YBCO” Vol 35 (16) pp 8778 –8781

70. R.P. Sharma, F.J. Rottela, J.D. Jorgensen C.E. Rehn (1991) “Neutron Diffraction and ion channeling investigation of atomic displacement in YBCO between 10-300K” Physica C 174 409-422

71. NN Kovaleva, AV Boris, T Holeden, AM Stoneham (2004) “c-axis Lattice dynamics in Bi-based cuprate superconductors” Phys Rev B 69 054511

72. J. Prade, A.D. Kulkarni, W. Kress (1989) “Calculation of Raman and infra-active modes of Bi-2212” Phys Rev B 39 (4) 2771

73. J. Maier, HL Tuller “Defect Chemistry and Transport in YBCO” J; Phys Rev B

74. R.D. Shannon, "Revised Effective Ionic Radii and Systematic Studies of Interatomic Distances in Halides and Chalcogenides", *Acta Cryst.* **A32** 751-767 (1976).

75. Sunshine, S. A., T. Siegrist, et al. (1988). "Structure and physical properties of single crystals of the 84-K superconductor Bi2.2Sr2Ca0.8Cu2O8+ [delta]." Physical Review B (Condensed Matter) 38(1): 893-896.

76. Buckley, R. G., J. L. Tallon, et al. (1988). "The influence of oxygen on the physical properties of the superconducting series bismuth calcium strontium copper oxide (Bi2.1(CaxSr1-x)n+1CunO2n+4+d)." Physica C:

Superconductivity and Its Applications (Amsterdam, Netherlands) 156(4): 629-34.

77. Grader, G. S., E. M. Gyorgy, et al. (1988). "Crystallographic, thermodynamic, and transport properties of the bismuth strontium calcium cuprate (Bi2Sr3-xCaxCu2O8+d) superconductor." Physical Review B: Condensed Matter and Materials Physics 38(1): 757-60.

78. Cheetham, A. K., A. M. Chippingdale, et al. (1989). "Chemical characterization of superconducting phases in the systems bismuth strontium calcium copper oxide and thallium barium calcium copper oxide; the evidence for cation deficiencies." Phase Transitions 19(4): 223-9.

79. Roth, R. S., C. J. Rawn, et al. (1989). "Phase equilibria of the system strontium oxide-calcium oxide-cupric oxide." Journal of the American Ceramic Society 72(8): 1545-9.

80. Zheng, H., R. Xu, et al. (1989). "Glass formation and glass structure of bismuth oxide (BiO1.5)-cupric oxide-calcium strontium oxide (Ca0.5Sr0.5O) system." Journal of Materials Research 4(4): 911-15.

81. Bohacek, P., J. Pracharova, et al. (1990). "Composition of phases and phase mixtures of the bismuth strontium calcium copper oxide system." Physica C: Superconductivity and Its Applications (Amsterdam, Netherlands) 171(1-2): 108-20.

82. Hong, B., J. Hahn, et al. (1990). "Phase composition and compatibilities in the bismuth-strontium-calcium-copper quaternary oxide system at 800 DegC in air." Journal of the American Ceramic Society 73(7): 1965-72.

83. Roth, R. S., C. J. Rawn, et al. (1990). "Crystal chemistry of the compound strontium bismuth copper oxide (Sr2Bi2CuO6)." Journal of Materials Research 5(1): 46-52.

84. Schulze, K., P. Majewski, et al. (1990). "Phase equilibria in the system bismuth(III) oxide-strontia-calcia-copper(II) oxide with emphasis on the high-Tc superconducting compounds." Zeitschrift fuer Metallkunde 81(11): 836-42.

85. Chow, H. M., X. P. Jiang, et al. (1991). "Effects of annealing on the microstructure and phase chemistry of directionally solidified bismuth strontium calcium copper oxide (Bi2Sr2CaCu2O8)." Journal of the American Ceramic Society 74(6): 1391-6.

86. Golden, S. J., F. F. Lange, et al. (1991). "Processing and characterization of thin films of the one-layer phase in the bismuth-strontium-calcium-copper-oxygen system: calcium solubility." Journal of the American Ceramic Society 74(4): 797-800.

87. Hong, B. and T. O. Mason (1991). "Solid-solution ranges of the n = 2 and n = 3 superconducting phases in bismuth strontium calcium copper oxide [Bi2(SrxCa1-x)n+1CunOy] and the effect on Tc." Journal of the American Ceramic Society 74(5): 1045-52.

88. Majewski, P., B. Hettich, et al. (1991). "The phase equilibria of bismuth strontium calcium copper oxide (Bi2Sr2Ca2Cu3O10) in the system bismuth sesquioxide-strontium oxide-calcium oxide-cupric oxide." Physica C: Superconductivity and Its Applications (Amsterdam, Netherlands) 185-189(Pt. 1): 469-70.

89. Majewski, P., B. Hettich, et al. (1991). "The phase equilibrium diagram of bismuth oxide (Bi2O3)-strontium oxide-calcium oxide-cupric oxide - a tool of processing the high-Tc superconducting bismuth-compounds." Advanced Materials (Weinheim, Germany) 3(1): 67-9.

90. Normura, S., T. Yamashita, et al. (1991). "Cation deficiency in bismuth (strontium, calcium) cuprate (Bi2(Sr,Ca)3Cu2O8+d)." Journal of the American Ceramic Society 74(10): 2711-14.

91. Presland, M. R., J. L. Tallon, et al. (1991). "General trends in oxygen stoichiometry effects on Tc in bismuth and thallium superconductors." Physica C: Superconductivity and Its Applications (Amsterdam, Netherlands) 176(1-3): 95-105.

92. Schweizer, T., R. Mueller, et al. (1991). "Phase equilibria of the superconducting phases in the bismuth strontium calcium copper oxide system." Ceramic Transactions 18(Supercond. Ceram. Supercond. 2): 23-9.

93. Heeb, B., S. Oesch, et al. (1992). "Microstructure of melt-processed bismuth strontium calcium copper oxide (Bi2Sr2CaCu2Oy) and reaction mechanisms during post heat treatment." Journal of Materials Research 7(11): 2948-55.

94. Holesinger, T. G., D. J. Miller, et al. (1992). "Characterization of the phase relations and solid-solution range of the bismuth strontium calcium copper oxide (Bi2Sr2CaCu2Oy) superconductor." Physica C: Superconductivity and Its Applications (Amsterdam, Netherlands) 202(1-2): 109-20.

95. List, F. A., H. Hsu, et al. (1992). "Phase development in the bismuth strontium calcium copper oxide (Bi2Sr2CaCu2Oy) system. Effects of oxygen pressure." Physica C: Superconductivity and Its Applications (Amsterdam, Netherlands) 202(1-2): 134-40.

96. Lo, W. and B. A. Glowacki (1992). "A study of the formation processes of the 2212 phase in the bismuth-based superconductor systems." Physica C: Superconductivity and Its Applications (Amsterdam, Netherlands) 193(3-4): 253-63.

97. Majewski, P. and B. Hettich (1992). "The single phase regions and the phase stability of the high-Tc superconducting compounds bismuth strontium calcium copper oxide Bi2+x(Sr,Ca)3Cu2O8+d (2212) and Bi2+x(Sr,Ca)4Cu3O10+d (2223)." Materials Research Society Symposium Proceedings 275(Layered Superconductors: Fabrication, Properties and Applications): 627-32.

98. Majewski, P., H. L. Su, et al. (1992). "The high-Tc superconducting solid solution bismuth strontium calcium copper oxide (Bi2+x(Sr,Ca)3Cu2O8+d) (2212 phase) - chemical composition and superconducting properties." Advanced Materials (Weinheim, Germany) 4(7-8): 508-11.

99. Mueller, R., T. Schweizer, et al. (1992). "Compositional range of the bismuth strontium calcium copper oxide (Bi2Sr2CaCu2Ox) HTc-superconductor and its surrounding phases." Physica C: Superconductivity and Its Applications (Amsterdam, Netherlands) 203(3-4): 299-314.

100. Paul, W., B. Heeb, et al. (1992). "Critical current densities Jc(H,T) and current-voltage characteristics in melt processed bismuth-2212 with and without preferential orientation." Materials Research Society Symposium Proceedings 275(Layered Superconductors: Fabrication, Properties and Applications): 383-7.

101. Assmus, W. and W. Schmidbauer (1993). "Crystal growth of HTSC materials." Superconductor Science and Technology 6(8): 555-66.

102. Knizek, K., E. Pollert, et al. (1993). "Single-phase region of the 2212-Bi---Sr---Ca---Cu---O superconductor." Physica C: Superconductivity 216(1-2): 211-218.

103. Heeb, B., L. J. Gauckler, et al. (1993). "Microstructure and properties of melt-processed Bi-2212 bismuth strontium calcium copper oxide (Bi2Sr2CaCu2Ox)." Journal of Electronic Materials 22(10): 1279-83.

104. Heeb, B., L. J. Gauckler, et al. (1993). "From imperfect to perfect bismuth strontium calcium copper oxide (Bi2Sr2CaCu2Ox) (Bi-2212) grains." Journal of Materials Research 8(9): 2170-6.

105. Holesinger, T. G., D. J. Miller, et al. (1993). "Solid solution region of the Bi2Sr2CaCu2Oy superconductor." Physica C: Superconductivity 217(1-2): 85-96.

106. Majewski, P., S. Kaesche, et al. (1993). "Enhanced pinning properties of \"(Bi,Pb)2Sr2Ca2Cu3O10+d\" bulk ceramics." Appl. Supercond., [Pap. Eur. Conf.], 1st 1: 129-32.

107. Majewski, P., B. Hettich, et al. (1993). "The influence of the phase equilibria on the critical temperatures Tc of the high-Tc bismuth strontium calcium copper oxide and yttrium barium copper oxide compounds." Journal of Electronic Materials 22(10): 1259-62.

108. Schartman, R. R., R. Sakidja, et al. (1993). "Supersolidus phase investigation of the bismuth strontium calcium copper oxide system in silver tape." Journal of the American Ceramic Society 76(3): 724-8.

109. Buhl, D., T. Lang, et al. (1994). "Processing, properties and microstructure of melt-processed Bi-2212 thick films." Physica C: Superconductivity (Amsterdam) 235-240(Pt. 5): 3399-400.

110. Heeb, B., D. Buhl, et al. (1994). "Processing and properties of Bi-2212 thick films." Process. Long Lengths Supercond., Proc. Symp.: 213-19.

111. Heinrich, H., G. Kostorz, et al. (1994). "Modeling the atomic displacements in Bi2Sr2Can-1CunOx superconductors." Physica C: Superconductivity and Its Applications (Amsterdam, Netherlands) 224(1-2): 133-42.

112. Idemoto, Y., S. Kobayashi, et al. (1994). "Phase diagrams and ionic defects in the 2212 and 2201 phases of the bismuth system." Physica C: Superconductivity and Its Applications (Amsterdam, Netherlands) 229(1-2): 47-58.

113. Kato, M., W. Ito, et al. (1994). "Dependence of Tc on the excess oxygen content d in Bi2Sr2CaCu2O8+d annealed under high pressures of oxygen." Physica C: Superconductivity and Its Applications (Amsterdam, Netherlands) 226(3-4): 243-9.

114. Majewski, P., B. Hettich, et al. (1994). "Increased pinning in \"Bi2Sr2CaCu2O8\" ceramics." Applied Superconductivity 2(2): 93-9.

115. Majewski, P., S. Elschner, et al. (1994). "Pinning in BSCCO superconductors." Process. Long Lengths Supercond., Proc. Symp.: 205-11.

116. Majewski, P., H.-L. Su, et al. (1994). "The oxygen content of the high-temperature superconducting compound Bi2+xSr3-yCayCu2O8+d as a function of the cation concentration." Physica C: Superconductivity and Its Applications (Amsterdam, Netherlands) 229(1-2): 12-16.

117. Majewski, P., S. Elschner, et al. (1994). "The increase of pinning in (Bi, Pb)2Sr2Ca2Cu3O10+d bulk ceramics." Superconductor Science and Technology 7(7): 514-17.

118. Majewski, P., S. Kaesche, et al. (1994). "The Pb solubility of the Bi-based high-Tc superconductors \"Bi2Sr2CaCu2O8\" and \"Bi2Sr2Ca2Cu3O10\" as a function of temperature." Physica C: Superconductivity and Its Applications (Amsterdam, Netherlands) 221(3-4): 295-8.

119. Rawn, C. J., R. S. Roth, et al. (1994). "Phase equilibria and crystal chemistry in portions of the system SrO-CaO-1/2Bi2O3-CuO: V, the system SrO-CaO-1/2Bi2O3." Journal of the American Ceramic Society 77(8): 2173-8.

120. Schweizer, T., R. Mueller, et al. (1994). "A wet-chemistry method to determine the Bi and Cu valencies in Bi-Sr-Ca-Cu-O (2212) high-temperature superconductors." Physica C: Superconductivity and Its Applications (Amsterdam, Netherlands) 225(1-2): 143-8.

121. Singh, K. K., D. E. Morris, et al. (1994). "Stability of Ba, Sr and Ca cuprate phases as a function of oxygen pressure." Physica C: Superconductivity and Its Applications (Amsterdam, Netherlands) 231(3-4): 377-82.

122. Boiko, J., P. Majewski, et al. (1995). "Pancake vortex- defects interaction and flux pinning in strongly anisotropic high-temperature superconductors." Advances in Science and Technology (Faenza, Italy) 8(Superconductivity and Superconducting Materials Technologies): 129-134.

123. Idemoto, Y., T. Toda, et al. (1995). "Comparison of Bi-rich and Cu-rich oxides of the Bi-2212 phase." Physica C: Superconductivity (Amsterdam) 249(1&2): 123-32.

124. Lang, T., D. Buhl, et al. (1995). "Decomposition and reformation of Bi-2212 during the partial melt processing in oxygen." Institute of Physics Conference Series 148 (Vol. 1): 111-14.

125. Leonyuk, L., G. J. Babonas, et al. (1995). "Study of isostructural phases in 2212-type high-Tc superconductors." Superconductor Science & Technology 8(1): 53-59.

126. MacManus-Driscoll, J. L., J. C. Bravman, et al. (1995). "Pseudo-quaternary phase relations near Bi2Sr2CaCu2O8+x in reduced oxygen pressures." Physica C: Superconductivity (Amsterdam) 251(1&2): 71-88.

127. Majewski, P. (1995). "The use of phase diagrams for the engineering of flux pinning centers in Bi2Sr2CaCu2O8 ceramics." Applied Superconductivity 3(5): 289-301.

128. Majewski, P., S. Elschner, et al. (1995). "Enhanced pinning by second-phase precipitates in Sr rich \"Bi2Sr2CaCu2O8\" ceramics." Physica C: Superconductivity (Amsterdam) 249(3&4): 234-40.

129. Mueller, R., M. Cantoni, et al. (1995). "Phase compatibilities in the Bi-poor region of the system Bi-Sr-Ca-O at 820 and 900 DegC in air." Physica C: Superconductivity (Amsterdam) 243(1&2): 103-12.

130. Kaesche, S., P. Majewski, et al. (1996). "Phase equilibria in the system Bi2O3-PbO-SrO-CaO-CuO with special regard to the (Bi, Pb)2+cSr2Ca2Cu3O10+d phase." Zeitschrift fuer Metallkunde 87(7): 587-593.

131. Nevriva, M., K. Knizek, et al. (1996). "Determination of phase diagram cuts in the BiO1.5-SrO-CaO-CuO system." Superconductor Science & Technology 9(4): 279-83.

132. Su, H.-L., F. Vasiliu, et al. (1996). "The influences of the Sr/Ca and Bi/Pb ratio upon the structural modulation of the Bi-2212 phase." Physica C: Superconductivity (Amsterdam) 256(3&4): 345-52.

133. Buhl, D., T. Lang, et al. (1997). "Phase composition and grain alignment in partial melt processed Bi-2212 thick films." Applied Superconductivity 4(7/8): 299-317.

134. Lang, T., D. Buhl, et al. (1997). "Sample-substrate interactions during melting of Bi2212 on Ag." Superconductor Science & Technology 10(5): 311-317.

135. Lang, T., D. Buhl, et al. (1997). "Melting of Bi-2212 under controlled oxygen partial pressures with silver." Physica C: Superconductivity (Amsterdam) 275(3&4): 284-292.

136. Majewski, P., H.-L. Su, et al. (1997). "Relationships between chemical composition and properties of the high-temperature superconductor Bi2+xSr3-yCayCu2O8+d." Journal of Materials Science 32: 5137-5141.

137. T. Di Luccio, V. Lukic, S. Oh, L. Maritato, and J. N. Eckstein (2003) “Complete substitution of Sr for Ca in $Bi_2Sr_{2+x}Ca_{1-x}Cu_2O_{8+\ delta}$” Phys. Rev. B 67, (2003)

138. Wong-Ng, W. K., L. P. Cook, et al. (1998). "Melting equilibria of the Bi-Sr-Ca-Cu-O (BSCCO) system in air: the primary crystallization phase field of the 2212 phase and the effect of silver addition." Journal of the American Ceramic Society 81(7): 1829-1838.

139. Kulakov, A. B., I. G. Naumenko, et al. (2001). "The primary crystallization field and growth of Bi-2212 crystals in platinum and gold crucibles." Journal of Crystal Growth 231(1-2): 194-202.

140. Kobel, S., R. Nussbaumer, et al. (2002). "Ceramic substrates for Bi2Sr2CaCu2Ox melt processing." Physica C: Superconductivity and Its Applications (Amsterdam, Netherlands) 377(4): 507-515.

141. Kobel, S., D. Schneider, et al. (2003). "Processing and properties of Bi2Sr2CaCu2Ox thick films on polycrystalline magnesium oxide substrates." Physica C: Superconductivity and Its Applications (Amsterdam, Netherlands) 399(3&4): 107-119.

142. Kobayashi, N., H. Iwasaki, et al. (1988). "Upper and lower critical fields of REBa2Cu3Oz compounds." Physica C: Superconductivity 153-155(Part 2): 1525-1526.

143. Manthiram, A. and J. B. Goodenough (1988). "Dependence of T[sub c] on hole concentration in the superconductors Bi[sub 4]Sr[sub 3]Ca[sub 3 - x]Y[sub x]Cu[sub 4]O[sub 16 + delta]." Applied Physics Letters 53(5): 420-422.

144. Nishida, N., H. Miyatake, et al. (1988). "Observation of antiferromagnetic ordering in Bi2Sr2YCu2Oy above room temperature by the muSR method." Physica C: Superconductivity 156(4): 625-628.

145. Yoshizaki, R., Y. Saito, et al. (1988). "Superconducting and magnetic properties of Bi2Sr2Ca1-xYxCu2Oy (0<x<1)." Physica C: Superconductivity 152(5): 408-412.

146. Koike, Y., Y. Iwabuchi, et al. (1989). "Correlation between Tc and hole concentration in the cation-substituted Bi2Sr2CaCu2O8+[delta] system." Physica C: Superconductivity 159(1-2): 105-110.

147. Lindberg, P. A. P., Z.-X. Shen, et al. (1989). "The electronic structure of Bi2.0Sr1.8La0.3Ca0.8Cu2.1O8+[delta] superconductors studied using ultraviolet and X-ray photoelectron spectroscopy." Physica C: Superconductivity 159(5): 649-653.

148. Olivier, S., W. A. Groen, et al. (1989). "On the solid solutions in the systems Bi2Sr2Ca1-xYxCu2O8+[delta], Bi2Sr2-xLaxYCu2O8+[delta] and Bi2Sr2Y1-xCexCu2O8+[delta]." Physica C: Superconductivity 157(3): 531-536.

149. Xue, Y. Y., P. H. Hor, et al. (1989). "The study and formation of the antiferromagnetic insulators Bi2(Gd1-xCax)ySr2Cu2O[delta]." Physica C: Superconductivity 158(1-2): 211-216.

150. Yoshizaki, R., H. Ikeda, et al. (1989). "Superconducting properties and phonon spectra of Bi2Sr2Y1-xCaxCu2Oy." Physica C: Superconductivity 162-164(Part 1): 67-68.

151. Groen, W. A., D. M. de Leeuw, et al. (1990). "Hole concentration and Tc in Bi2Sr2CaCu2O8+[delta]." Physica C: Superconductivity 165(1): 55-61.

152. Nishida, N., S. Okuma, et al. (1990). "Internal magnetic fields at [mu]+ sites and the magnetic phase diagram of Bi2Sr2Y1-xCaxCu2Oy system studied by the [mu]SR method." Physica C: Superconductivity 168(1-2): 23-28.

153. Yoshizaki, R., J. Fujikami, et al. (1990). "Substitution effect of rare earth (R) for calcium in the bismuth strontium calcium rare earth copper oxide (Bi2Sr2Ca1-xRxCu2O8+y) system." Physica C: Superconductivity and Its Applications (Amsterdam, Netherlands) 171(3-4): 315-20.

154. Zandbergen, H. W., W. A. Groen, et al. (1990). "Structure and properties of (Bi, Pb)2Sr2(Ca, Y)Cu2O8+[delta]." Physica C: Superconductivity 168(3-4): 426-449.

155. Adachi, S., H. Adachi, et al. (1991). "Studies on Sr/Ca ratio and Ln substitution in (Pb/Cu)Sr2(Y/Ca)Cu2Oy." Physica C: Superconductivity 185-189(Part 1): 671-672.

156. Fueki, K., Y. Idemoto, et al. (1991). "Substitution of allovalent ions for cations in the (2201) and (2212) phases and its effect on Tc." Physica C: Superconductivity 185-189(Part 1): 679-680.

157. Fujikami, J., R. Yoshizaki, et al. (1991). "Site-selective substitution effect on Tc in the bismuth strontium calcium rare earth copper oxide (Bi2(Sr2-xCax)(Ca0.8R0.2)Cu2O8+y) system (R = rare-earth)." Physica C: Superconductivity and Its Applications (Amsterdam, Netherlands) 174(4-6): 359-64.

158. Rentschler, T. and S. Kemmler-Sack (1991). "Superconducting properties of ceramics in the 2212 system bismuth lead strontium calcium neodymium copper oxide (Bi2-wPbwSr2-xCa1-yNdx+yCu2O8+z)." Physica C: Superconductivity and Its Applications (Amsterdam, Netherlands) 176(4-6): 445-50.

159. Tang, I. M., S. Leelaprute, et al. (1991). "Optimization of the hole concentration in the two-layer bismuth superconductors." Physica C: Superconductivity and Its Applications (Amsterdam, Netherlands) 177(1-3): 57-60.

160. Tang, I. M., S. Leelaprute, et al. (1991). "Lanthanide substitution into low hole concentration bismuth superconductors." Physica C: Superconductivity 175(3-4): 250-254.

161. Ummat, P. K., R. K. Nkum, et al. (1991). "The effect of gallium substitution on the superconductivity of the BiSrCaCuO system." Physica C: Superconductivity 180(5-6): 407-410.

162. Wang, N. L., M. C. Tan, et al. (1991). "Cation substitution in bismuth-strontium-calcium-copper-oxygen system." Physica C: Superconductivity and Its Applications (Amsterdam, Netherlands) 185-189(Pt. 2): 799-800.

163. Weber, M., A. Amato, et al. (1991). "Electronic carrier density in doped bismuth-based high-Tc superconductors." Physica C: Superconductivity and Its Applications (Amsterdam, Netherlands) 185-189(Pt. 2): 749-50.

164. Yasuoka, H., M. Kakihana, et al. (1991). "Effect of carrier concentration on the superconducting property of Bi2Sr2Ca1-xYxCu2Oy." Physica C: Superconductivity 185-189(Part 2): 803-804.

165. Awana, V. P. S., S. K. Agarwal, et al. (1992). "Superconductivity and resistivity studies in Bi2Sr2Ca1-xMxCu2O8+y (M=Eu, Dy, Tm and 0[les]x[les]0.6)." Physica C: Superconductivity 191(1-2): 43-51.

166. Babushkina, N. A., M. V. Dobrotvorskaya, et al. (1992). "Charge state of copper in Bi2Sr2Ca1-xYxCu2O8+[delta]." Physica C: Superconductivity 197(3-4): 299-302.

167. Calestani, G., M. G. Francesconi, et al. (1992). "Structural modulation and superconducting properties in bismuth lead strontium yttrium calcium copper oxide (Bi,Pb)2Sr2 (Y,Ca)Cu2Oz)." Physica C: Superconductivity and Its Applications (Amsterdam, Netherlands) 197(3-4): 283-98.

168. Gopala Krishna, B., R. Gundakaram, et al. (1992). "Effect of sodium substitution on superconductivity in Bi-based (2212) system." Physica C: Superconductivity 200(3-4): 425-433.

169. Munakata, F., T. Kawano, et al. (1992). "Oxygen nonstoichiometry effect on structural modulation in bismuth-2212 cuprate superconductors." Physica C: Superconductivity and Its Applications (Amsterdam, Netherlands) 190(4): 471-6.

170. Ruscher, C. H., M. Gotte, et al. (1992). "Coexistence of localized and delocalized states in Bi-2212 Y/Ca : An investigation of the infrared and optical absorption." Physica C: Superconductivity 204(1-2): 30-42.

171. Jordan, F., O. Pena, et al. (1994). "Cerium substitution in the 2212 bismuth cuprate : Bi2Sr2Ca1-xCexCu2O8+[delta]." Physica C: Superconductivity 235-240(Part 2): 945-946.

172. Jordan, F. and O. Pena (1994). "Superconductivity in the cerium-substituted 2212 bismuth cuprate: Bi2Sr2Ca1-xCexCu2O8+[delta]." Physica C: Superconductivity 231(3-4): 311-318.

173. Lemmens, P., T. Suzuki, et al. (1994). "Specific heat measurements across the metal-insulator transition in Bi2Sr2(CazRE1-z)Cu2O8 with RE=Y, Pr, Nd and Gd." Physica B: Condensed Matter (Amsterdam, Netherlands) 194-196: 467-8.

174. Nanda Kishore, K., S. Satyavathi, et al. (1994). "Effect of Y3+ substitution for Ca on the superconducting and the normal state properties of Bi(2223) system (Bi1.7Pb0.3Ca2-xYxSr2Cu3Oy)." Physica C: Superconductivity (Amsterdam) 235-240(Pt. 2): 1521-2.

175. Ruyter, A., C. Simon, et al. (1994). "Irreversibility lines of Yb and Pb substituted Bi-2212 single crystals." Physica C: Superconductivity and Its Applications (Amsterdam, Netherlands) 225(3-4): 235-9.

176. Stassen, S., R. Cloots, et al. (1994). "Magnetic alignment in rare-earth substituted Bi-based 2212 superconducting materials." Physica C: Superconductivity (Amsterdam) 235-240(Pt. 1): 515-16.

177. Jordan, F. and O. Pena (1995). "Texturation and critical currents in cerium-substituted cuprates Bi2Sr2Ca1-xCexCu2O8 + [delta]." Journal of Magnetism and Magnetic Materials 140-144(Part 2): 1315-1316.

178. Koike, Y., K. Sasaki, et al. (1995). "Carrier doping through iodine intercalation into Bi2Sr2CaCu2O8+[delta] with different [delta] values." Physica C: Superconductivity 245(3-4): 332-340.

179. Suvarna, A. M. and C. S. Sunandana (1995). "Magnetic penetration depth in polycrystalline Bi-2212 Bi2Sr2Ca1-xNaxCu2O8+[delta] (x = 0-0.3)." Physica C: Superconductivity 254(3-4): 355-358.

180. Vasiliu-Doloc, L., A. H. Moudden, et al. (1995). "Antiferromagnetic order of Cu2+ spins and structural fluctuations in Bi2Sr2PrCu2O8+d." Physica B: Condensed Matter (Amsterdam) 213&214(1-4): 63-5.

181. Sattar, A., J. P. Srivastava, et al. (1996). "Effect of Er-substitution on superconducting and metal-insulator transitions in 2212 bismuth cuprate." Physica C: Superconductivity 266(3-4): 335-344.

182. Hu, A., N. Sakai, et al. (2001). "A comparative study of enhanced flux pinning among melt-processed SmBa2Cu3O7-[delta], (Sm0.5Eu0.5)Ba2Cu3O7-[delta], EuBa2Cu3O7-[delta] superconductors." Physica C: Superconductivity 357-360(Part 1): 461-465.

183. Koblischka, M. R., T. Higuchi, et al. (1998). "Magnetic measurements in NdBa2Cu3O7-[delta] single crystals: magnetization, flux pinning and creep." Applied Superconductivity 6(2-5): 225-234.

184. Koblischka, M. R., M. Muralidhar, et al. (1999). "Engineering of pinning sites in melt-processed (Nd0.33Eu0.33Gd0.33)Ba2Cu3Oy superconductors." Materials Science and Engineering B 65(1): 58-65.

185. Koblischka, M. R., M. Muralidhar, et al. (2000). "Flux pinning sites in melt-processed (Nd0.33Eu0.33Gd0.33)Ba2Cu3Oy superconductors." Physica C: Superconductivity 337(1-4): 31-38.

186. Murakami, M., N. Sakai, et al. (1997). "Flux pinning in melt processed RE---Ba---Cu---O." Physica C: Superconductivity 282-287(Part 1): 371-374.

187. Muralidhar, M., K. Segawa, et al. (1999). "Enhancement of critical current density in (Nd, Eu, Gd)-Ba-Cu-O superconductors." Materials Science and Engineering B 65(1): 42-47.

188. Muralidhar, M. and M. Murakami (2000). "Superconducting properties of (Nd, Eu, Gd)-123." Physica C: Superconductivity 341-348(Part 4): 2431-2432.

189. Muralidhar, M. and M. Murakami (2001). "Microstructure and flux pinning in oxygen-controlled melt-growth processed (Nd0.33Eu0.33Gd0.33)Ba2Cu3Oy." Physica C: Superconductivity 363(1): 19-24.

190. Muralidhar, M. and M. Murakami (2002). "A new technique for pinning enhancement in ternary REBa2Cu3Oy systems." Physica C: Superconductivity 378-381(Part 1): 627-630.

191. Muralidhar, M., S. Nariki, et al. (2002). "Flux pinning by Gd-211 particles in ternary (Nd0.33Sm0.33Gd0.33)Ba2Cu3Oy melt-processed superconductors." Physica C: Superconductivity 378-381(Part 1): 746-749.

192. Muralidhar, M., M. Jirsa, et al. (2002). "High flux pinning in ternary (Nd-Eu-Gd)Ba2Cu3Oy superconductors at 77 K." Physica C: Superconductivity 378-381(Part 1): 750-754.

193. Muralidhar, M., N. Sakai, et al. (2003). "Superconductors for high-field use at 77 K." Physica C: Superconductivity 392-396(Part 1): 567-570.

194. Yoshizawa, K., S. Nariki, et al. (2003). "Effect of pinning on the flux motion of Gd-Ba-Cu-O bulk superconductors." Physica C: Superconductivity 392-396(Part 1): 391-395.

195. Koike, K., S. Kambe, et al. (1997). "Study on physical properties of Bi-2201, Bi-2212 and Bi-2223 superconductors." Physica C: Superconductivity 282-287(Part 3): 1211-1212.

196. Prabhakaran, D. and C. Subramanian (1997). "Metal-insulator transition in the Pr substituted Bi-2212 bulk textured crystals." Physica C: Superconductivity (Amsterdam) 291(1&2): 73-78.

197. Prabhakaran, D., A. Thamizhavel, et al. (1997). "Morphology and characterization studies of Y doped Bi-2212 single crystals." Physica C: Superconductivity (Amsterdam) 288(3&4): 249-254.

198. Villard, G., D. Pelloquin, et al. (1997). "Growth and superconductivity of Bi2Sr2Ca1-xYxCu2O8+d single crystals in the Tc optimum region." Physica C: Superconductivity (Amsterdam) 278(1&2): 11-22.

199. Villard, G., D. Pelloquin, et al. (1997). "Growth and superconductivity of Bi2Sr2Ca1-xYxCu2O8+[delta] single crystals in the Tc optimum region." Physica C: Superconductivity 278(1-2): 11-22.

200. Villard, G., D. Pelloquin, et al. (1998). "Doping dependence of the in-plane penetration depth and fishtail in Bi2Sr2Ca1-xYxCu2O8+d single crystals." Physical Review B: Condensed Matter and Materials Physics 58(22): 15231-15237.

201. Jin, H. and J. Kotzler (1999). "Effect of La-doping on growth and superconductivity of Bi-2212 crystals." Physica C: Superconductivity and Its Applications (Amsterdam) 325(3&4): 153-158.

202. Khan, M. N. and M. Khizar (1999). "Effect of rare-earth substitutions on superconducting properties of the Bi1.7Pb0.3Sr2Ca2-xRxCu3Oy (R = Eu,Yb,Ag) system." Journal of Materials Science 34(23): 5833-5838.

203. Manifacier, L., G. Collin, et al. (1999). "Correlations between crystallographic and physical properties in (Bi, Pb)2Sr2(Ca, Y)Cu2O8+[Delta] superconductors." Physica B: Condensed Matter 259-261: 562-563.

204. Pop, A. V., G. Ilonca, et al. (1999). "Effects of Y and rare earth ion substitution for Ca in (Bi,Pb):2223 superconductor." Modern Physics Letters B 13(8): 255-259.

205. Hsu, Y. Y., Y. Huang, et al. (2000). "Low field flux dynamics of Pr-doped Bi-2212 single crystals." Physica C: Superconductivity 341-348(Part 2): 1159-1160.

206. Pop, M., G. Borodi, et al. (2000). "Gd substitution effect on the formation of Bi-based superconducting glass ceramics." Modern Physics Letters B 14(2): 59-63.

207. Sorkin, B. and P. Konsin (2000). "Doping dependences of the superconducting transition temperature and the chemical potential shift in La2-xSrxCuO4 and Bi2Sr2Ca1-xYxCu2O8+[delta]: theory and experiment." Physica B: Condensed Matter 284-288(Part 1): 1055-1056.

208. Yasuoka, H., S. Tochihara, et al. (2000). "Hole concentration of sintered Bi2-xPbxSr2Ca1-yYyCu2O8+d." Physica B: Condensed Matter 284-288(Part 1): 1087-1088.

209. Sato, Y., M. Kakihana, et al. (2001). "Synthesis of high-purity (CaxLa1.00-x)(Ba1.75-xLa0.25+x)Cu3Oz tetragonal superconductor by an aqueous solution technique using citric acid." Physica C: Superconductivity 357-360(Part 1): 260-264.

210. Wang, X. L., H. K. Liu, et al. (2001). "Study of the peak effect in pure, Pb and Pb+Y doped Bi-2212 single crystals." Physica C: Superconductivity 364-365: 622-625.

211. Kawai, T., T. Horiuchi, et al. (1989). "Effect of alkaline metal substitutions to Bi-Sr-Ca-Cu-O superconductor." Physica C: Superconductivity 161(5-6): 561-566.

212. Uchinokura, K., T. Yabe, et al. (1989). "Effect of substitution of 3d metals for Cu in Bi2(Sr0.6Ca0.4)3Cu2Oy." Physica C: Superconductivity 162-164(Part 2): 981-982.

213. Dou, S. X., H. K. Liu, et al. (1990). "Melt processing of alkali element doped Bi2Sr2CaCu2O8." Physica C: Superconductivity 172(3-4): 295-303.

214. Horiuchi, T., T. Kawai, et al. (1990). "Li substitution in the Bi2Sr2Ca1Cu2O8 superconductor." Physica C: Superconductivity 168(3-4): 309-314.

215. Matsubara, I., H. Tanigawa, et al. (1990). "Growth of Li-doped and dopant-free Bi-Sr-Ca-Cu-O superconducting whiskers." Physica C: Superconductivity 167(5-6): 503-508.

216. Tang, H., Z. Q. Qiu, et al. (1990). "A study of iron-doped bismuth-strontium-calcium-copper superconductors." Hyperfine Interactions 62(1-2): 65-71.

217. Tang, H., Z. Q. Qiu, et al. (1990). "Structural and superconducting properties of Bi-Sr-Ca-Cu superconductors studied by Fe doping." Journal of Applied Physics 67(9): 4512-4514.

218. Dou, S.-X., W.-M. Wu, et al. (1991). "Mechanism of the Tc enhancement in Bi2Sr2CaCu2O8+y by sodium doping." Physica C: Superconductivity 185-189(Part 2): 811-812.

219. Engkagul, C., K. Eaiprasertsak, et al. (1991). "Lithium/strontium exchange in '2212' bismuth superconductors." Physica C: Superconductivity 181(1-3): 63-67.

220. Hibble, S. J., P. C. C. Welch, et al. (1991). "Lithium-doped Bi2Sr2CuO6." Physica C: Superconductivity 185-189(Part 1): 631-632.

221. Horiuchi, T., K. Kitahama, et al. (1991). "1.1 substitution to Bl---Sr---Ca---Cu---O superconductor." Physica C: Superconductivity 185-189(Part 1): 629-630.

222. Ishikawa, N., N. Kuroda, et al. (1991). "Effects of substitution for Cu in La1.82Sr0.18Cu1-yMyO4 (M=Co, Ni, Ga, Zn)." Physica C: Superconductivity 185-189(Part 2): 805-806.

223. Poullain, G., T. Brousse, et al. (1991). "In-situ growth of Li-doped Bi2Sr2CaCu2O8 thin films by laser deposition." Physica C: Superconductivity 182(1-3): 143-148.

224. Xin, Y., Z. Z. Sheng, et al. (1991). "Comparison of Pb, Pb---Sb, Pb---V, P---Mo and Pb---W substituted Bi---Sr---Ca---Cu---O." Physica C: Superconductivity 176(1-3): 179-188.

225. Boekholt, M., T. Bollmeier, et al. (1992). "Structural and superconducting properties of bismuth strontium calcium copper cobalt oxide (Bi2Sr2Ca(Cu1-yCoy)2O8+d) single crystals." Physica C: Superconductivity and Its Applications (Amsterdam, Netherlands) 198(1-2): 33-41.

226. Hoshizaki, H., S. Kawabata, et al. (1992). "Direct observation of crystal growth and preparation of 2212-phase single crystals in Li-doped Bi-Sr-Ca-Cu-O system." Journal of Crystal Growth 121(1-2): 53-61.

227. Ishikawa, N., N. Kuroda, et al. (1992). "Spin-correlation in La1.82Sr0.18Cu1-yMyO4 (M = Ga, Zn, Ni, Co)." Physica C: Superconductivity 203(3-4): 284-292.

228. Lonnberg, B., T. Lundstrom, et al. (1992). "Substitution of vanadium and chromium for copper in Bi2Sr2CaCu2O8." Physica C: Superconductivity 191(1-2): 147-150.

229. Matsubara, I., T. Ogura, et al. (1992). "Effects of Li doping on the superconducting properties of Bi-based superconducting whiskers." Physica C: Superconductivity 201(1-2): 83-94.

230. Nkum, R. K., A. Punnett, et al. (1992). "Substitution of 3d metals for copper in bismuth lead strontium calcium copper oxide ((Bi,Pb)2Sr2Ca2Cu3Oy)." Physica C: Superconductivity and Its Applications (Amsterdam, Netherlands) 202(3-4): 371-8.

231. Moehlecke, S., C. H. Westphal, et al. (1993). "Enhancement of the intergranular superconducting properties in Bi2Sr2CaCu2O8 with Li additions." Physica C: Superconductivity 211(1-2): 113-120.

232. Sumana Prabhu, P., M. S. Ramachandra Rao, et al. (1993). "Structure and superconductivity studies on Fe and Co doped Bi-2212." Physica C: Superconductivity and Its Applications (Amsterdam, Netherlands) 211(3-4): 279-87.

233. Gu, G. D., K. Takamuku, et al. (1994). "Growth and superconductivity of Bi2.1Sr1.9Ca1.0(Cu1-yFey)2Ox single crystal." Journal of Crystal Growth 137(3-4): 472-8.

234. Horiuchi, T., K. Kitahama, et al. (1994). "Preparation of Li-containing Bi2Sr2CaCu2O8 single crystals and their Li solubility limit." Physica C: Superconductivity 221(1-2): 143-148.

235. Wu, S., J. Schwartz, et al. (1995). "Superconducting properties and microstructural evolution of Li doped Bi2Sr2CaCu2Ox." Physica C: Superconductivity 246(3-4): 297-308.

236. Noetzel, R., B. vom Hedt, et al. (1996). "Magnetic irreversibility lines and critical currents of Bi(2212) single crystals doped by Fe, Ni, Co and Zn." Physica C: Superconductivity 260(3-4): 290-296.

237. Chen, L.-X., H. Ikeda, et al. (1997). "Effect of Zn impurities on the mixed state Hall effect in Bi-2212 single crystal." Physica C: Superconductivity 282-287(Part 3): 1205-1206.

238. Fujiwara, M., M. Nakanishi, et al. (1997). "Electrochemical lithium intercalation into the Bi-2212 phase." Physica C: Superconductivity 279(3-4): 219-224.

239. Gu, G. D., G. J. Russell, et al. (1997). "Magnetism and flux pinning of Bi2.1Sr1.9Ca1(Cu1-yFey)2O8+x single crystals." Physica C: Superconductivity (Amsterdam) 282-287(Pt. 4): 2107-2108.

240. Gu, G. D., G. J. Russell, et al. (1997). "Effect of growth conditions and compositions on the morphology and stability of the solid-liquid interface of Bi-Sr-Ca-Cu-O grown by a floating zone method." Physica C: Superconductivity (Amsterdam) 282-287(Pt. 2): 865-866.

241. Ha, D. H., K. W. Lee, et al. (1997). "Magnetization of Y- and Ni-substituted Bi-2212 single crystals." Physica C: Superconductivity (Amsterdam) 282-287(Pt. 4): 1981-1982.

242. Joko, H., M. Fujiwara, et al. (1997). "Li doping into a Pb-substituted Bi-2212 phase." Funtai oyobi Funmatsu Yakin 44(8): 792-796.

243. Li, T. W., R. J. Drost, et al. (1997). "Enhanced flux pinning in Bi-2212 single crystals by planar defects introduced via Ti-substitution." Physica C: Superconductivity (Amsterdam) 274(3&4): 197-203.

244. Taniguchi, M., H. Ikeda, et al. (1997). "Second peak and magnetization jump in Bi2Sr2Ca(Cu1-xNix)2O8+d single crystals." Advances in Superconductivity IX, Proceedings of the International Symposium on Superconductivity, 9th, Sapporo, Oct. 21-24, 1996 1: 187-190.

245. Traeholt, C., H. W. Zandbergen, et al. (1997). "TEM analysis of planar defects induced by Ti doping in Bi-2212 single crystals." Physica C: Superconductivity 290(3-4): 239-251.

246. Wang, Y.-Z., Z.-R. Li, et al. (1997). "Superconducting properties of Bi1.8Pb0.4Sr2Ca2Cu3.2-xGexOy compounds." Physica C: Superconductivity (Amsterdam) 282-287(Pt. 3): 1447-1448.

247. Bandyopadhyay, B., J. B. Mandal, et al. (1998). "Variation of Tc and the thermopower of Bi2Sr2Ca1-yYy(Cu1-xMx)2O8 (M = Co and Zn) system." High Temperature Superconductivity: 302-305.

248. Chen, W. M., J. J. Jiang, et al. (1998). "The effects of substitution of Sn for Cu in Bi1.75Pb0.25Sr2CaCu2.3-xSnxSnxOy." Journal of Superconductivity 11(4): 437-441.

249. Gu, G. D., Z. W. Lin, et al. (1998). "Effect of Fe on the crystal growth morphology of Bi-Sr-Ca-Cu-O." Superconductor Science & Technology 11(10): 1129-1132.

250. Kouno, H., H. Ikeda, et al. (1998). "Out-of-plane transport properties of Bi2Sr2Ca(Cu1-xZnx)2O8+d single crystals." Advances in Superconductivity X, Proceedings of the International Symposium on Superconductivity, 10th, Gifu, Japan, Oct. 27-30, 1997 1: 135-138.

251. Movshovich, R., M. Jaime, et al. (1998). "Low-temperature phase transition in Bi2Sr2Ca(Cu1-xNix)208." Journal of Physics and Chemistry of Solids 59(10-12): 2100-2104.

252. Prabhakaran, D., A. Thamizhavel, et al. (1998). "Growth and texturing studies of Bi2.1Y0.1Sr1.9CaCu2 - xLixO8 crystals grown by floating-zone technique." Journal of Crystal Growth 183(4): 573-580.

253. Zhigadlo, N. D., V. V. Petrashko, et al. (1998). "The effects of Cs doping, heat treatments on the phase formation and superconducting properties of (Bi,Pb)-Sr-Ca-Cu-O ceramics." Physica C: Superconductivity 299(3-4): 327-337.

254. Volkov, M. P., B. T. Melekh, et al. (1999). "Effect of Li doping on the critical temperature and glass formation in the Bi-Sr-Ca-Cu-O system." Physics of the Solid State (Translation of Fizika Tverdogo Tela (Sankt-Peterburg)) 41(1): 15-17.

255. Watanabe, I., M. Akoshima, et al. (1999). "m+SR study on Bi2Sr2Ca1-xYx(Cu1-yZny)2O8+d around the hole concentration of per Cu." Journal of Low Temperature Physics 117(3/4): 503-507.

256. Watanabe, I., M. Akoshima, et al. (1999). "mSR study on the magnetic state of the Zn-substituted Bi-2212 system." Physica B: Condensed Matter (Amsterdam) 259-261: 557-558.

257. Gu, G. D. and Z. W. Lin (2000). "Single crystal growth of high-temperature superconductor Bi2.1Sr1.9Ca1.0Cu2.0AlyOx." Superconductor Science and Technology 13(8): 1197-1201.

258. Ilonca, G., A. V. Pop, et al. (2000). "Transport phenomena in Zn-substituted Bi2Sr2Ca1-xGdx(Cu1-yZny)2O8+d." Physica B: Condensed Matter (Amsterdam) 284-288: 1099-1100.

259. Jaime, M., R. Movshovich, et al. (2000). "Heat capacity of Ni-doped Bi2Sr2CaCu2O8 single crystals." Physica B: Condensed Matter 284-288(Part 1): 1069-1070.

260. Sun, Y. P., W. H. Song, et al. (2000). "Improved flux pinning and anomalous magnetization peak in heavily overdoped Bi2-xPbxSr2CaCu2-yCryO8+d single crystals." Applied Physics Letters 76(25): 3795-3797.

261. Wang, X. L., J. Horvat, et al. (2000). "Enhanced flux pinning by Fe point defects in Bi2Sr2Ca(Cu1-xFex)2O8+[delta] single crystals." Physica C: Superconductivity 337(1-4): 221-224.

262. Watanabe, I., M. Akoshima, et al. (2000). "Muon-spin-relaxation study on the Cu-spin state of Bi2Sr2Ca1-xYx(Cu1-yZny)2O8+d around the hole concentration of (1)/(8) per Cu." Physical Review B: Condensed Matter and Materials Physics 62(21): 14524-14530.

263. Zhao, X., S. Nakao, et al. (2000). "STM/STS observations of Co impurities in Bi2.1Sr1.8Ca(Cu1-xCox)2O8+y single crystals." Physica B: Condensed Matter 284-288(Part 1): 1065-1066.

264. Albino Aguiar, J., C. L. S. Lima, et al. (2001). "Structural and magnetic properties of NiS doped Bi-2212 superconductors." Physica C: Superconductivity and Its Applications (Amsterdam, Netherlands) 354(1-4): 363-366.

265. Zhao, X. R., K. Kitazawa, et al. (2002). "Effects of impurities on magnetization in Bi2.1Sr1.8Ca(Cu1-xMx)2Oy (M=Co, Zn) single crystals." Physica C: Superconductivity 370(1): 44-52.

266. Ilonca, G., T. R. Yang, et al. (2003). "Critical currents of Bi:2212 doped by Fe and Ni." Physica C: Superconductivity 388-389: 425-426.

267. Poddar, A., B. Bandyopadhyay, et al. (2003). "Effects of Co-substitution on superconductivity and transport in Tl2Ba2Ca1-xYx(Cu1-yCoy)2O8+d." Physica C: Superconductivity and Its Applications (Amsterdam, Netherlands) 390(2): 120-126.

268. Uthayakumar, S., E. Srinivasan, et al. (2003). "Growth of Bi2Sr2Ca(Cu1-xMnx)2O8 bulk textured crystals by IHFZ technique." Physica C: Superconductivity 392-396(Part 1): 463-467.

269. Kase, N. Irisawa, T. Morimoto, K. Kumakura, D.R. Dietderich, H. Maeda, Appl. Phys. Lett. 56, 970 (1990)

270. J. Tenbrink, K. Heine, H. Krauth, A. Szulczyk, M. Thoner, VDI Berichte 733, 399 (1989)

271. J. Tenbrink, K. Heine, H. Krauth, Cryogenics 30, 422 (1990)

272. W. Paul, Th. Baumann, Physica C 175, 102 (1991)

273. S. Nomura, H. Yoshino, K. Ando, Physica C 196, 323 (1992)

274. K. Shibutani, T. Egi, S. Hayashi, R. Ogawa, Y. Kawate, Japan, J. Appl. Phys. 30, 3371 (1991)

275. Th. Lang, D. Buhl, L.J. Gauckler, Physica C 275, 284 (1997)

276. D. Buhl, T. Lang, M. Cantoni, D. Risold, B. Hallstedt, L.J. Gauckler, Physica C 257, 151 (1996)

277. J.L. MacManus-Driscoll, J.C. Bravman, R.B. Beyers, Physica C 251, 71 (1995)

278. R. Wesche, A. M. Fuchs, B. Jakob, G. Pasztor, “Development and Processing of Bi-2212/Ag Superconducting Wires and Tapes” , In *Processing of Long Lengths of Superconductors*, U. Balachandran, E.W. Collings and A. Goyal, eds., TMS, Warrendale, USA (1994)

279. A.P. Baker, B.A. Glowacki, Physica C 223, 383 (1994)

280. P.Majewski, H.-L. Su, F. Aldinger, Physica C 229, 12 (1994)

281. J.F. Mitchell, J.A. Garcia, D.G. Hinks, Physica C 245, 126 (1995)

282. Krishnaraj, P, Lelovic M, Eror N.G, Balachandran U; (1994) “Synthesis and oxygen stoichiometry of Bi-2212;” Phys C 234(3-4) 311-8

283. Krishnaraj, P, Lelovic M, Eror N.G, Balachandran U; (1995) “Oxygen stoichiometry, structure and superconductivity of Bi-2212;” Phys C 246(3-4) 271-6

284. M'Hamdi E.M, Lacour C; (1992) "Synthese du composeBi-2212 sans Pba partird'unepoudre Lyophilise" Annales de Chimie et Physique; 17, 421-32

285. M'Hamdi E.M, Lacour C; (1992) "Synthese du composeBi-2212 sans Pba partird'unepoudre Lyophilise" Annales de Chimie et Physique; 17, 421-32

286. M.Azuma, Z.Hiroi, M.Takano, Y.Bando & Y.Takeda (1992) "Superconductivity at 110 K in the infinite-layer compound $(Sr_{1-x}Ca_x)_{1-y}CuO_2$" *Nature* 356, 775 - 776

287. Balachandran; Uthamalingam, Poeppel; Roger B. Emerson; James E., Johnson; Stanley A. United States Patent No *5,086,034;* Calcination and solid state reaction of ceramic-forming components to provide single-phase superconducting materials having fine particle size; February 4, 1992

288. Yu. D. Tretyakov, NN Oleynikov and OA Shlyakhtin; "Cryochemical Technology of advanced Materials" Chapman and Hall, 1997. ISBN 0412639807

289. C.P. Bean. "Magnetization of High-Field Superconductors" Rev. Mod. Phys. 36(1), 31–39 (1964)

290. I. Bozovic and J. N. Eckstein "Atomic-level engineering of cuprates and manganites", Applied Surface Science, Volumes 113-114, April 1997, Pages 189-197